NASA CR-72733

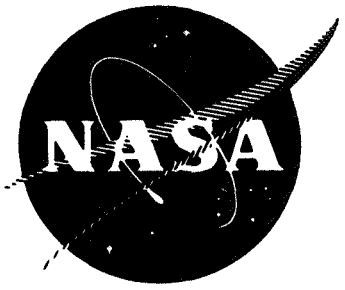

FINAL REPORT

CRYOGENIC ALLOY SCREENING

November 1970

By F. R. Schwartzberg, R. D. Keys,
and T. F. Kiefer

Prepared under Contract No. NAS3-11203 by
MARTIN MARIETTA CORPORATION
Denver, Colorado
for
NATIONAL AERONAUTICS AND SPACE ADMINISTRATION

NASA CR-72733

FINAL REPORT
CRYOGENIC ALLOY SCREENING

By F. R. Schwartzberg, R. D. Keys, and T. F. Kiefer

November 1970

Technical Management
NASA Lewis Research Center
Cleveland, Ohio
Liquid Rocket Technology Branch
J. R. Faddoul

Prepared under Contract No. NAS3-11203 by
MARTIN MARIETTA CORPORATION
Denver, Colorado

for

NATIONAL AERONAUTICS AND SPACE ADMINISTRATION

FOREWORD

This final report was prepared by Martin Marietta Corporation under contract Number NAS3-11203, "Cryogenic Alloy Screening," for the Lewis Research Center of the National Aeronautics and Space Administration. The work was administered under the technical direction of the Liquid Rocket Technology Branch, with Mr. James Faddoul acting as Project Manager.

Mr. F. R. Schwartzberg served as Martin Marietta Program Manager and Mr. R. D. Keys as Technical Director. Mr. T. F. Kiefer was responsible for the testing effort. The authors gratefully acknowledge the assistance of the following colleagues: L. M. Hanzlick, J. LeBeau, S. H. Osgood, and H. J. Brown.

CRYOGENIC ALLOY SCREENING

by

F. R. Schwartzberg, R. D. Keys and T. F. Kiefer

ABSTRACT

Three materials, 2021-T81 and X7007-T6 aluminum alloys, and cryogenically stretched 301 stainless steel, were evaluated in order to determine their mechanical properties, static fracture toughness, cyclic flaw-growth behavior, and sustained load threshold stress intensity. Testing was performed for both parent metal and welded material at 70, -320, and -423°F. Surface flaw and compact tension specimens were used for the fracture mechanics portion of the evaluation.

The results showed that the two aluminum alloys were quite tough. The 2021-T61 alloy is not greatly superior to 2014-T6 from a strength standpoint, but may be desirable from a weldability standpoint. X7007-T6 exhibits excellent static and cyclic strength properties but appears to have a low sustained load crack growth threshold. The cryogenically stretched stainless steel exhibits an excellent combination of properties.

CONTENTS

Figure

SUMMARY

The objective of this program was to characterize the routine mechanical properties, static fracture toughness, cyclic flaw-growth behavior, and sustained load threshold stress intensity of two newly developed aluminum alloys, 2021-T81 and X7007-T6 and a cryogenically stretched type 301 stainless steel. The three alloys were evaluated in both the parent metal and welded conditions at 70, -320, and -423°F.

The mechanical property data showed the two aluminum alloys to be slightly stronger than the currently used compositions. The stainless steel exhibits excellent strength properties; compared with titanium compositions on a strength/density basis we find it comparable to 6Aℓ-4V titanium at 70°F but inferior in the cryogenic range.

The static fracture toughness behavior of the two aluminum alloys is comparable to currently used compositions. The stainless steel exhibits excellent toughness at 70°F, over 100 ksi $\sqrt{\text{in.}}$, but despite a marked decrease with decreasing temperature, its toughness at -423°F is quite high, considering that its strength is about 350 ksi.

Cyclic growth behavior of the three alloys is similar to the aluminum and titanium compositions used to compare mechanical property and static toughness behavior.

Sustained load behavior was conducted using a limited number of specimens and as a result was only approximate. However, our data indicate that the parent metal X7007-T6 and welded 2021-T81 exhibit low threshold levels at 70°F. Under other conditions, the threshold levels appeared normal. Tests performed under a deleterious environment showed the typical decrease in threshold properties anticipated for 2000 and 7000 series alloys.* Unnotched corrosion tests failed to show any unusual behavior. The 301 stainless steel exhibits threshold levels clearly lower than reported for titanium alloys.

I. INTRODUCTION

The objective of the work described in this final report was to evaluate the cryogenic mechanical properties, fracture toughness, and flaw-growth characteristics of Aℓ 2021-T81, Aℓ X7007-T6, and Type 301 stainless steel in the parent metal and welded conditions. To do so, conventional mechanical properties were determined for each alloy and condition and used to establish baseline data at 70, -320, and -423°F. The static fracture toughness, cyclic crack-growth behavior, and sustained-load crack-growth behavior for each alloy were determined in the same way.

Cryogenic metallic materials available on the market have invariably been compositions whose properties represent a compromise. There have been few attempts to develop alloys specifically for low-temperature applications. The two new aluminum alloys recently developed by Alcoa* (2021-T81 and X7007-T6) that are intended to provide high strength, toughness, and weldability represent the first attempt to meet the needs of those designing and building structures that must withstand low temperatures. Cryogenically stretched type 301 stainless steel, chemically modified to provide improved toughness compared with cryogenically stretched, normal-grade type 301, is another new material made specifically for cryogenic service.

The entire program consisted of eight tasks. Brief descriptions of each task are as follows:

Task I - Literature Survey

The literature survey was conducted to obtain information on fabrication techniques, mechanical properties, and methods of acceptance testing of the three alloys to determine their suitability for structural applications.

Task II - Parent Metal Properties

Characterization of mechanical properties, static fracture toughness, cyclic crack-growth behavior, and sustained-load crack-growth behavior of the three subject alloys in the parent metal condition.

Task III - Weld Metal Properties

Same as Task II except for welded joints.

Task IV - Influence of Welding Procedure on Fracture Toughness of Aluminum Alloys

*Work performed under NASA Contract NAS8-5452.

Determination of the effect of welding procedure and defect location on the static fracture toughness of 2021-T81 and X7007-T6 aluminum alloys. Alloy 2014-T6 was included for comparison purposes.

Task V - Static Fracture Toughness Characterization of Aluminum Welds

Determination of behavior of optimized welds and effect of weld repair of same alloys evaluated in Task IV.

Task VI - Environmental Threshold Stress Intensity Evaluation

Determination of effect of defect location and a deleterious environment on sustained load threshold of the alloys evaluated in Tasks IV and V.

Task VII - Response of Materials to a Corrosion Environment

Determination of general and stress corrosion resistance of the three aluminum alloys described above plus several additional aluminum alloys for control purposes.

Task VIII - Data Evaluation

Analysis of test data from all tasks data and comparison of behavior with compositions currently being utilized for structural service.

This program was performed in two parts. The original portion consisted of the first three tasks. An interim report (Ref 1) was issued describing the results of these tasks. As a result of our initial findings it was decided to perform the work described in Tasks IV thru VII.

In this final report, we have extracted the pertinent data from the interim report to insure continuity and have presented the detailed findings of Tasks IV thru VII.*

*These data are presented in Appendix A and summarized in the body of the report.

II. BACKGROUND AND ANALYTICAL TECHNIQUES

A. STRESS INTENSITY FOR SURFACE-FLAWED SPECIMENS

Irwin (Ref 2) has estimated the effect of shape on stress intensity in a semielliptical surface flaw subject to a normal load by using the following equation:

$$K_I = \frac{M_1 \sqrt{\pi a}\ \sigma \left(\sin^2 \varphi + \frac{a^2}{c^2} \cos^2 \varphi\right)^{\frac{1}{4}}}{\left[\Phi^2 - 0.212 \left(\frac{\sigma}{\sigma_{ys}}\right)^2\right]^{\frac{1}{2}}}$$

where:

M_1 is a front surface correction factor generally taken as 1.1;

σ is the applied tensile stress;

a is the length of the semiminor axis;

φ is the angle between the major axis and any point on the flaw front;

c is the length of the semimajor axis;

Φ is the complete elliptical integral of the second kind and may be expressed by:

$$\Phi = \int_0^{\pi/2} \sqrt{1 - \frac{c^2 - a^2}{c^2} \sin^2 \varphi}\ d\varphi.$$

The term $\left[\Phi^2 - 0.212 \left(\frac{\sigma}{\sigma_{ys}}\right)^2\right]$ is commonly called Q. By letting φ = 90° the limiting equation for stress intensity can be expressed as:

$$K_I = 1.1 \sqrt{\pi}\ \sigma \left(\frac{a}{Q}\right)^{\frac{1}{2}}$$

Several modifications have been made to the above approximate solutions in order to account for the effect of the proximity of the back face. These have been reported by Kobayashi (Ref 3) and Smith (Ref 4). Recent experiments performed by Larson (Ref 5) and Smith (Ref 6) using cast epoxy specimens indicate that the back-surface correction factors are approximately 20 to 25% lower than those predicted by Smith (Ref 4).

In this work, attempts were made to avoid making cracks deep enough to require back-surface correction of the stress-intensity factor. Back-surface correction factors were not used because there is still some uncertainty as to the magnitude of the elastic magnification factors, and in addition, the effects of plasticity have still not been assessed.

B. STRESS INTENSITY FOR COMPACT-TENSION SPECIMENS

Optimization studies of the Westinghouse WOL (wedge opening loading) specimen have resulted in a modification of the T design to accommodate dual pin loading. The resulting design has been designated the compact-tension (CT) specimen. Figure II-1 illustrates the geometry of these two specimens. Increasing the crack length-to-width ratio (a/W) to a nominal value of 0.5 has effected a reduction in the size and load requirements. The principal advantage of the CT specimen is that it has a higher toughness measurement capacity than the WOL specimen. For example, the WOL specimen has a tentative capacity $\left(\text{defined by the ratio } K_{Ic}/\sigma_{ys}\right)$ of 0.45; the CT specimen is estimated to have a capacity of 0.63. For the rather tough aluminum materials tested in this program, a high measurement capacity was essential.

Wessel (Ref 7) shows that the stress intensity equation for the CT specimen is of the form:

$$K_I = Y \frac{P\sqrt{a}}{BW},$$

where:

$$Y = 23.12 - 67.67\left(\frac{a}{W}\right) + 97.31\left(\frac{a}{W}\right)^2 \text{ for } \frac{a}{W} = 0.4 \text{ to } 0.6$$

$$\text{and } \frac{H}{W} = 0.60;$$

W = 2·55 B
a = 1·0 B
H = 1·24 B
D = ·70 B
W_1 = 3·2 B
T = ·625 B

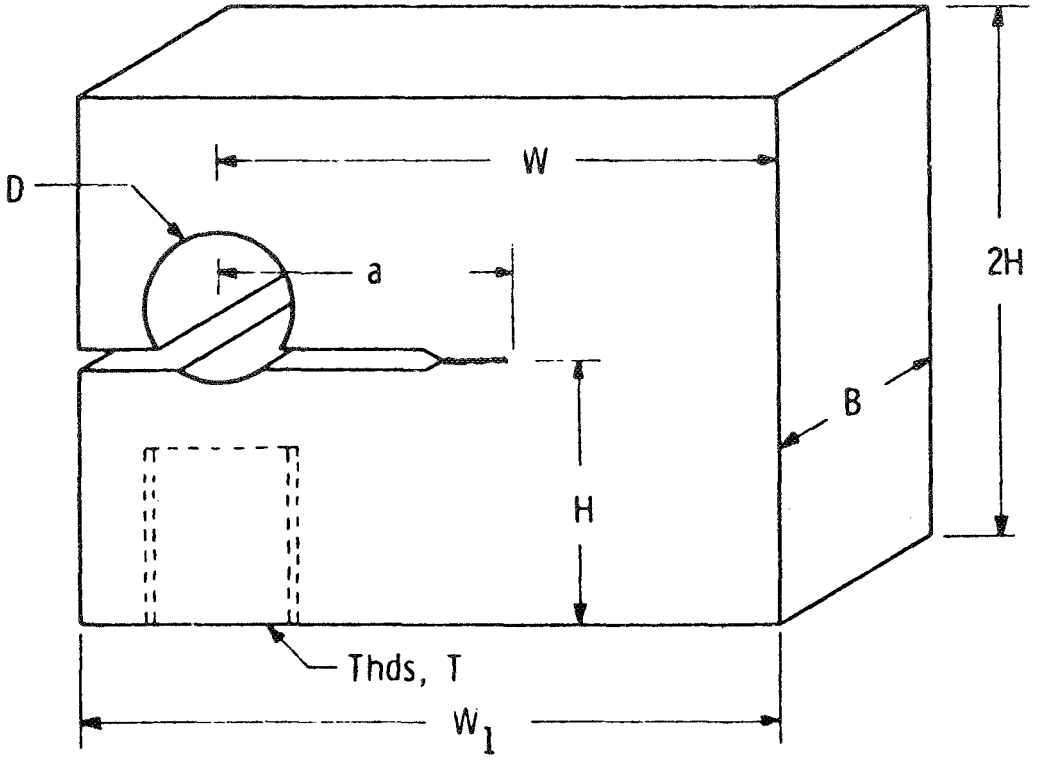

'T' Type WOL Specimen

W = 2·0 B
a = 1·0 B
H = 1·2 B
D = 0·5 B
W_1 = 2·5 B
H_1 = 0·65 B

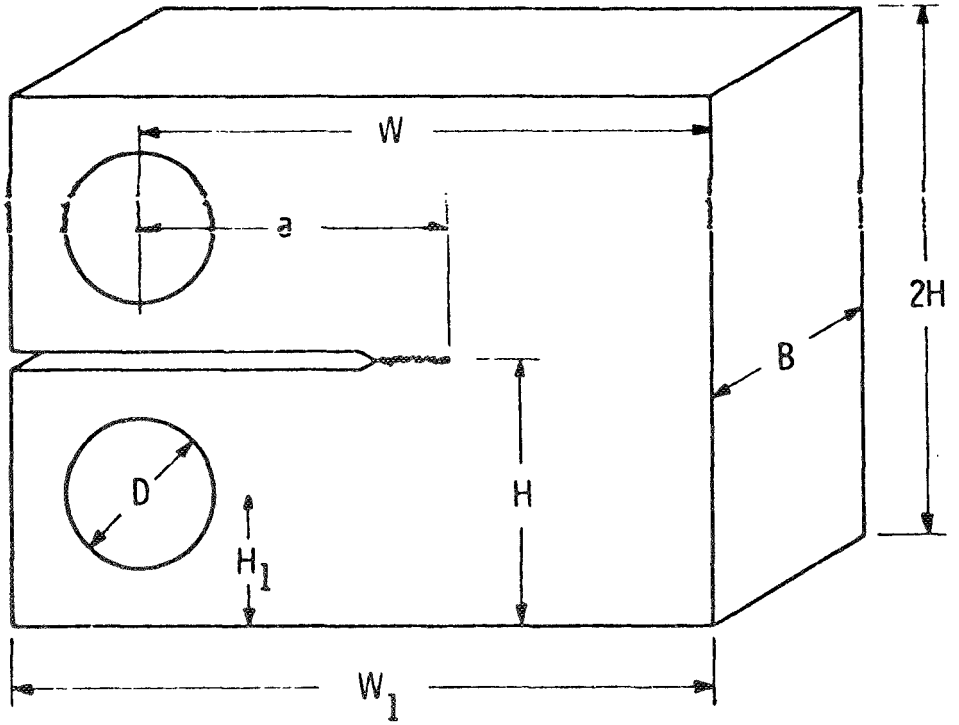

Compact Tension Specimen

Fig. II-1 Geometries of Two Crackline Loaded Fracture Toughness Specimens

H = half beam height;

P = load;

a = crack length;

B = thickness;

W = beam width.

Experience with the use of compact-tension specimens has shown that the crack front does not grow uniformly. Normally, the crack front grows in a convex manner -- that is, deeper in the center. Therefore, it is necessary to adjust the crack-length measurements to provide a weighted average.

$$a_{average} = \frac{4a_{\text{at midthickness}} + a_{\text{left face}} + a_{\text{right face}}}{6}$$

The proposed ASTM method for plane strain fracture toughness testing of metallic materials covers the compact tension specimen. In section 7.2.3 of this method the technique for crack measurement is described. Their method does not agree with that used in this work. In the ASTM method the crack length at the center and midway between the center and end of the crack front on each side is measured. The crack length is taken as the average of these three measurements. If the difference between any two measurements exceeds 5% of the average or if any part of the crack front is within 5% of the length of the machined notch root, the test is considered invalid. If the surface trace is less than 90% of the average crack length, the test is also invalid.

The proposed method was published subsequent to performance of the bulk of our data analysis and as a result was not utilized. Due to crack front curvature, many of the aluminum specimens used in this program would not have met these ASTM criteria.

C. CYCLIC FLAW GROWTH

During cyclic loading, a small amount of growth is considered to have occurred during each load cycle. If the increment of crack extension that occurs during a specific number of cycles can be determined, it is possible to prepare a crack extension curve of crack length (a) vs number of cycles (N). The slope of the curve at any point is the crack growth rate (da/dN). From an experimental standpoint, this technique is relatively simple to

apply for through-cracked specimens. However, for semielliptical surface flawed specimens this is not readily accomplished because the critical crack parameter, the crack depth, is not visually measurable from the surface. Because the shape of the crack usually changes as the crack grows in depth, determining the crack width, which is readily discernible on the surface, does not provide quantitative information.

Boeing (Ref 8 and 9) has evaluated flaw-growth behavior in surface-flawed specimens using the "end point analysis" method. In this method, the initial stress intensity $\left(K_{Ii}\right)$ is plotted against the number of cycles to failure, and these data are converted to an initial crack size (a/Q) vs N curve at a given stress. From this curve, the slope or crack growth rate $[d(a/Q)/dN]$ can be obtained for a specific a/Q. The latter can be converted to a value of K_I at a given stress, and as a result, a stress intensity vs growth rate curve can be obtained.

This method is dependent on several factors:

1) The specimen must be taken to fracture;
2) The critical crack depth must be sufficiently less than the thickness to avoid plasticity effects;
3) The critical crack size must be distinguishable from the rapid fracture;
4) A semielliptical shape must be maintained.

Satisfying these criteria gives a simple method for determining crack growth.

Another method, used in this program, can be called the "linear interpolation" technique. This approach is to minimize the amount of flaw growth, thereby making the initial and final stress intensities similar enough so that a rate based on the initial and final crack sizes is a valid linear interpolation of the slope of the crack size vs number of cycles curve. It is important to make a small linear interpolation because the error that can result in a power function relationship, in this case one theorized to be a fourth power relationship, can be quite significant. As described elsewhere in this report, using the linear interpolation method, multiple data can be obtained from a single surface-flawed specimen by flexural fatiguing between increments of axial cyclic growth.

III. EXPERIMENTAL PLAN

The object of this investigation was to characterize the mechanical properties and behavior of the three subject alloys and compare them to those of currently-used structural alloys.

The program consisted of the following tasks:

Task I - Literature Survey;*

Task II - Parent-Metal Evaluation;*

Task III - Weld Metal Evaluation;*

Task IV - Influence of Welding Procedure on Fracture Toughness of Aluminum Alloys;

Task V - Static Fracture Toughness Characterization of Aluminum Welds;

Task VI - Environmental Threshold Stress Intensity Evaluation;

Task VII - Response of Materials to a Corrosive Environment;

Task VIII - Data Evaluation.

The following sections discuss the nature of the work required under each task.

A. TASK I -- LITERATURE SURVEY

Two literature surveys were conducted, one for the aluminum alloys and one for the stainless steel, to collect data on the mechanical properties, fabrication techniques, and acceptance tests associated with each material.

The aluminum survey was conducted by Martin Marietta Corporation and is included in this report. The stainless steel survey was subcontracted to Arde, Inc. As the developers of the cryogenic stretch-forming process, they were the obvious choice for the performance of this subtask. The stainless steel survey was presented in Appendix B of the interim report (Ref 1).

*The results of part of Task I and all of Tasks II and III were presented in an interim report (Ref 1).

B. TASK II -- PARENT-METAL EVALUATION

The following nominal thicknesses were planned for use in this evaluation:

Cryoformed Stainless Steel = 0.125 in.;
Aℓ 2021-T81 = 1.00 in.;
Aℓ X7007-T6 = 1.00 in.

Tests were conducted at three temperatures:

70°F (ambient air);
-320°F (liquid nitrogen);
-423°F (liquid hydrogen).

1. Mechanical Property Tests

The uniaxial tensile data gathered for each alloy included:

1) Ultimate strength;
2) Yield strength;
3) Elongation;
4) Reduction in area;
5) Elastic modulus;
6) Strain-hardening exponent;
7) Poisson's ratio;
8) Conventional stress-strain behavior;
9) True stress-strain behavior.

The testing was conducted in both the longitudinal and transverse directions. Six replicate tests were performed for each condition and temperature.

2. Static Fracture-Toughness Tests

Static fracture-toughness tests were conducted for each alloy in the longitudinal and transverse directions. Triplicate tests were performed for each condition and temperature.

3. Cyclic-Load Flaw-Enlargement Tests

Cyclic-load flaw-enlargement tests were conducted for each alloy and temperature in one grain direction. Triplicate specimens were tested for each condition and temperature.

4. Sustained-Load Flaw-Enlargement Tests

Sustained-load flaw-enlargement tests were conducted for each alloy and temperature in one grain direction. Triplicate specimens were tested for each condition and temperature.

C. TASK III -- WELDED METAL EVALUATION

The testing conducted in this task was essentially identical to that described in the preceding section. Flaws were oriented parallel to the weld centerline. The aluminum alloys were tested in the as-welded condition; the stainless steel was tested in the aged condition.

D. TASK IV -- INFLUENCE OF WELDING PROCEDURE ON FRACTURE TOUGHNESS OF ALUMINUM ALLOYS

In this task the effect of overheating was compared to the normal procedure used in Task III. The effect of defect location (heat affected zone, fusion line, and weld centerline) was also evaluated. For comparison purposes, alloy 2014-T6 were also studied. A second heat of 2021-T81 and X7007-T6 was obtained for this work

E. TASK V -- STATIC FRACTURE TOUGHNESS CHARACTERIZATION OF ALUMINUM WELDS

Using an optimized weld procedure from Task IV, toughness was determined for the three alloys (2021-T81, X7007-T6, and 2014-T6). The effect of weld repairing was also determined.

F. TASK VI -- ENVIRONMENTAL THRESHOLD STRESS INTENSITY EVALUATION

The effect of defect location and environment (air and salt solution) on the sustained load threshold stress intensity of the three alloys (2021-T81, X7007-T6, and 2014-T6) was determined.

G. TASK VII -- RESPONSE OF MATERIALS TO A CORROSIVE ENVIRONMENT

In this task, the general and stress corrosion resistance (using both laboratory tests and actual seacoast environment) of the three above alloys, plus several additional aluminum alloys for control purposes, was evaluated.

H. TASK VIII -- DATA EVALUATION

The data obtained from the alloy tests described in the preceding sections was compared to the data for currently-used alloys in order to determine whether the new alloys were superior to present materials.

IV. MATERIAL PROCUREMENT AND PROCESSING

A. ALUMINUM ALLOYS

The aluminum alloy plate (2021-T81 and X7007-T6) purchased from Alcoa was 84 to 96 in. long, 36 in. wide, 1 in. thick, and was fully heat-treated. Material of each alloy for Tasks II and III was obtained from a single heat; stock for Tasks IV through VII was purchased at a later date and was from a different heat. Alcoa's certification report lists transverse room temperature properties in the following tabulation.

Aluminum Alloy*	Lot No.	Used in Indicated Task	Tensile Strength (ksi)	Yield Strength (ksi)	Elongation (%)
X2021-T8E31	105-267	II, III	72.0	63.0	3.8
2021-T8E31	713-581	IV - VII	72.2	62.5	7.0
X7007-T6E136	105-266	II, III	72.2	66.7	14.0
X7007-T6E136	717-781	IV - VII	76.5	71.8	12.5

*The designations for the alloys are those used at the time the plates were purchased. The experimental or X designation for the 2021 alloy has since been removed. In this report, the two alloys will be designated as 2021-T81 and X7007-T6.

Because the elongation level of the Aℓ 2021 from lot 105-267 appeared abnormally low, standard 0.505-in.-diameter round bars were machined and tested in both the longitudinal and transverse grain directions. The test data shown below confirmed that the transverse elongation was low.

Grain Direction	Tensile Strength (ksi)	Elongation (%)
Longitudinal	72.2 71.6	8.0 8.5
Transverse	70.8 70.6	4.5 4.5

Alcoa was contacted to determine whether this material was representative of the subject alloy. Photomicrographs of the structure and a small quantity of material were forwarded to Alcoa for their review and analysis. Alcoa reviewed the complete processing records for this material and found no basis for recommending that the material be rejected, although they did confirm that the ductility was at the low end of the specification limit.

At the request of the NASA project engineer, the Aℓ 2021 was further evaluated to determine whether the cryogenic ductility was adversely affected. The test results showed that there was no further loss of ductility with reductions in temperature, rather only the normal increase in elongation observed for aluminum alloys (see Table IV-1).

Table IV-1 Strength and Ductility of Parent Metal Specimens* (2021-T81 Aluminum Alloy; Lot 105-267)

Temperature (°F)	Ultimate Strength (ksi)		Elongation (%)	
	Longitudinal Direction	Transverse Direction	Longitudinal Direction	Transverse Direction
70	70.9	71.0	9.0	4.0
	72.0	71.7	8.5	5.0
	71.4	71.4	8.8	4.5
-320	86.7	88.4	11.5	6.5
	87.5	87.7	11.2	7.9
	87.1	88.0	11.4	7.2
-423	99.9	101.7	13.4	11.0
	99.8	99.7	14.4	11.0
	99.8	100.7	13.9	11.0

*0.250-in.-diameter round bar specimens.

The 2014-T6 aluminum alloy obtained for comparison purposes in Tasks III thru VII was purchased as commercial material, and as a result, no certification was obtained. Similarly, the other aluminum alloys (2219-T87 and 7075-T6) used for the corrosion tests (Task VII) were obtained without certification.

Panels were prepared for welding in the following manner. First the alloys were degreased in trichloroethylene vapor, soaked in an alkaline solution for 15 minutes, and deoxidized for 10 minutes. Then the edges were filed, and after the corners were broken slightly, a 1-in.-wide surface next to the edge was cleaned with a wire brush. The specimens were welded transverse to the grain direction using a direct-current, straight-polarity, 800-amp Sciaky Zero Error supply and an Airline Welding fixture. One pass was made on each side without using filler wire. This was followed by making a second pass on each side using filler wire. Filler wires were as indicated in the following tabulation.

Alloy Designation	Filler Designation
2021	2319
X7007	5356
2014	4043
2219*	2319

*2219-T87 material was obtained in the form of a welded panel from the Boeing Company; this material was excess from Contract NAS3-10290. The final report for NAS3-10290 gives complete mechanical property data (Ref 11).

Weld panels were air cooled to room temperature after each pass.

Welding parameters used for this work are given in Table IV-2. The normal weld procedure was used for all work reported under Tasks II and III. In subsequent discussion, welds should be considered to be of normal procedure, without weld repair, unless otherwise noted.

Radiographic inspection of all welds showed no evidence of defects or porosity and the welds were declared acceptable. No postweld aging was used for the X7007 and 2014 welds. Alloy 2021 was evaluated in the as-welded and postweld aged conditions. Data for 2021 alloy welds should be considered to be in the as-welded condition unless otherwise noted.

Table IV-2 Welding Parameters for Aluminum Alloys

Welding Parameters	Normal Weld			Overheated Weld		
	2021	X7007	2014	2021	X7007	2014
Current (amp)						
1st Pass	550-575	580-600	570	600	650-660	630
2nd Pass	350-375	350-375	340	500	400	375
Voltage (v)						
1st Pass	10.7-12	10.7-11.5	103	10.8	10.6	10.3
2nd Pass	11.8-13	12-13	113	12.0	11.8-12.6	11.3
Torch Speed (in./minute)						
1st Pass	4-6	4-6	5	3.6	3.6	4.5
2nd Pass	6-6.5	6-6.5	6.5	5.2-5.4	3.6-5.4	5.5
Wire Feed (in./minute)						
2nd Pass	12-15	10-12	12	12	12-15	12
Helium Gas Coverage (cfh)						
All Passes	90-110	90-110	70	80	90-100	70

Specimens for weld repair were welded in the normal manner and then routed using a U-shaped milling cutter that gave a 3/8-in. wide x 3/8 in. deep recess. Multipass automatic welding was used for repairing; two to four passes were required to provide full weld buildup.

Metallographic examination of the two new alloys showed structures typical for 2000- and 7000-series alloys. Figure IV-1 shows a longitudinal section of 2021-T81 parent metal. This alloy exhibits slightly more second-phase precipitate than lower-strength 2000-series compositions. A macro section of a 2021 welded joint is shown in Fig. IV-2. The heat-affected zone (see Fig. IV-3) shows depletion, presumably of copper, along the grain boundary and around the intermetallic particles. This depletion might cause reductions in strength and in stress-corrosion resistance.

An examination of the X7007-T6 alloy showed the highly-oriented structure typical for high-strength 7000-series compositions. The amount of second-phase precipitate in the X7007 (Fig. IV-4) was slightly less than that observed in 7075 alloy (Fig. IV-5). Figure IV-6 shows a macrosection of a X7007 welded joint; the rather significant mushrooming effect noted near the surface in the heat-affected zone probably results from deformation at the welding temperature, due to the rather low yield strength of aluminum-zinc alloys at high temperatures. An examination of the heat-affected zone showed grain-boundary coarsening rather than the recrystallization that commonly is found in other aluminum alloys.

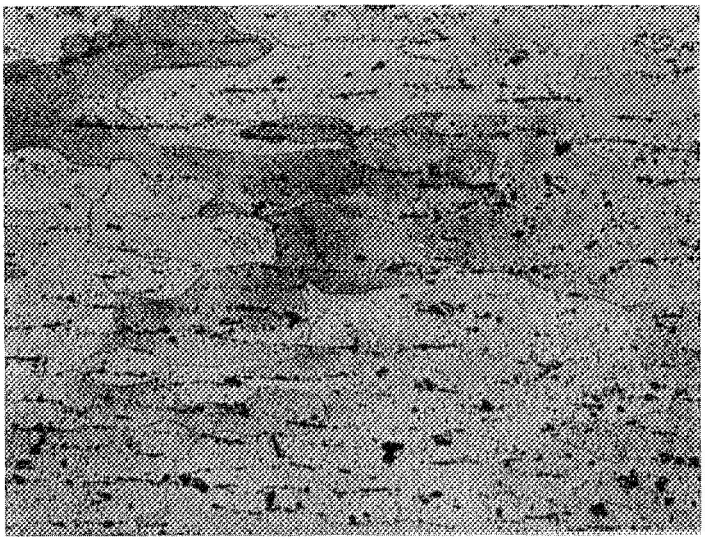

Fig. IV-1 Microstructure of Parent-Metal 2021-T81; Longitudinal Direction (Enlarged 100X)

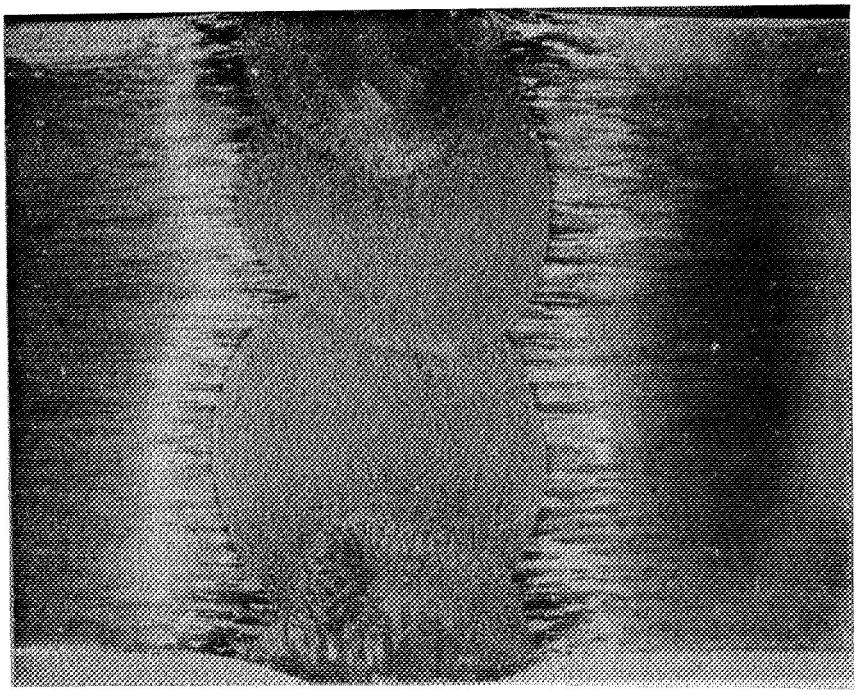

Fig. IV-2 Macrosection of a 2021-T81 Welded Joint (Enlarged 3X)

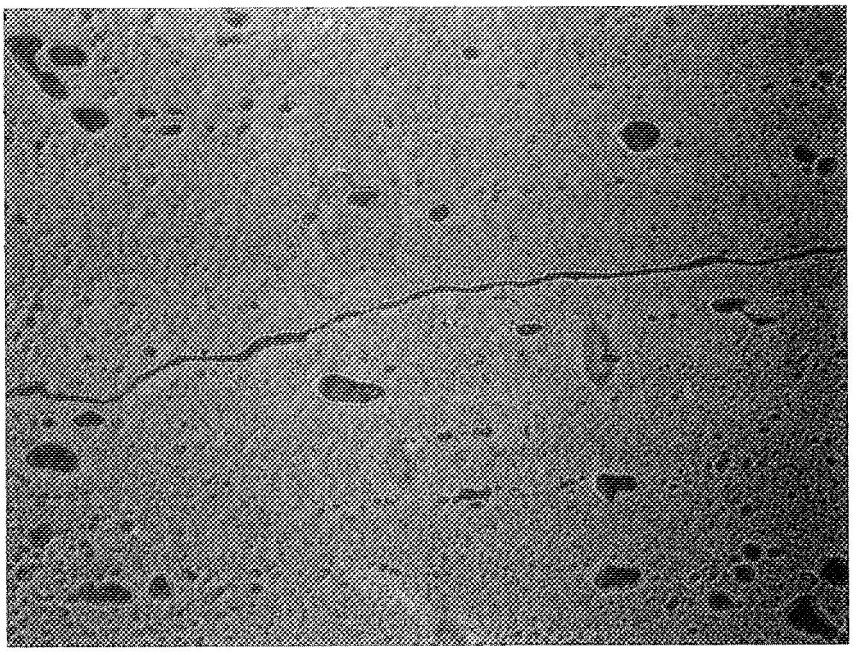

Fig. IV-3 Microstructure of 2021-T81 Heat-Affected Zone Showing Depleted Zones (White Areas) (Enlarged 400X)

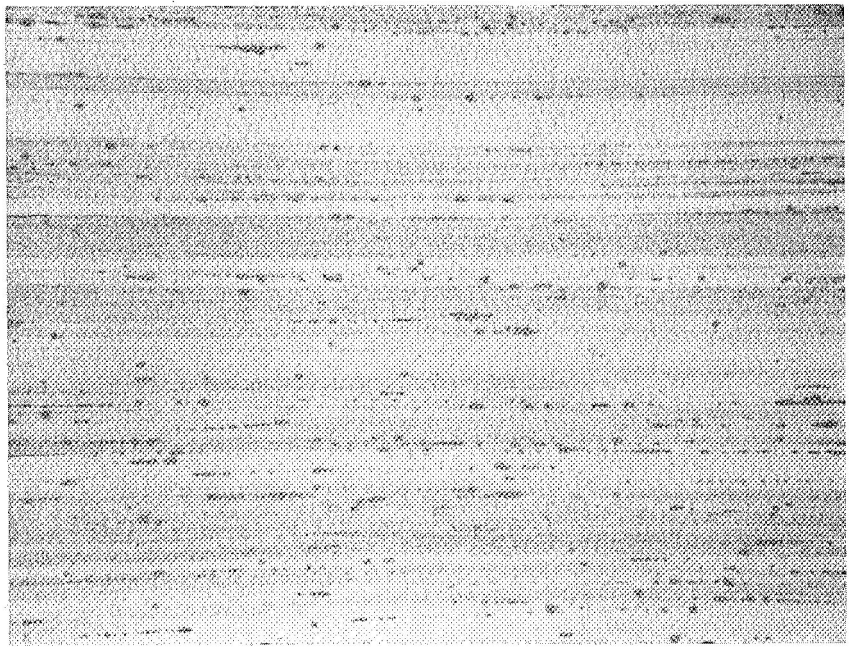

Fig. IV-4 Microstructure of Parent-Metal X7007-T6; Longitudinal Direction (Enlarged 100X)

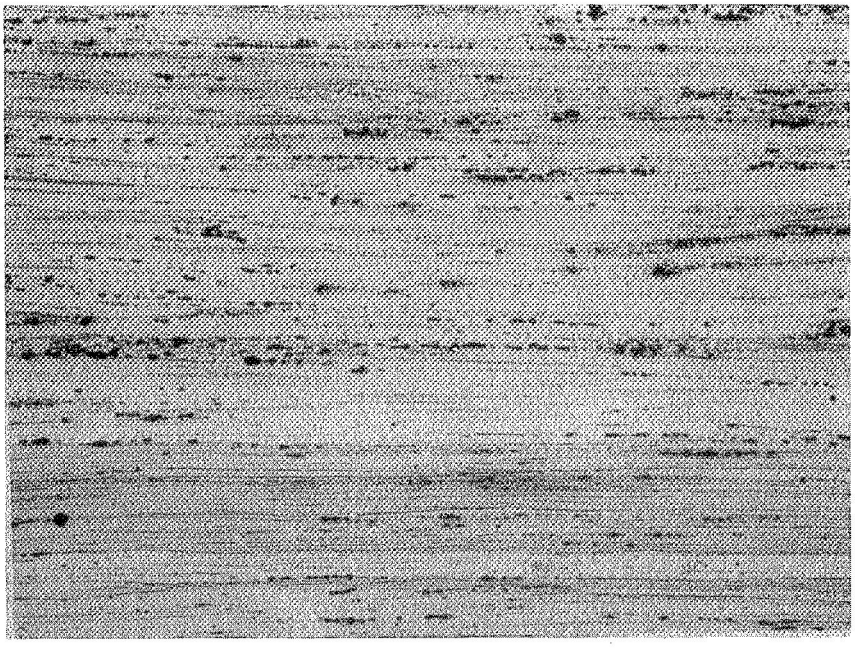

Fig. IV-5 Microstructure of Parent-Metal 7075-T6; Longitudinal Direction (Enlarged 100X)

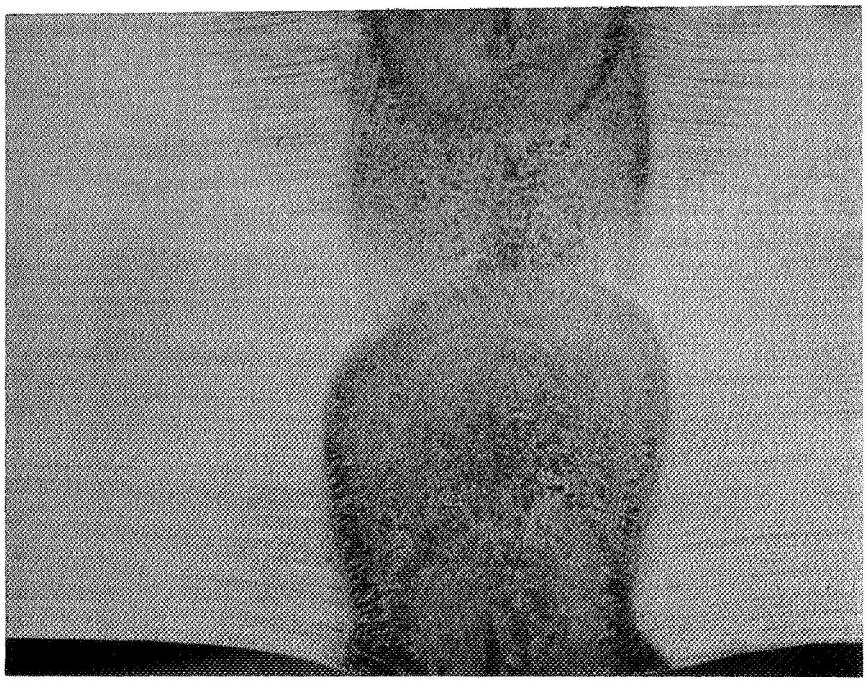

Fig. IV-6 Macrosection of an X7007-T6 Welded Joint (Enlarged 3X)

B. STAINLESS STEEL ALLOY

Arde, Inc supplied three 120-in.-long by 36-in.-wide by 0.140-in.-thick sheets of modified, Type 301, low-silicon (less than 0.1%) stainless steel (Latrobe Heat No. 50793) to Martin Marietta.

Martin Marietta cut the material into panels for subsequent cryogenic stretching in liquid nitrogen (-320°F). These panels had a gage width of 13 in. and a reduced section length of 48 in.

Next, the panels were sent back to Arde, Inc, where they were welded, re-annealed, pickled, and passivated. Then the panels were shipped back to Denver, where they were stretched and machined into test coupons. Finally, the coupons were returned to Arde for aging, cleaning, and passivating.

The panels were stretched in our 500,000-lb testing machine. The machine was placed horizontally and a large pan, approximately 10 ft long x 3 feet wide x 1½ ft deep, was placed in the throat of the machine to provide the environmental control for stretching. A typical stretched panel is shown in Fig. IV-7.

Of the first nine panels stretched, six were satisfactory. In the other three, there were premature failures in the joint between the grip and the test section. This weld was to have been made automatically, but was found to be a manual weld that exhibited very poor weld penetration. Three additional panels were fabricated using automatic welding equipment. A fourth panel, which showed indications of cracks, was returned to Arde for automatic rewelding, but was only repaired. Back at Denver, the three automatically-welded panels were stretched satisfactorily, but the repaired panel failed during stretching.

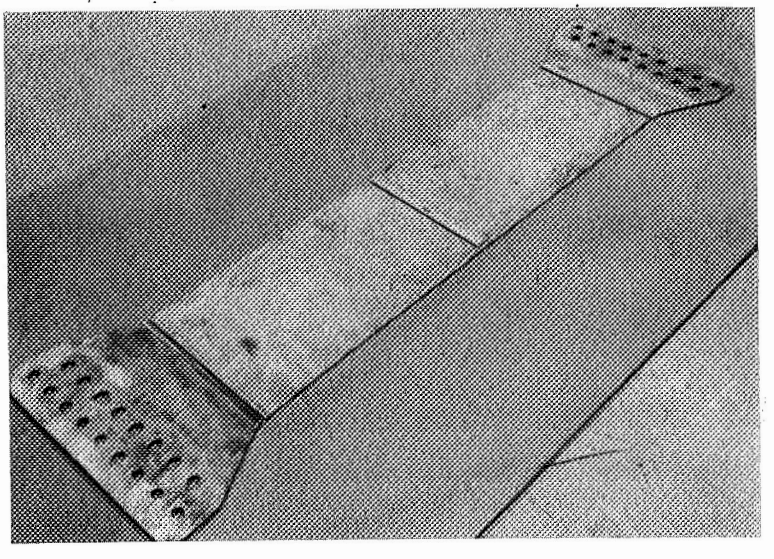

Fig. IV-7 Typical Cryogenically Stretched Stainless Steel Panel

Single tension specimens were machined from each of the first nine stretched panels. No tensile specimens were taken from the four additional panels. These specimens were aged at 790°F for 2 hr, air-cooled, and then tensile-tested at 70°F. Except for Panel 4, which obviously did not receive enough prestress to achieve the desired strength level, there was good agreement between the tensile properties of each panel. Panels 6 and 7, which failed prematurely, were as strong as the panels that were given the full prestress, and were deemed satisfactory for use (Table IV-3).

Table IV-3 Tensile Properties of Cryogenically-Stretched Parent Metal Specimens*

Panel Number	Cryogenic Prestress (kips)	Ultimate Strength (ksi)	Yield Strength (ksi)	Elongation (%)
1	400	235.2	232.9	7.3
2	400	234.4	228.7	8.0
3	410	236.1	231.6	6.8
4	325†	217.0	208.2	8.0
5	400	237.6	236.9	7.5
6	364†	237.3	233.5	8.0
7	380†	236.6	235.1	7.8
8	405	244.3	241.3	6.8
9	403	241.8	236.5	7.3

*Single tensile specimen removed from each panel.

†Failed during stretching.

A metallographic examination of the cryogenically-stretched stainless steel showed that the material structure was typical of that for a strain-hardened austenitic stainless steel. Twins were noted in many of the grains. The microstructure showed a very low level of inclusions or foreign matter. Aging appeared to only slightly increase the size of the carbides deposited along the grain boundary. Figures IV-8 and IV-9 show the unaged and aged structures. The welded joint (see Fig. IV-10) appeared quite normal; there was no evidence of excessive carbide precipitation.

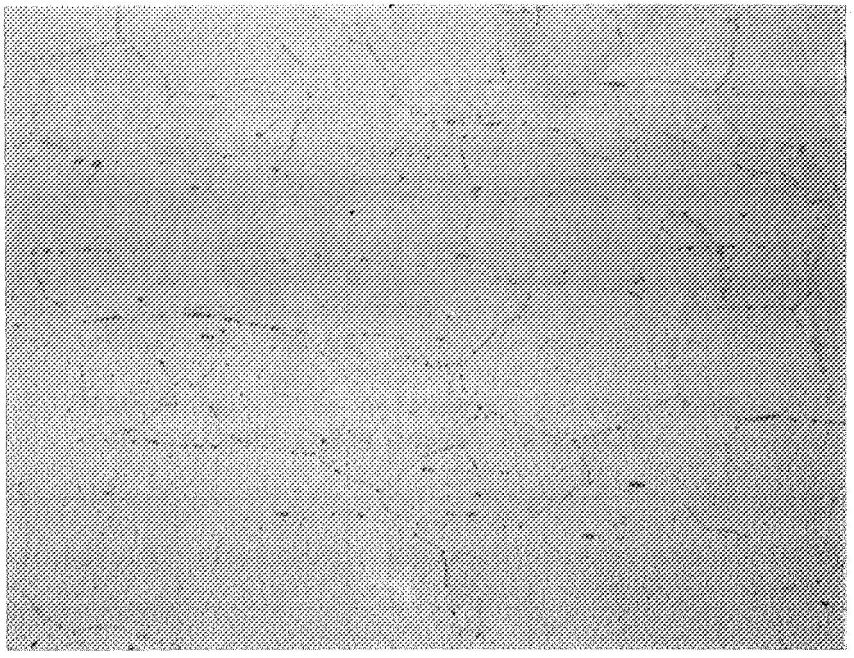

Fig. IV-8 Microstructure of Unaged, Cryogenically Stretched Type 301 Stainless Steel; Parent Metal; Longitudinal Direction (Enlarged 250X)

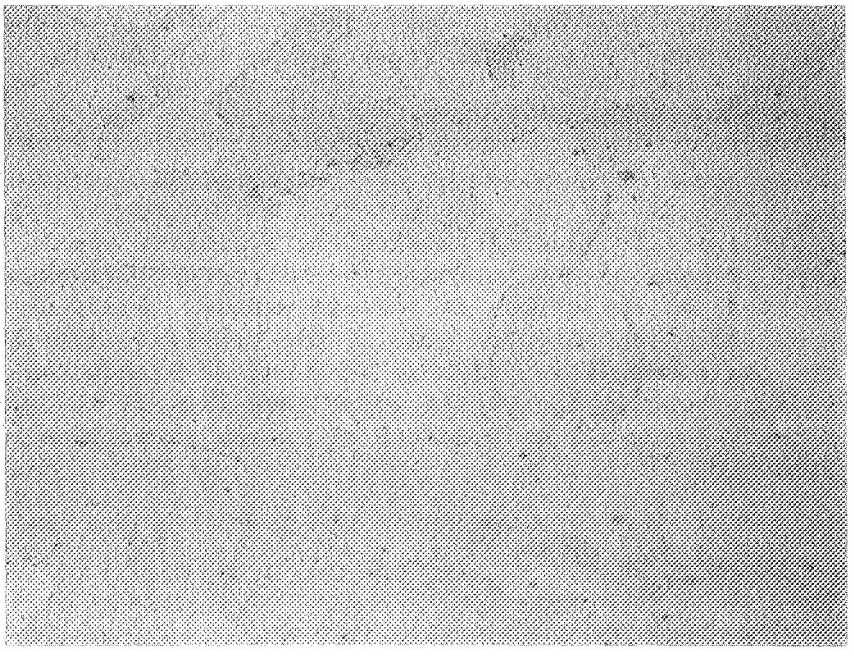

Fig. IV-9 Microstructure of Aged, Cryogenically Stretched Type 301 Stainless Steel; Parent Metal; Longitudinal Direction (Enlarged 250X)

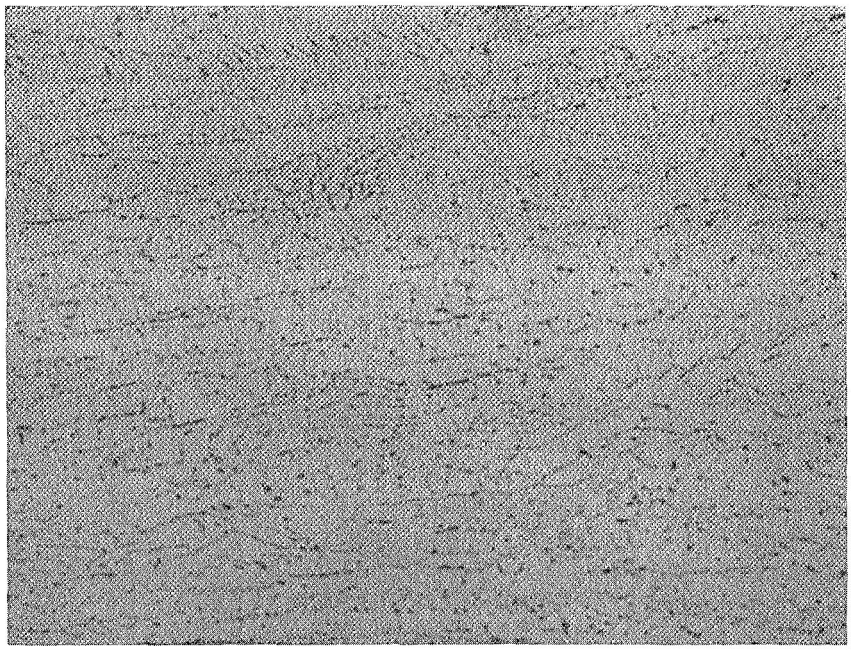

Fig. IV-10 Microstructure of Aged, Cryogenically Stretched Type 301 Stainless Steel; Welded Metal; Longitudinal Direction (Enlarged 250X)

V. EXPERIMENTAL PROCEDURE AND TECHNIQUES

A. MECHANICAL PROPERTY TESTING

The mechanical property testing techniques used in this program were relatively routine. Emphasis was placed on obtaining multiple strain data, and as a result, many resistance strain gages were used.

1. Specimen Design

Two types of tensile specimens were used in the aluminum investigation. The evaluation of welded materials was performed using full-thickness specimens, and though this approach necessitated using loads that were higher than those on the round bar specimens, it was considered superior because it allowed us to evaluate the entire weld cross-section. The room-temperature specimens were friction-gripped; the cryogenic specimens were pin-loaded (Fig. V-1). Some parent metal tests were performed using full-thickness specimens.

The remainder of the parent metal aluminum specimens was machined to the standard diameter of 0.505 in. so that their elongation, which depends on shape and gage length, could be compared with that of other alloys.

The stainless steel specimens were machined according to our standard design for sheet gage materials and were pin-loaded at all temperatures. Figure V-2 gives the specifications for these specimens.

On both the aluminum and the stainless-steel specimens, the weld beads were machined flush with the surface.

2. Instrumentation

Bonded resistance strain gages and strain beam extensometers were used to determine the strains. Bonded foil gages were used to obtain elastic-modulus and deformation data into the yield-strength range. We used series-connected gages, mounted on opposite surfaces, to compensate for small misalignments and bending. Our approach in using strain gages is to establish a full bridge circuit of strain gages and to compensate for temperature

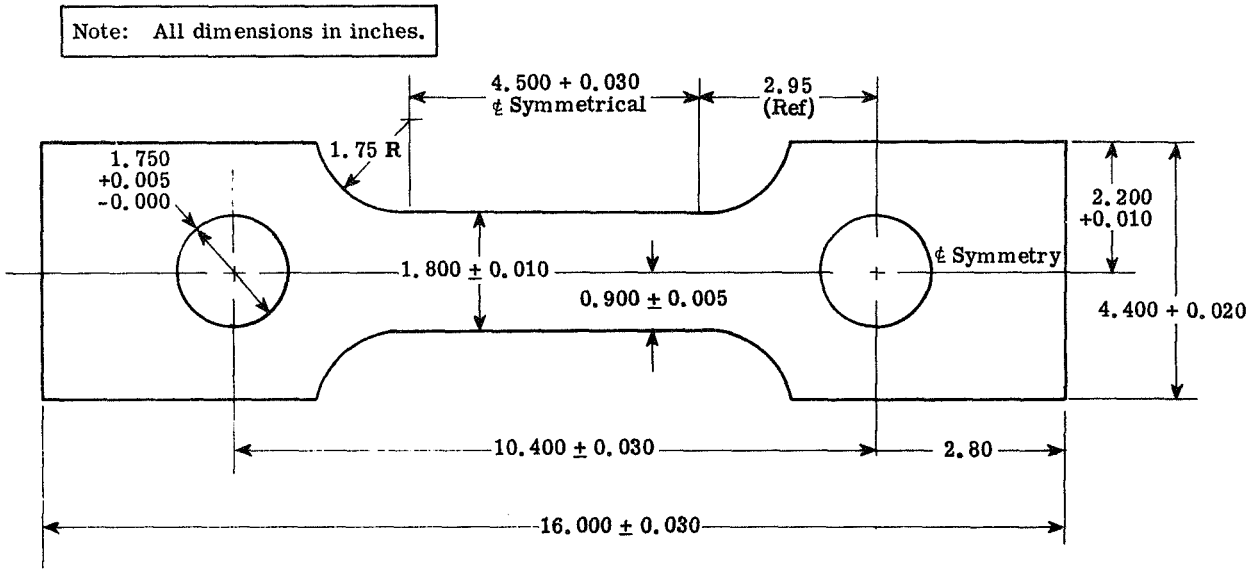

Fig. V-1 Specifications for Cryogenic Aluminum Tensile Specimen

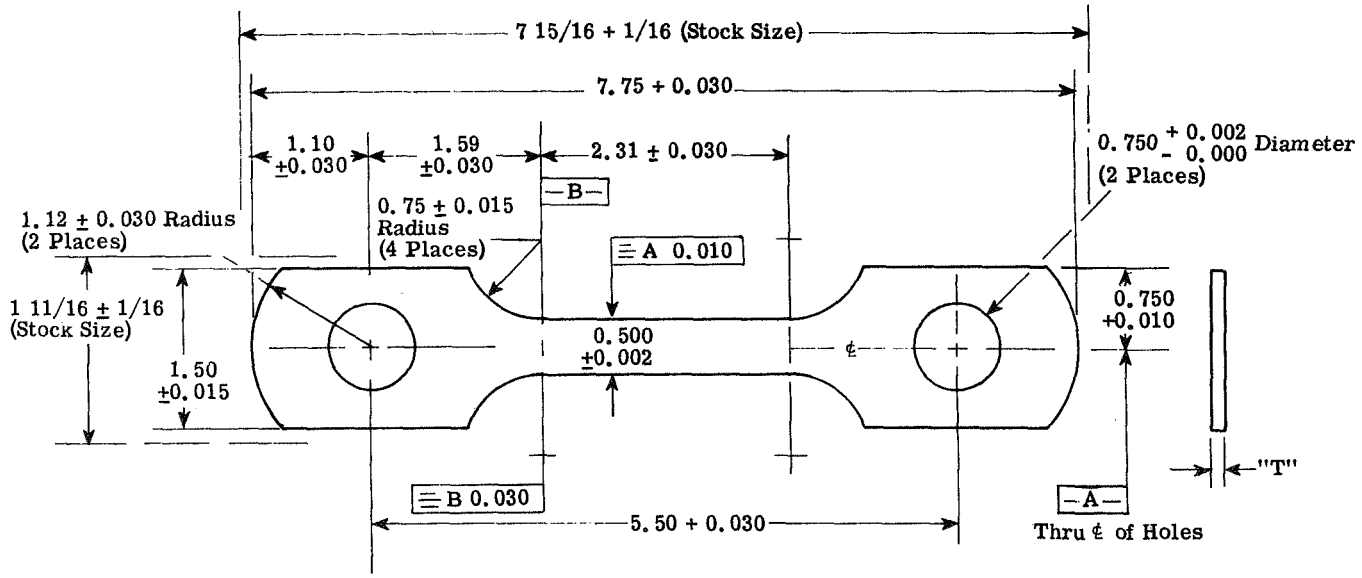

Fig. V-2 Specifications for Stainless Steel Tensile Specimen

effects in the bridge by bonding the strain gage to dummy boards made of the same type of material being evaluated. For cryogenic testing, the entire bridge is submerged in the liquid. Using this technique, no external resistors or balancing systems are required. 120-ohm constantan gages (Micromeasurements No. EA-13-500-BH-120L) were used for 70°F testing. For cryogenic testing, a special lot of 350-ohm nichrome gages (Micromeasurements EK-13-500-BH-350LE) was obtained.

Strain data was obtained using both a mechanical extensometer, for the entire stress vs strain curve to failure, and a bonded resistance strain gage for the elastic plus initial plastic range. Separate records of each strain measuring device were obtained. This system was utilized so that a maximum amount of data could be recorded simultaneously. This was achieved using dual Baldwin-Lima-Hamiltion (B-L-H) SRA-7 strain recorders mounted in tandem on the testing machine or by using a single SRA-7 recorder and an X-Y plotter (see Fig. V-3 and V-4).

Poisson's ratio was determined using bonded resistance strain gages mounted on test specimens in the longitudinal and transverse directions. The specimens were loaded below the elastic limit and the data were autographically recorded.

3. Testing Procedure

Tensile specimens were tested at -320°F using a liquid nitrogen bath in an open-mouthed, foam-insulated cryostat. The tests at -423°F were performed using liquid hydrogen in sealed, double-walled, vacuum-jacketed cryostats. The stainless steel specimens were tested in our 50,000-lb cryostat (see Fig. V-5), and the aluminum alloy specimens were tested in the 400,000-lb-capacity cryostat system shown in Fig. V-6.

B. STATIC FRACTURE TOUGHNESS TESTING

1. Specimen Design

The original plans called for all static fracture toughness tests to be performed using surface-flawed specimens. During the course of the experimental program, however, we found it necessary to also test aluminum 1T compact-tension specimens in order to provide baseline data for the cyclic and sustained-load tests.

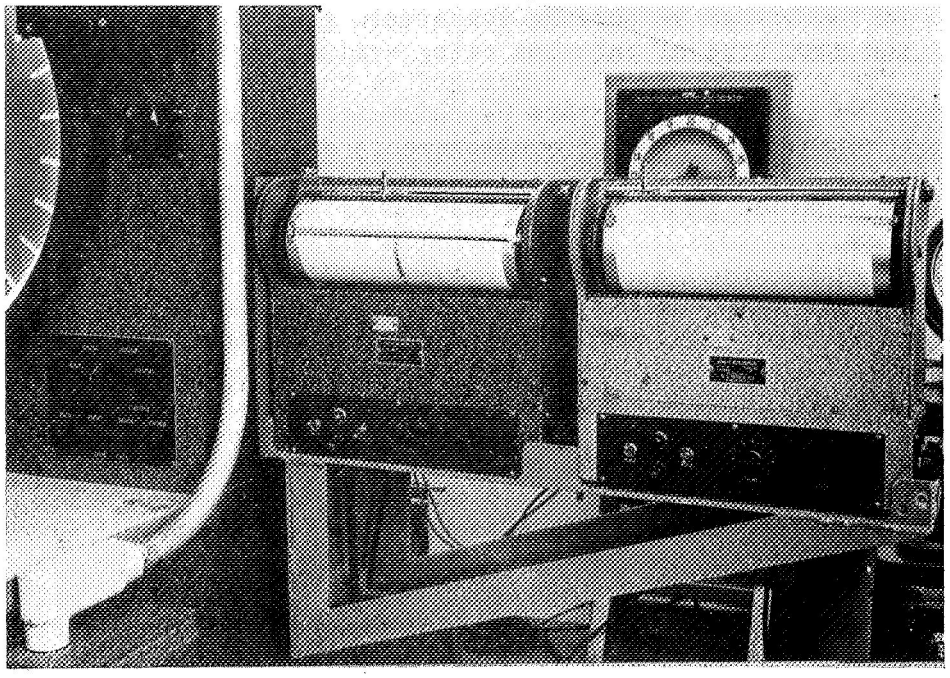

Fig. V-3 Dual SRA-7 Autographic Strain Recorders Mounted on Universal Testing Machine

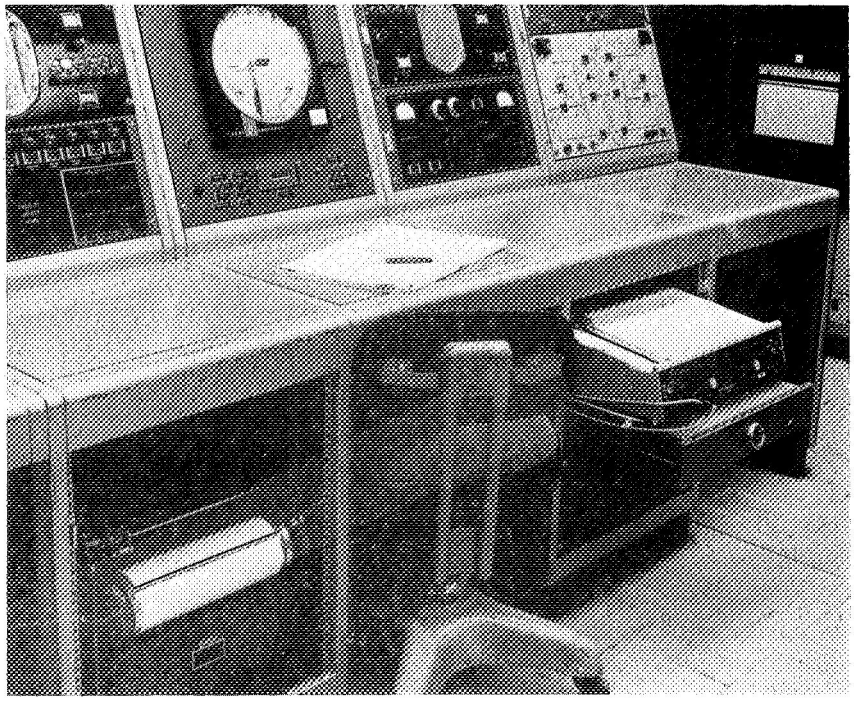

Fig. V-4 SRA-7 Recorder and X-Y Plotter Used with 400,000-lb Testing Machine

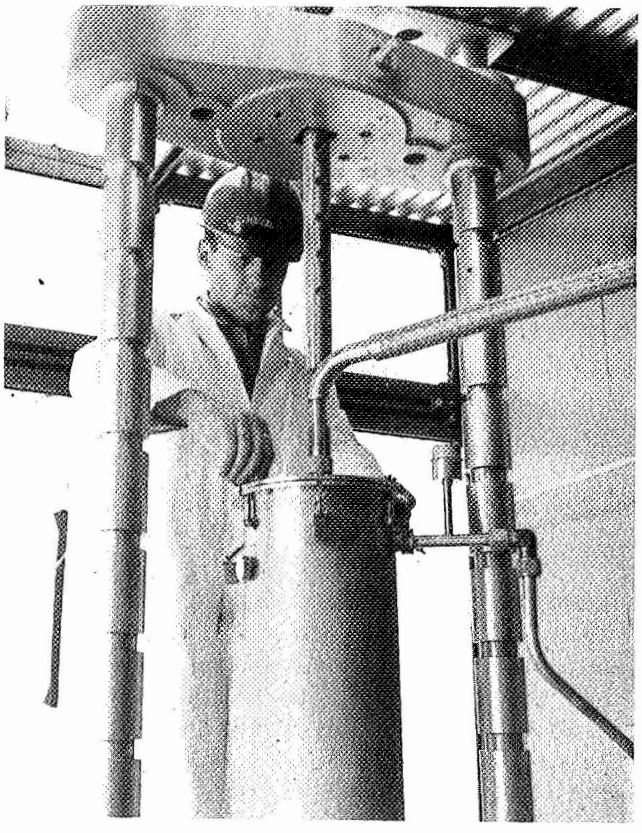

Fig. V-5 50,000-lb Liquid-Hydrogen Testing System

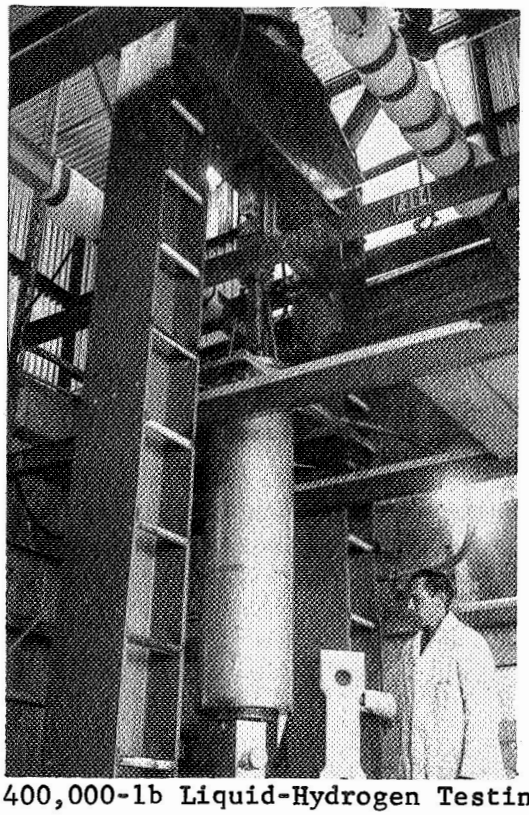

Fig. V-6 400,000-lb Liquid-Hydrogen Testing System

The specimens that were tested are depicted in the following figures:

Figure No.	Description
V-7	Aluminum surface-flawed specimen;
V-8	Aluminum compact-tension specimen;
V-9	Stainless-steel surface-flawed specimen.

2. Specimen Preparation

In all welded specimens, the weld bead was machined flush with the surface.

Surface flaws were introduced into the aluminum specimens by using a very thin slitting saw to machine precracks. The saw blades used in this machine are available in diameters from one in. up and range in thickness from 0.010 to 0.015 in. Next, the precracks were scored with a razor blade, and the specimens were fatigued in flexure to sharpen the cracks. Figure V-10 shows the apparatus used to produce these surface cracks. The maximum outer fiber stress was 30 ksi for the parent-metal specimens and 15 ksi for the welded-joint specimens. In a few cases, high $\frac{a}{2c}$ ratios were desired and electro-discharge machining was used.

Compact-tension specimen flaws were prepared by notching the specimens with a razor and then fatiguing them in axial tension to sharpen the cracks.

Flaws in stainless-steel specimens were introduced by grinding a shallow starter notch and then arc-burning this notch to create local embrittlement. The crack was extended by bending the specimens at a maximum outer fiber stress of 90 ksi.

3. Instrumentation

Normally, no instrumentation is used when testing surface-flawed specimens. However, because "pop-in" behavior was encountered during some of the parent-metal aluminum tests, small (1/32- to 1/4-in.) resistance strain gages were located near the ends of the crack in an attempt to detect the load at which "pop-in" occurred. This technique was successful when the "pop-in" zone was sufficiently large. In contrast, attempts to calculate critical stress intensities from the "pop-in" load and the direction of the initial fracture were unsuccessful.

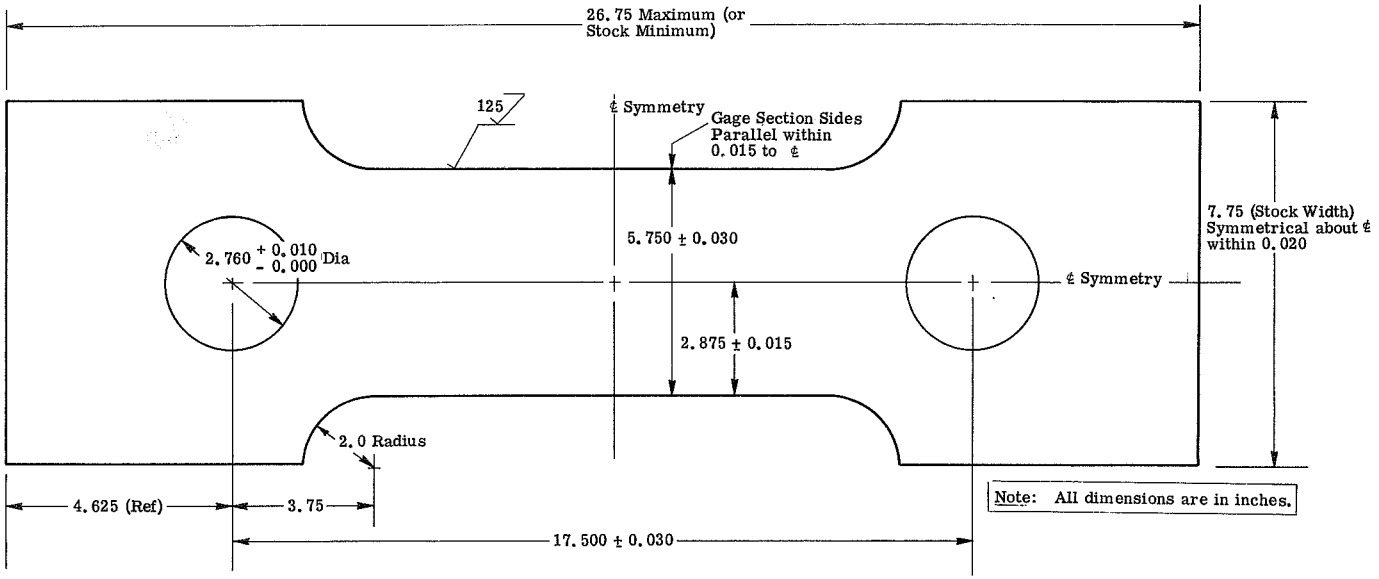

Fig. V-7 Specifications for Surface-Flawed Fracture Toughness Specimens (Aluminum Alloy)

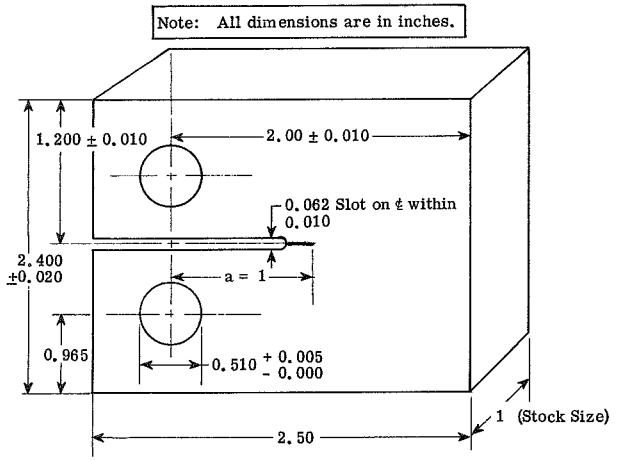

Fig. V-8 Specifications for Compact Tension Specimens

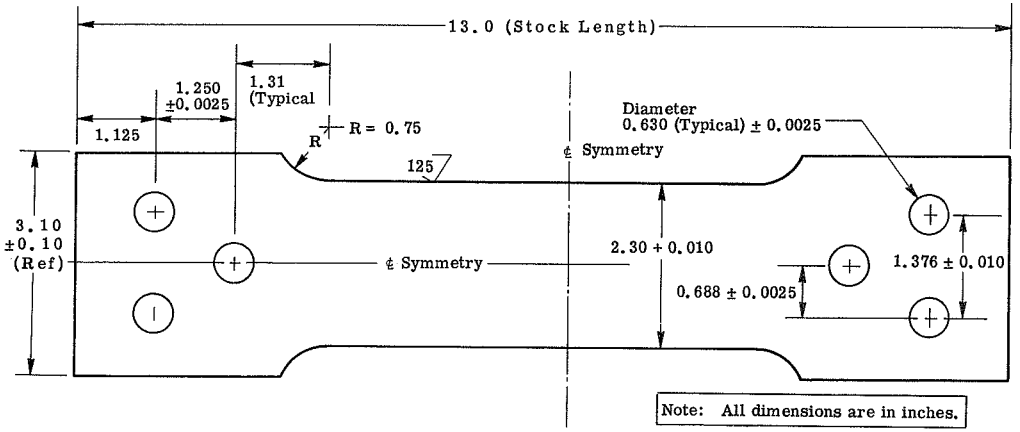

Fig. V-9 Specifications for Surface-Flawed Fracture Toughness Specimens (Type 301 Stainless Steel)

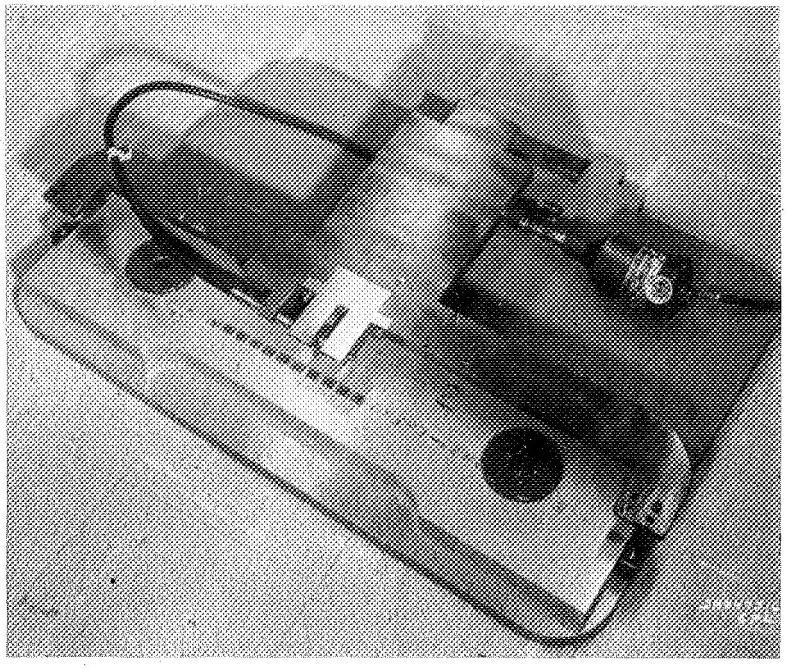

(a) Overall View

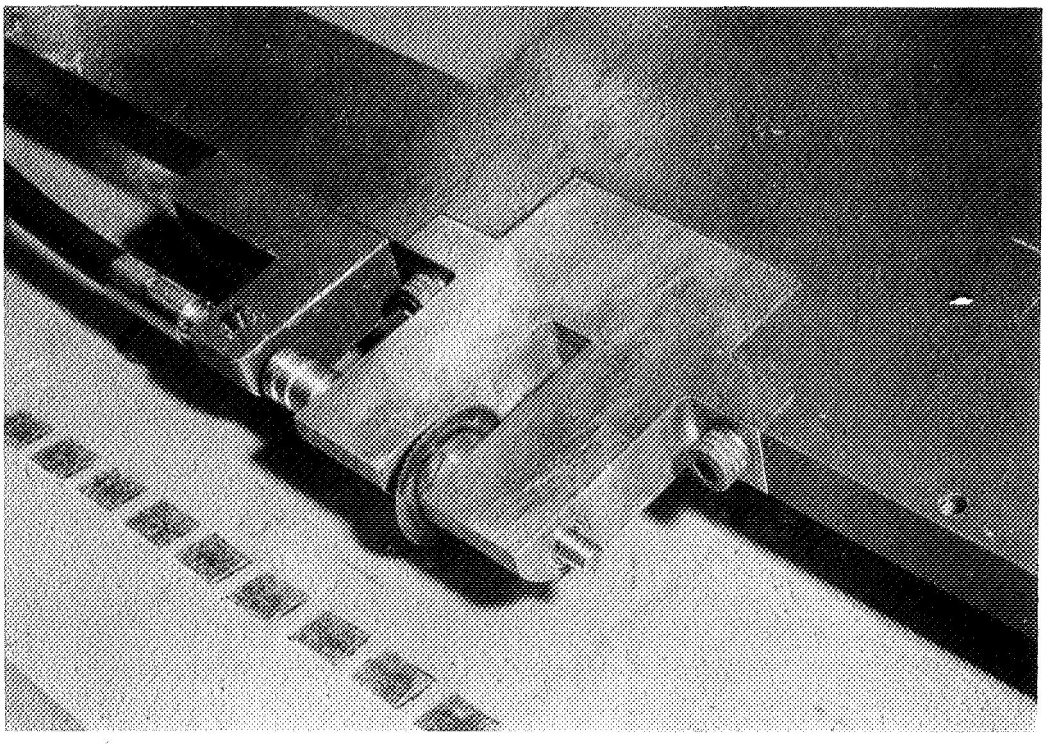

(b) Close-up View

Fig. V-10 Apparatus for Machining Precrack in Aluminum Fracture Toughness Specimens

In the latter portions of this work (Tasks IV and V) audible noises suggesting crack advancement were heard during testing of the surface flawed room temperature weld specimens. The strain gages placed adjacent to the edge of the crack were only successful in detecting large amounts of crack growth or small amounts when it occurs very close to the front face. The strain gages were not providing any indications of crack growth that explained the noise. Therefore, it was decided to use acoustic monitoring techniques in an attempt to ascertain what was happening.

The acoustic emission technique is a method of monitoring the noise produced by a solid material as a result of the relaxation of internal stresses due to 1) crack initiation or growth, or 2) localized plastic deformation. It is currently becoming a popular tool for fracture mechanics research because it can be used to detect small increments of crack extension that are undetectable by other means.

The technique developed to monitor internal flaw growth utilized an accelerometer which was adhesively bonded along the centerline of the surface flawed specimen, approximately two inches from the flaw. The accelerometer output was originally fed through a charge amplifier into a filter network, passing only signals above 10 kHz, then recorded along with load signal on magnetic tape. The acoustic output during test was also monitored with a dual-trace storage oscilloscope.

As specimen loading was increased, small increments of crack growth were usually detected well below the more obvious critical growth load levels. (This incremental crack growth was especially noticeable on the X7007 alloy tests, due to the out-of-plane cracking nature of the alloy.) Only the 2014 and 2021 weld centerline flaws failed to show incremental flaw growth before failure.

Monitoring growth through the storage oscilloscope proved to be sufficiently accurate for later tests, and the use of the band pass filter/tape recorder system was abandoned.

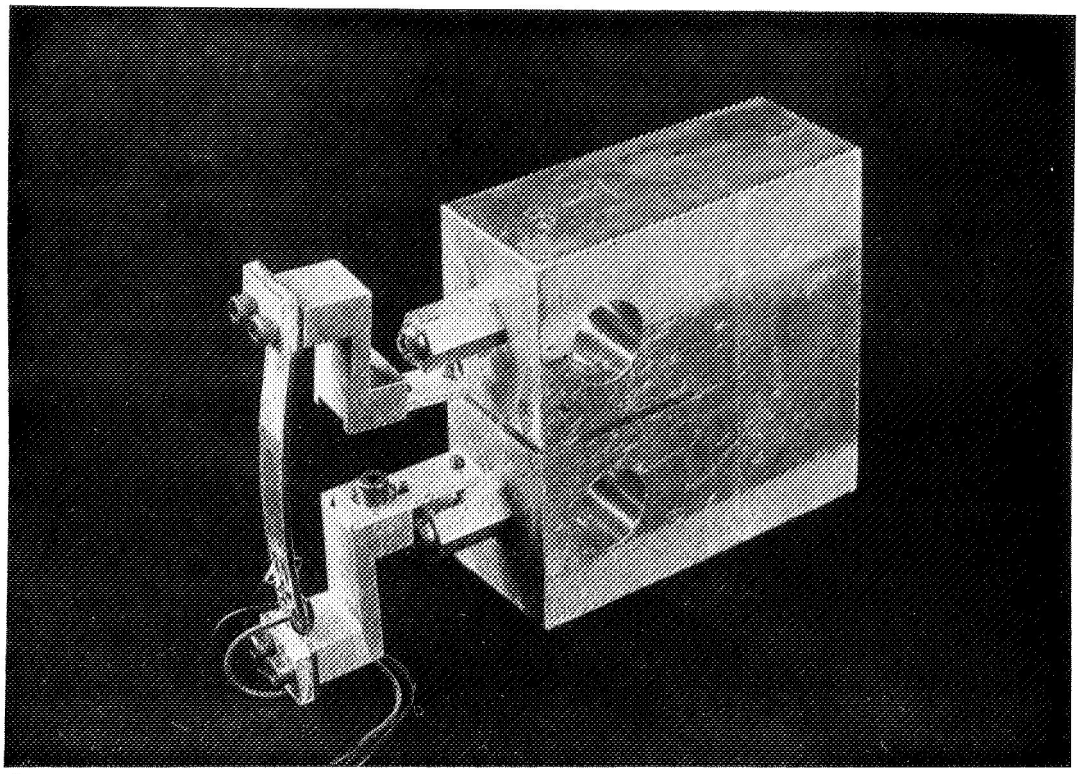

Fig. V-11 Compact-Tension Specimen with Strain Beam Extensometer

"Pop-in" in compact-tension specimens was measured with a simple beam extensometer that was clipped into standoffs attached to the edge of the specimen with self-tapping screws (see Fig. V-11). This technique is simpler, just as accurate, and less expensive than machining mounting slits across the defect.

4. Testing Procedure

Aluminum surface-flawed specimens were tested to failure or to a high percentage of the yield strength in our 500,000-lb-capacity testing machine. This testing was performed at a rate in excess of 40,000 psi per minute.

Compact-tension specimens were tested in a variety of conventional machines whose capacities ranged from 10,000 to 50,000 lb.

Stainless-steel surface-flawed specimens were tested at 70 and -320°F in a 150,000-lb-capacity system and were tested at -423°F in our 50,000-lb-capacity system.

C. CYCLIC-LOAD FLAW-ENLARGEMENT TESTS

Cyclic-load flaw-enlargement tests were performed on both surface-flawed and compact-tension specimens, using the same machines that had been used for the static fracture-toughness tests.

Parent metal tests were performed using only compact-tension specimens because of the unusual behavior noted during the static fracture-toughness tests. All cyclic-test specimens were identical to those used in the static tests (ref Fig. V-7 thru V-9) and were prepared according to the procedures described in the preceding section.

No instrumentation was used for cyclic testing. Instead, we attempted to obtain multiple data for each welded-aluminum, surface-flawed specimen. For example, we applied axial loads to each specimen to extend the crack, tried to mark the extent of the crack by flexurally fatiguing the specimen, and repeated this process several times. Although this technique worked reasonably well, in several cases it was virtually impossible to distinguish each cyclic growth band.

We attempted to produce a minimum amount of crack growth in the compact-tension specimens so that the initial and final stress intensities would be similar. In this way, the linear interpolation of the slope of the crack-growth-rate vs stress-intensity curve would be reasonably accurate. The stainless-steel specimens were cycled in a similar manner. No attempts were made to obtain multiple data from the compact-tension or stainless-steel, surface-flawed specimens.

D. SUSTAINED-LOAD FLAW-ENLARGEMENT TESTS

Sustained-load flaw-enlargement tests were performed to determine the stress intensity below which crack growth does not occur. Compact-tension specimens were used to determine the behavior of the parent metal and the welded aluminum alloys, and surface-flawed specimens were used to determine the behavior of the Type 301 stainless steel. No instrumentation was used for testing the stainless steel specimens. Many of the aluminum specimens were compliance-checked before and after being exposed to the sustained load to determine where significant growth had occurred. All specimens were fatigue-marked after being exposed to the load in order to clearly show the presence or absence of slow crack extension.

The aluminum specimens were tested in 20,000-lb (dead weight) creep frames. For the -423°F tests, a creep rack was moved to our liquid hydrogen laboratory and equipped with a large cryostat (see Fig. V-12). The cryostat had a high thermal efficiency and could be operated for periods of seven or eight hours before it had to be filled with liquid hydrogen. As a result, continuous testing was achieved without the need for constant monitoring.

Because the sustained load on the stainless-steel specimens had to be greater than 20,000 lb, these specimens were tested in tensile machines which incorporated a load-holding feature. The cryostat used to test these specimens at -423°F also had a high thermal efficiency, and required a minimum of refilling.

All the tests at -320°F were performed using cryostats which had automatic fill controllers to maintain the level of the liquid nitrogen.

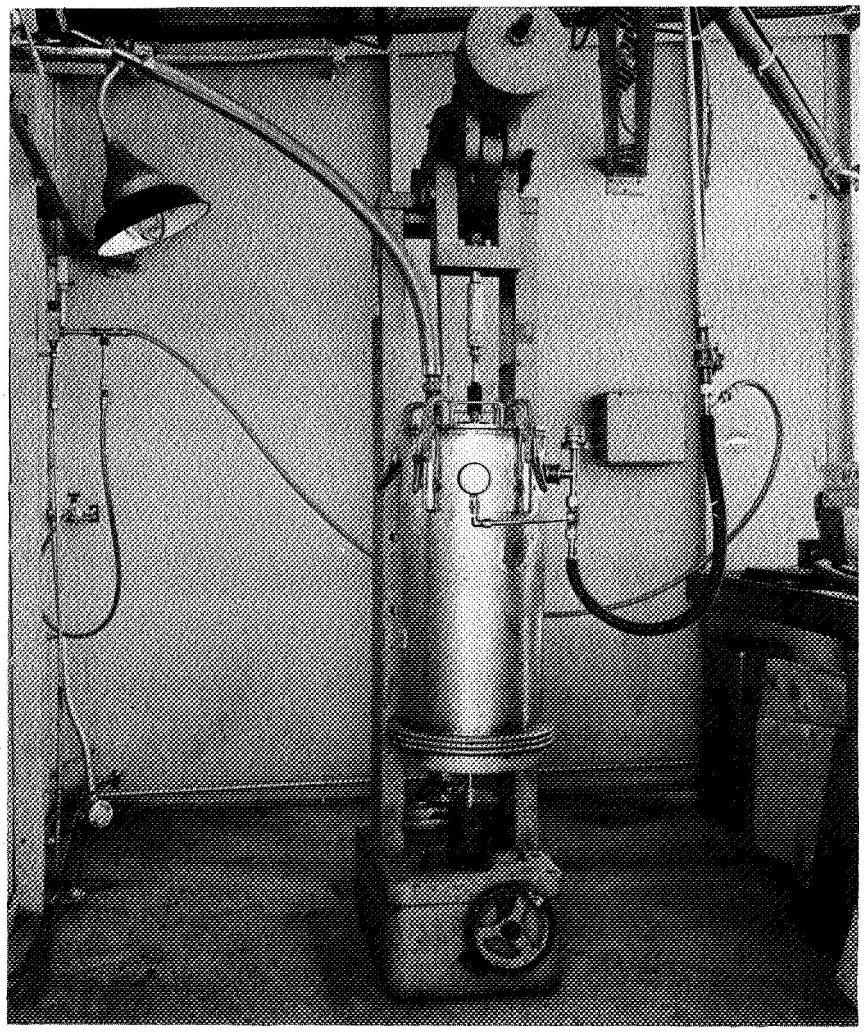

Fig. V-12 Creep Rack with Liquid-Hydrogen Cryostat

E. CORROSION TESTS

1. General Corrosion

Specimens for general corrosion testing of the aluminum alloys were obtained by sectioning the 1-in.-thick plate to obtain "bacon slices." In this manner the entire cross section of the material was subjected to the corrosive environment, rather than just the surfaces. This was particularly desirable for the welded joints since there can be such a great variability in the cross section of a weld joint.

Specimen blanks 1 in. wide x 8 in. long x 0.100-in. thick were exposed in the laboratory to a 30-day test in 20% salt fog according to the method outlined in ASTM specification B-117-64.

Similar specimens were sent to International Nickel Company's Francis L. LaQue Corrosion Laboratory at Kure Beach, N. Carolina and exposed for a 90-day period in a sea coast environment.

2. Stress Corrosion

Stress corrosion testing was achieved by use of self-stressing specimens similar to those described in NASA Technical Note TND-2011. Our specimens were fabricated from the same type of bacon-slices described above. Strips 1 in. wide x 11 in. long x 0.100 in. thick were bent to a predetermined angle at a distance of 1½ in. from each end. The bent ends of matched specimen pairs were spot welded together so that the entire central 8-in. portion was bowed and subjected to the required stress. The spot welded ends were coated with chem-mill masking in order to avoid bend-line attack or development of any possible preferential corrosion cells. Figure V-13 shows a typical stress corrosion specimen ready for test.

Specimens of each alloy and condition were stressed to various percentages of their yield strengths as determined from tensile testing. Depending upon the anticipated behavior, stress levels were 65, 80, and 90% or 65, 70, and 80% of yield strength.

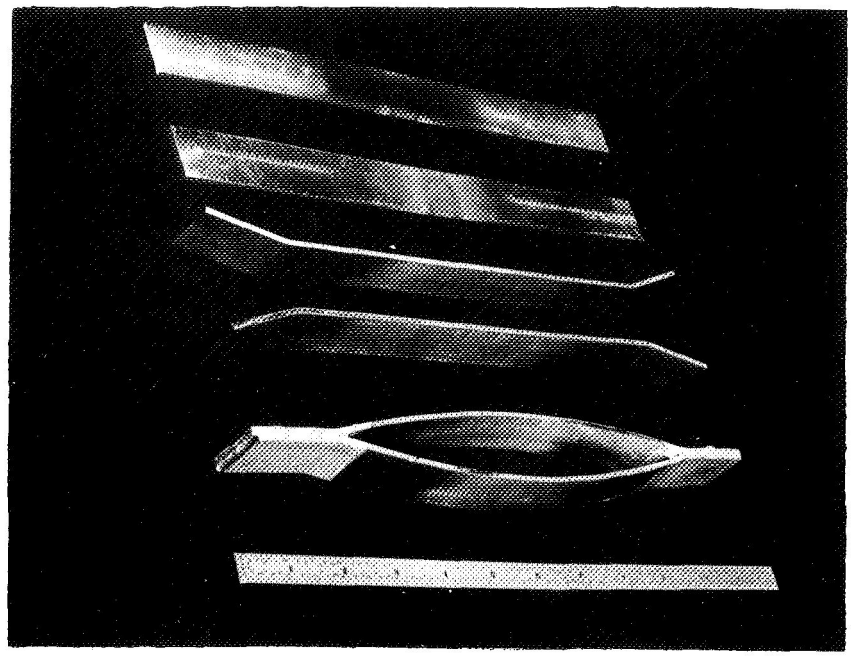

Fig. V-13 Construction Sequence of Typical Stress Corrosion Specimen

Half of the specimens were subjected to a laboratory exposure by alternate immersion for 30 days in a 3½% NaCℓ solution according to Federal Test Method 15113, Method 823. The remainder of the specimens were subjected to the sea coast environment at Kure Beach for 90 days. Figure V-14 shows the specimens in test at the Kure Beach facility.

Following test, all stress corrosion specimens were measured to determine the magnitude of stress relaxation that occurred during the exposure period.

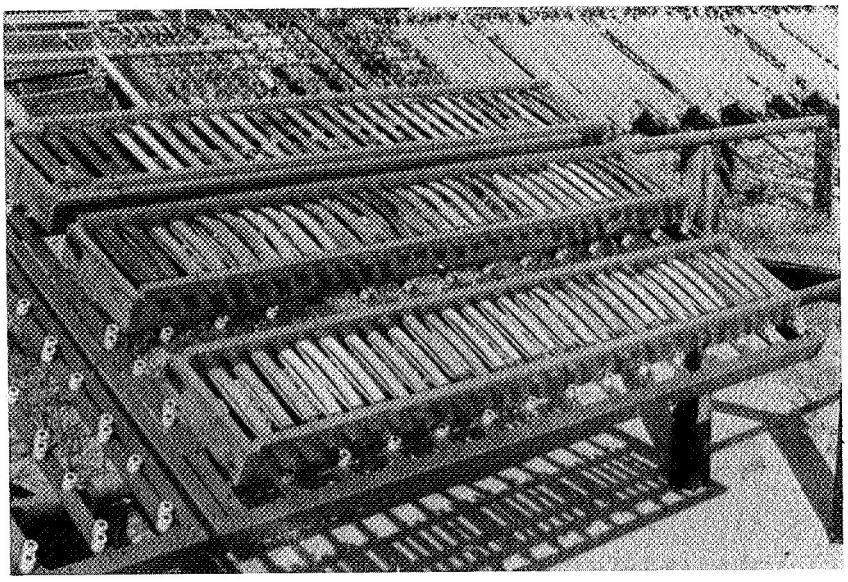

(a) Overall View

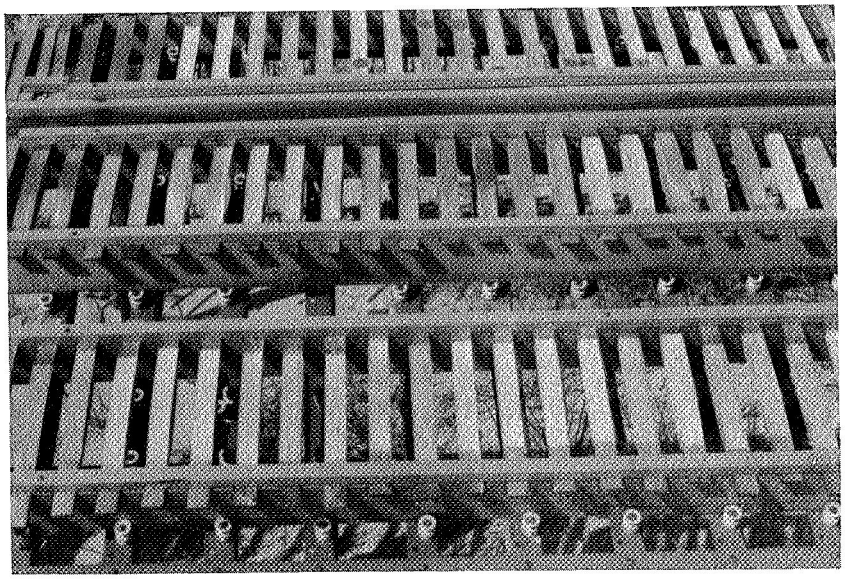

(b) Close-Up View

Fig. V-14 Testing Setup at Kure Beach

VI. EXPERIMENTAL DATA AND DISCUSSION OF RESULTS

This chapter summarizes test data in graphical and tabular form and discusses the test results. Data that have previously been presented in appendix form in the interim report (Ref 1) are not presented in this document.

A. MECHANICAL PROPERTY TESTS

Mechanical property data obtained in Tasks II, III, and IV are presented in this section.

1. Aluminum Alloys

a. Parent Metal Properties

Tensile properties of the 2021-T81 material from lot 105-267 are given in Table VI-1. Note the characteristic increase in strength that is typical of 2000-series aluminum alloys. (The ultimate strength is slightly more temperature dependent than the yield strength; and the elongation and the reduction in area increase with decreases in temperature.) The ultimate strength and yield strength exhibit little directionality, but the elongation and reduction in area do depend on the grain direction. In the transverse direction, the elongation and reduction in area are quite low. The tensile properties of the two lots of 2021-T81 show approximately the same strength levels (Table VI-1).

The tensile properties of Aℓ X7007-T6 from lot 105-266 are given in Table VI-2. At room temperature, the yield strength for Aℓ X7007-T6 is similar to that of Aℓ 2021-T81, but the elongation and reduction in area are significantly higher. The ultimate strength of Aℓ X7007-T6, however, is more temperature-dependent than that of Aℓ 2021-T81. The ultimate strength and yield strength of Aℓ X7007-T6 are somewhat lower in the transverse direction. As is typical for 7000-series alloys, the ductility decreases as the temperature drops.

Although ultimate strength, yield strength, elongation and reduction in area increase with lowering temperatures, the ultimate strength is slightly more temperature dependent than the yield strength.

Table VI-1 Summary of Parent Metal Property Data for 2021-T81 Aluminum Alloy

Temperature (°F)	Lot No.	Grain Direction	Ultimate Strength (ksi)	Yield Strength (ksi)	Elongation (%)	Reduction of Area (%)	Modulus of Elasticity (10^6 psi)	Poisson's Ratio	
								LT*	ST*
70	105-267	Longitudinal	71.4	62.7	8.0	10.5	10.6	0.30	0.33
-320			87.4	74.9	12.0	11.9	11.7	0.31	0.31
-423			99.5	79.8	12.0	18.8	11.8	0.39	0.42
70	105-267	Transverse	70.2	62.3	3.2	5.1	10.7	0.30	0.32
-320			87.7	73.6	6.3	7.7	11.8	0.31	0.31
-423			101.3	79.6	10.0	9.0	12.0	0.42	0.40
70	713-581	Longitudinal	69.8	64.9	11.0				

*LT = long transverse; ST = short transverse

Table VI-2 Summary of Parent Metal Property Data for X7007-T6 Aluminum Alloy

Temperature (°F)	Lot No.	Grain Direction	Ultimate Strength (ksi)	Yield Strength (ksi)	Elongation (%)	Reduction of Area (%)	Modulus of Elasticity (10^6 psi)	Poisson's Ratio	
								LT*	ST*
70	105-266	Longitudinal	73.3	69.0	13.8	36.0	10.3	0.30	0.32
-320			98.1	85.5	12.7	8.6	11.4	0.31	0.32
-423			114.0	91.7	13.0	--- †	11.4	0.39	0.41
70	105-266	Transverse	70.4	64.5	14.3	35.0	10.4	0.30	0.33
-320			92.0	80.0	11.7	15.2	11.6	0.31	0.31
-423			105.3	84.8	11.5	14.1	11.6	0.40	0.41
70	717-781	Longitudinal	77.4	73.4	13.5				

*LT = long transverse; ST = short transverse.

†No reduction of area could be measured because of excessive delamination.

The most significant observation made during the Aℓ X7007-T6 tension tests was that a different kind of fracture appeared at cryogenic temperatures. When the material was loaded in the longitudinal direction, it sheared for long distances in an interlaminar fashion, as shown vividly in Fig. VI-1.* (However, it should be emphasized that the fracture strain was quite high.) At room temperature, the material failed in a characteristic slant manner, but a tendency toward laminar fracture was noted (see Fig. VI-2). When the loads were applied in the transverse direction, indications of laminar fractures were found, but were much less pronounced.

Strength properties determined for the second lot of X7007-T6 (717-781) showed a significantly higher level of both yield and ultimate strengths, as reported in Table VI-2

The tendency toward interlaminar failures in the tensile test raised the question of whether the short transverse properties would be adversely affected. Miniature threaded and round bar specimens (0.156-in. gage diameter x 0.312-in. gage lengths) were machined from parent metal of each of the two alloys and tested at room temperature. No evidence of low strength or ductility deficiencies were noted. Results are given in the following tabulation.

Short Transverse Tensile Properties			
Alloy	Ultimate Strength (ksi)	Yield Strength (ksi)	Elongation (% in ¼ in.)
2021-T81	76.4	65.4	12
	78.1	65.6	8
	77.2 avg	65.5 avg	10 avg
X7007-T6	74.3	64.3	8
	74.1	63.9	8
	74.2 avg	64.1 avg	8 avg

Alloy 2014-T6 exhibited an ultimate strength level (73.1 ksi) slightly above typical, but not abnormal. The yield strength level (69.5 ksi) was surprisingly high for this composition. Ductility (10% elongation) was quite normal.

*From the available evidence, it appears that no delamination occurred before the materials fractured; rather, the interlaminar fracture was merely the mode of failure.

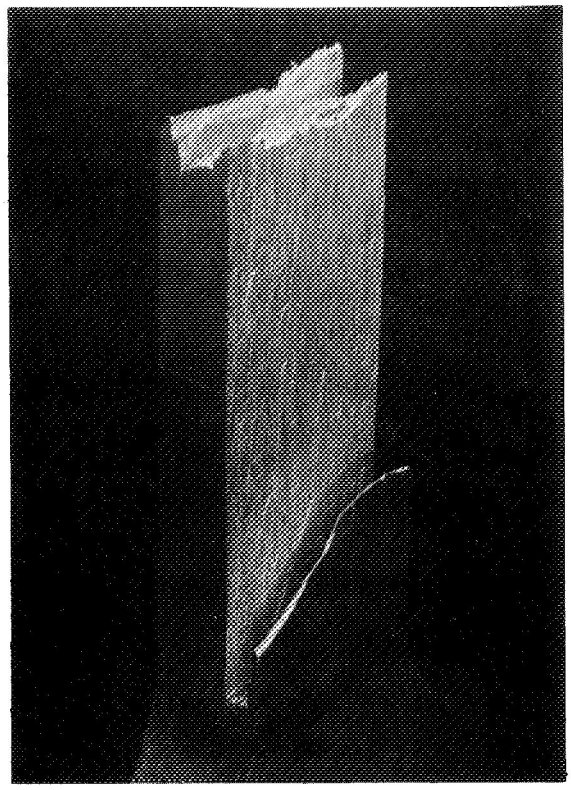

Fig. VI-1 Fractured Aℓ X7007-T6 Tension Specimen, Load Applied in Longitudinal Direction, Temperature = -320°F

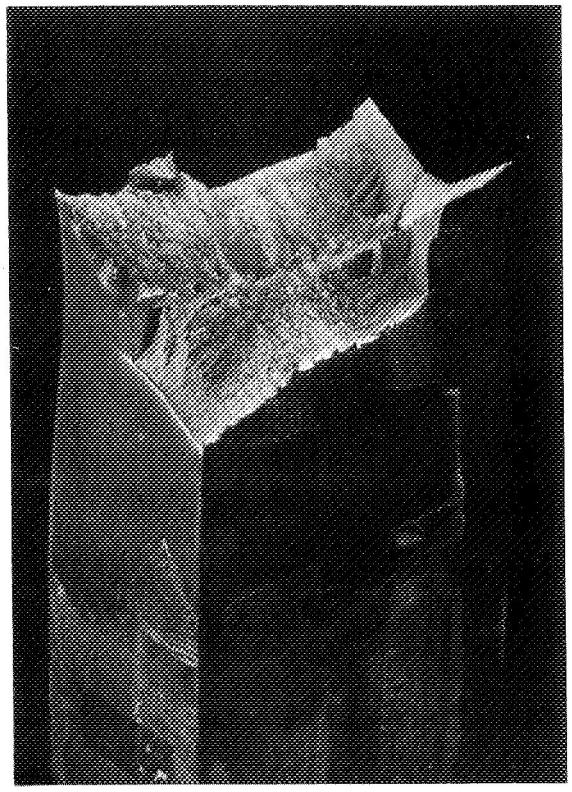

Fig. VI-2 Fractured Aℓ X7007-T6 Tension Specimen, Load Applied in Longitudinal Direction, Temperature = 70°F

Modulus of elasticity, Poisson's ratio, and stress vs strain data for 2021-T81 and X7007-T6 were presented in detail in the interim report. Summaries of the modulus and Poisson's ratio data are included in Tables VI-1 and VI-2, respectively. The reader is referred to the interim report (Ref 1) for additional information.

b. Weld Properties

The room temperature ultimate and yield strengths for the welded Aℓ 2021-T81 specimens (summarized in Table VI-3) were typical of those for 2000-series alloys. The yield strength (measured directly on the weld centerline or heat affected zone) was rather low, and the ductility (measured over a 1-in. gage length for a limited number of specimens) was quite high.

The as-welded strength properties for the two lots of material were quite similar. As expected, the heat-affected zone exhibited slightly higher yield strength than the weld centerline. Postweld aging (325°F/16 hr) increased the weld strength approximately 10%.

The overheated weld, although not showing metallographic evidence of overheating, did exhibit a slight reduction in strength below that of the normal as-welded condition. Postweld aging resulted in up to 10% strength increase.

Table VI-3 Summary of Room Temperature Weld Behavior

Condition	Lot No.	Ultimate Strength (ksi)	Yield Strength (ksi)	
			Weld Centerline	Heat Affected Zone
2021-T81				
AW	105-267	42.3	19.2	
	713-581	40.0	19.4	22.0
WA	713-581	44.3	23.4	25.0
OW	713-581	38.4	18.3	18.5
OWA	713-581	42.8	24.7	28.4
X7007-T6				
AW	105-266	50.7	36.5	
	717-781	54.0	39.9	40.4
OW	717-781	48.6	37.2	38.7
2014-T6				
AW	--	44.6	24.7	28.3
OW	--	40.9	21.0	27.4

Legend:

PM	Parent metal	WA	Welded plus aged
AW	As-welded	OW	Overheated weld
		OWA	Overheated weld plus aged

The effect of temperature on the properties of as-welded 2021-T81 is included in Table VI-4. Behavior is typical for a 2000-series alloy.

Room temperature data for welded X7007-T6 show excellent ultimate strength properties (over 50 ksi) and a remarkably high yield strength level (35 to 40 ksi). The overheated weld exhibited an obvious decrease in ultimate strength but only a modest decrease in yield strength. These data are summarized in Table VI-3.

Table VI-4 Summary of Data on Effect of Temperature on Weld Properties*

Temperature (°F)	Ultimate Strength (ksi)	Yield Strength (ksi)	Elongation (%)
2021-T81 (Lot 105-267)			
70	42.3	19.2	5.8
-320	57.4	23.8	7.6
-423	68.1	28.8	9.7
X7007-T6 (Lot 105-266)			
70	50.7	36.5	6.3
-320	68.6	42.2	10.7
-423	69.1	47.3	6.7
*As-welded condition.			

The effect of temperature on the tensile properties of the as-welded X7007-T6 is given in Table VI-4. Excellent strengthening is noted between 70°F and -320°F; but no additional strengthening occurred with further decrease in temperature. Ductility was satisfactory, but showed a decrease with decreasing temperature between -320 and -423°F.

Weld strength properties for 2014-T6 were typical for 1-in. plate. Overheating resulted in a 10% weld strength decrease. Table VI-3 summarizes these data.

The locations at which the fractures occurred and the appearances of the welded tension specimens after failure were quite interesting. The Aℓ X7007-T6 specimen that failed at 70°F exhibited necking in the heat-affected zone, approximately ½ in. from the centerline of the weld and, to a lesser degree, in the center of the weld bead; at -320°F failures occurred at the centerline of the weld, and although necking occurred in the heat-affected

zone, it was less pronounced than at 70°F. The Aℓ 2021-T81 exhibited a fracture at 70°F that completely followed the fusion line (see Fig. VI-3). At -320°F, however, the failure occurred through the center of the weld bead.

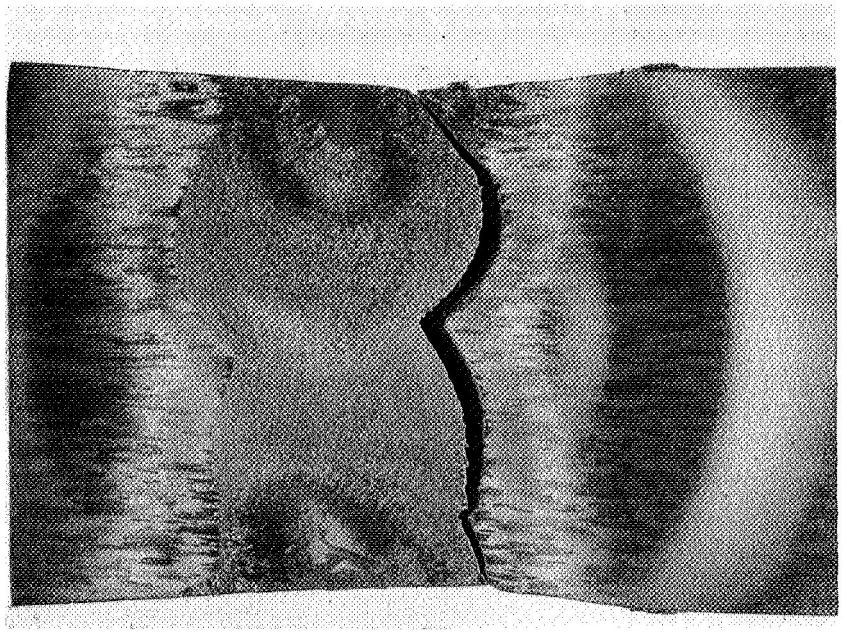

Fig. VI-3 Macrosection through the Center of a 1-Inch Thick Aℓ 2021-T81 Welded Tension Specimen

2. Cryogenically-Stretched Type 301 Stainless Steel

The tensile properties of unnotched, parent-metal, cryogenically-stretched Type 301 stainless steel are given in Table VI-5. As the temperature decreases from 70 to -423°F, the ultimate strength and the yield strength increase more than 100 ksi. The ductility increases as the temperature goes from 70 to -320°F, but then decreases as the temperature drops below -320°F. The elongation at -423°F (3.5%) is quite satisfactory, considering that the ultimate strength is over 350 ksi.

Welded, cryogenically-stretched specimens exhibited excellent strength properties, and the efficiency of the welded joint averaged approximately 95%. The ductility was similar to that observed for the parent metal.

Table VI-5 Tensile Properties of Cryogenically Stretched Type 301 Stainless Steel*

Temperature (°F)	Grain Direction	Ultimate Strength (ksi)	Yield Strength, 0.2% Offset (ksi)	Elongation (%)	Reduction in Area (%)	Modulus of Elasticity (x 10^6 psi)	Poisson's Ratio, μ
Parent Metal Specimens							
70	Longitudinal	244.5	239.1	7.8	34.8	27.2	0.32
-320	Longitudinal	310.1	306.4	12.3	41.1	29.6	0.28
-423	Longitudinal	355.8	350.7	3.5	30.0	29.6	0.37
70	Transverse	241.1	229.0	7.1	28.1	27.6	0.31
-320	Transverse	315.3	301.2	11.6	31.1	29.6	0.30
-423	Transverse	353.2	337.7	3.3	11.0	29.7	0.32
Welded Specimens							
70	Longitudinal	227.8	207.7	5.3	27.7		
-320	Longitudinal	301.2	292.8	9.2	33.1		
-423	Longitudinal	339.6	336.3	3.8	17.3		

*Nominal thickness = 0.135 in.

B. STATIC FRACTURE-TOUGHNESS TESTS

Appendix Guide - Static Fracture Toughness Tests		
Alloy	Description of Table	Appendix Table No.
Aℓ 2021-T81	Surface-Flawed Welded Specimens	A-1
Aℓ X7007-T6	Surface-Flawed Welded Specimens	A-2
Aℓ 2014-T6	Surface-Flawed Welded Specimens	A-3
Aℓ 2021-T81	Compact-Tension Welded Specimens	A-4
Aℓ X7007-T6	Compact-Tension Welded Specimens	A-5

1. Aluminum Alloys

a. Parent-Metal Tests*

Surface-cracked specimens of Aℓ 2021-T81 were tested for fracture toughness in the transverse orientation. At 70°F, their fracture strength was approximately 50% of the yield strength and their plane-strain fracture toughness averaged 33 ksi $\sqrt{\text{in}}$. (with nominal a/Q values of 0.25-0.30). We noted that the fatigued precrack did not have the smooth appearance that is typical of aluminum alloys; instead, it appeared very coarse; and the rapid-fracture area, although relatively flat, had laminar cracks in the region ahead of the semininor axis, but not in the regions away from this area. In tests at -320°F, cracks of a size equivalent to those tested at 70°F caused failure at stresses approaching 80% of the yield stress. The average plane-strain fracture toughness was 54 ksi $\sqrt{\text{in}}$. At -423°F, the fracture faces appeared much smoother than those observed in the 70°F tests, there was virtually no evidence of laminar cracking, and the plane-strain fracture toughness increased to 59 ksi $\sqrt{\text{in}}$.

The toughness of transverse compact-tension specimens increased as the temperature decreased. The toughness values for these specimens did not agree with those for the surface-flawed specimens, but this is not surprising since the cracks grow in

*Parent metal tests of 2021-T81 and X7007-T6 were conducted on Lots 105-267 and 105-266, respectively. These data were obtained as part of the Task II effort (Ref 1).

different directions. In edge-notched, compact-tension specimens, cracks grow into the width direction, but in surface-cracked specimens they grow into the thickness direction. Plane-strain fracture toughness levels for the two types of specimens are compared below.

Temperature (°F)	Critical Stress Intensity (ksi $\sqrt{in.}$)	
	Surface-Cracked Specimens	Compact-Tension Specimens
70	34	26
-320	54	36
-423	59	40

Test data for parent metal Aℓ 2021-T81 are included in Fig. VI-4. Note that in the longitudinal direction, surface-cracked specimens could not be fractured at stresses below the yield strength. After opening the first few specimens, we noted that a small area of "pop-in" existed near the front face, so we placed small (1/32 to 1/4 in.) resistance strain gages at the ends of the crack in an attempt to determine the "pop-in" load. The data we obtained were generally inconclusive, because the "pop-in" area was very small.

The fracture-toughness tests on the surface-cracked, parent-metal Aℓ X7007-T6 specimens produced some equally surprising results. In the longitudinal direction, the "pop-in" behavior was similar to that noted in the Aℓ 2021-T81 specimens, but was of much greater magnitude.

Delamination around the crack front prevented the Aℓ X7007-T6 specimens from fracturing below their yield strength. Figure VI-5 shows a typical specimen that was opened after being loaded to a high percentage of its yield strength at -320°F. From the appearance of this specimen we concluded that it failed when delamination occurred at the high-stress-intensity area at the front of the crack. Note that where this delamination occurred, the crack front is generally oriented in the width direction.

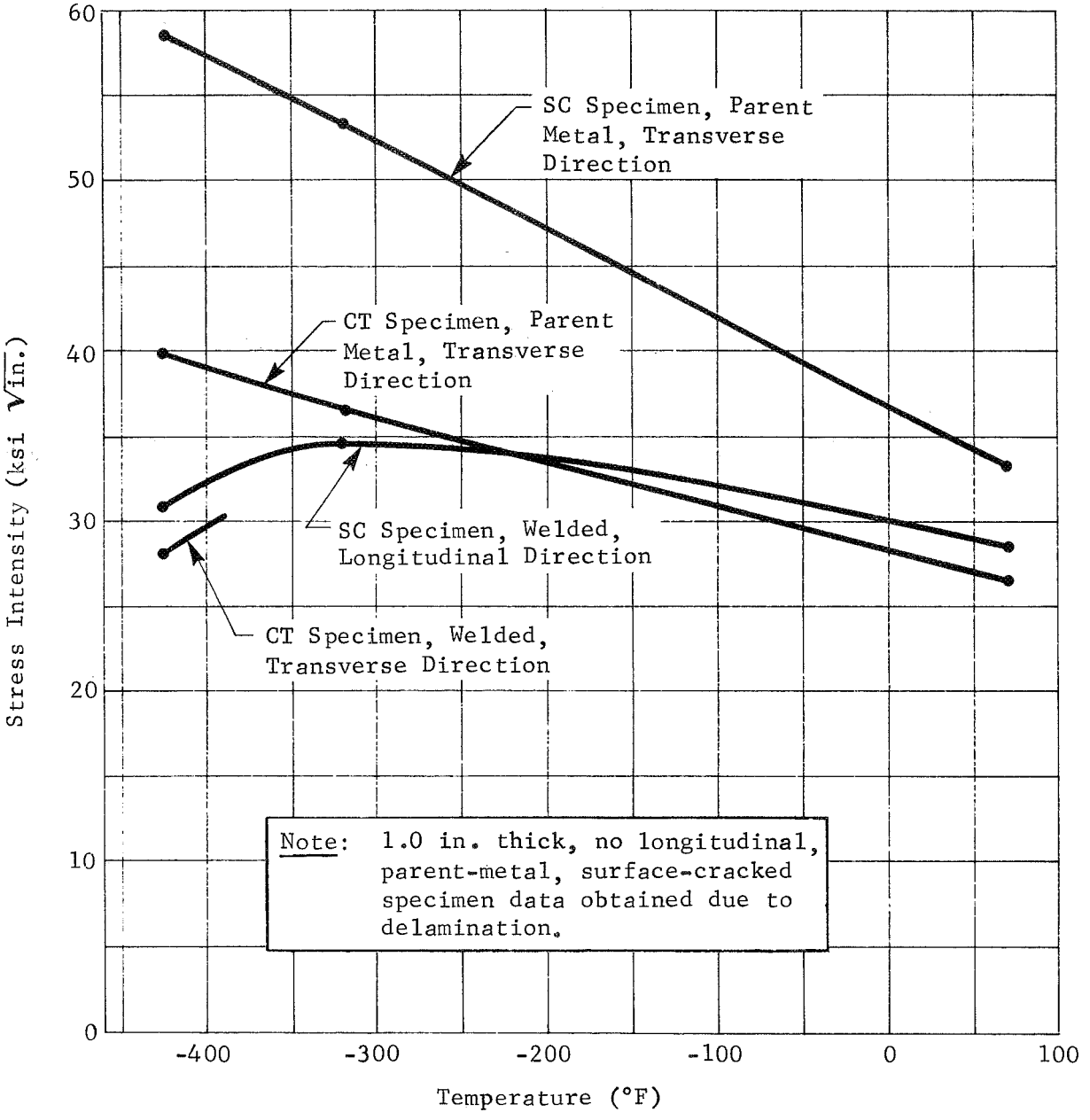

Fig. VI-4 Static Fracture Toughness of 2021-T81 Aluminum Alloy

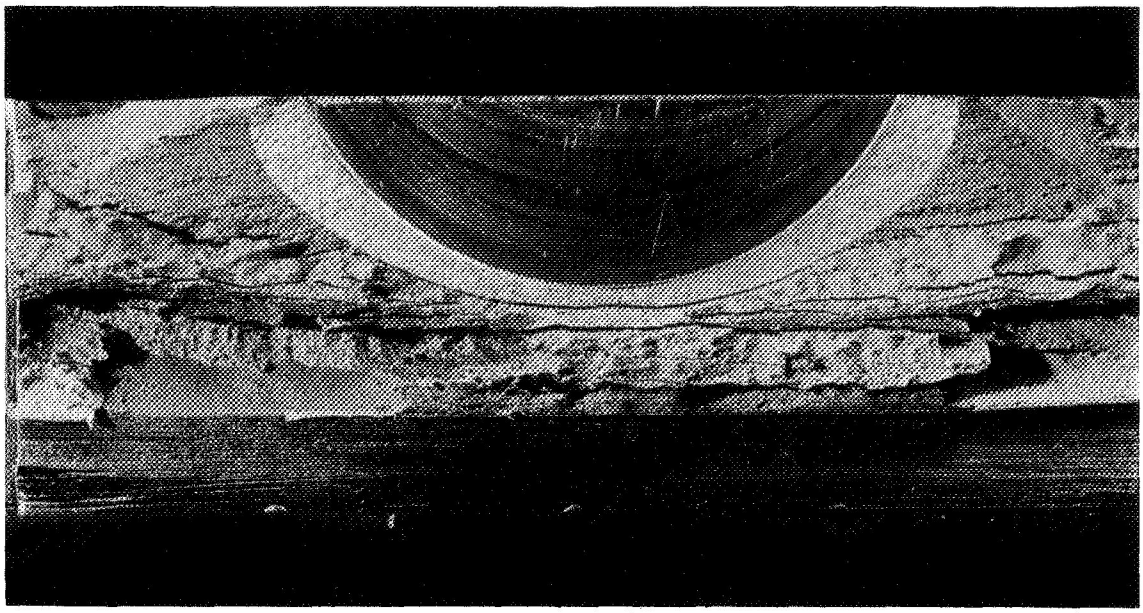

Fig. VI-5 Fracture Face of Aℓ X7007-T6 Surface-Flawed Specimen, Load Applied in the Longitudinal Direction, Temperature = -320°F

It appears that, when the specimen is loaded to a level that should be the critical stress intensity at the nose of the crack (the end of the semiminor axis), fracturing cannot occur because the crack front becomes blunted; and because the stress intensity decreases from a maximum at the nose of the crack to a minimum at the free face, fracturing cannot occur elsewhere along the crack front. Then, as the applied load is increased, the stress intensity increases until it reaches a critical value at some point on the crack front that is not blunted, and the fracture begins. However, as the crack begins to spread, laminar cracking occurs in the width direction and arrests the growth of the crack, and a region of higher fracture toughness near the surface prevents the crack from extending. When this occurs, a small fracture region appears near the face of the crack.

This type of "pop-in" behavior has been confirmed by staining the test specimens before opening them and by strain gage data (see Fig. VI-6) obtained during the tests. Figure VI-6 shows that there is local yielding at the end of the crack, although the nominal strain away from the crack is still elastic. At the "pop-in" load, the slope of the curve decreases abruptly.

Our attempts to calculate the critical stress intensities from the "pop-in" load and the direction in which the fractures began did not produce satisfactory data.

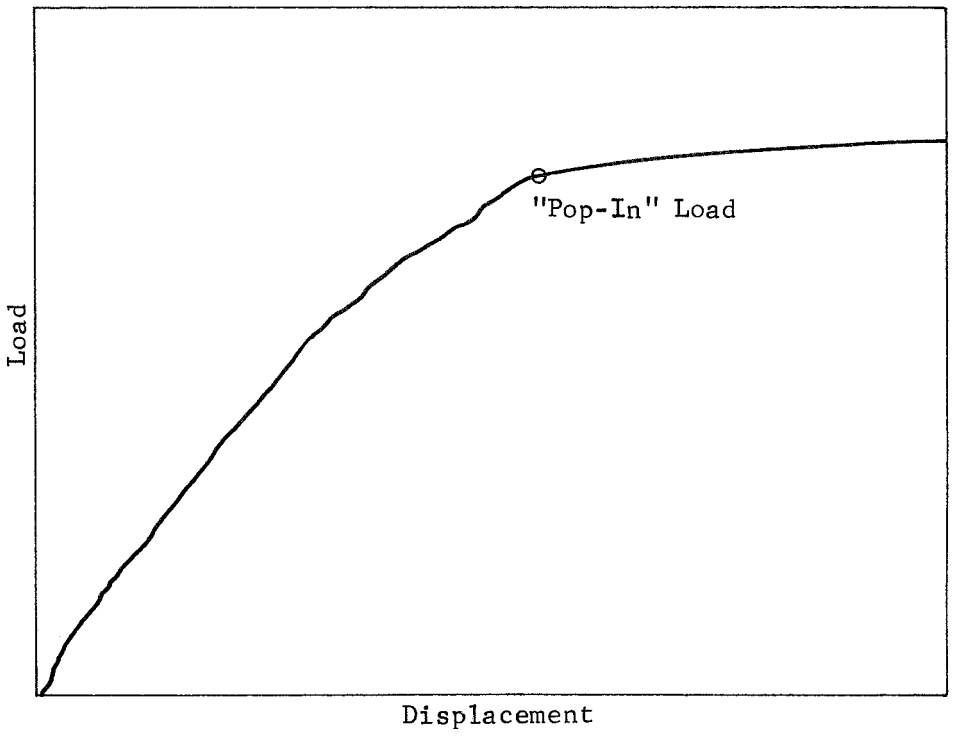

Fig. VI-6 Load vs Displacement for the Aℓ X7007-T6 Specimen Shown in Fig. VI-5

Toughness tests conducted at -423°F produced complete fractures that were not arrested. An examination of the fracture face (see Fig. VI-7) revealed the same type of crack blunting at the end of the semiminor axis and indicated that the fractures began near the front face. However, unlike the fractures produced at 70 and -320°F, the cracks proceeded for a significant distance on each side of the defect. The resulting fractures apparently progressed via shearing in the thickness direction.

In the transverse direction, the Aℓ X7007-T6 surface-cracked parent metal specimens fractured at stresses below the yield strength. In these cases, the fractures did not appear to begin at the nose of the precrack. Examinations disclosed that these fractures also began near the surface, like those that occurred in longitudinally-loaded specimens of the parent metal (see Fig. VI-8). In these cases, however, the laminar cracking was not extensive enough to arrest the growth of the crack. Although complete fractures occurred, toughness data calculated for this series of tests are not reliable, and have not been included in this report.

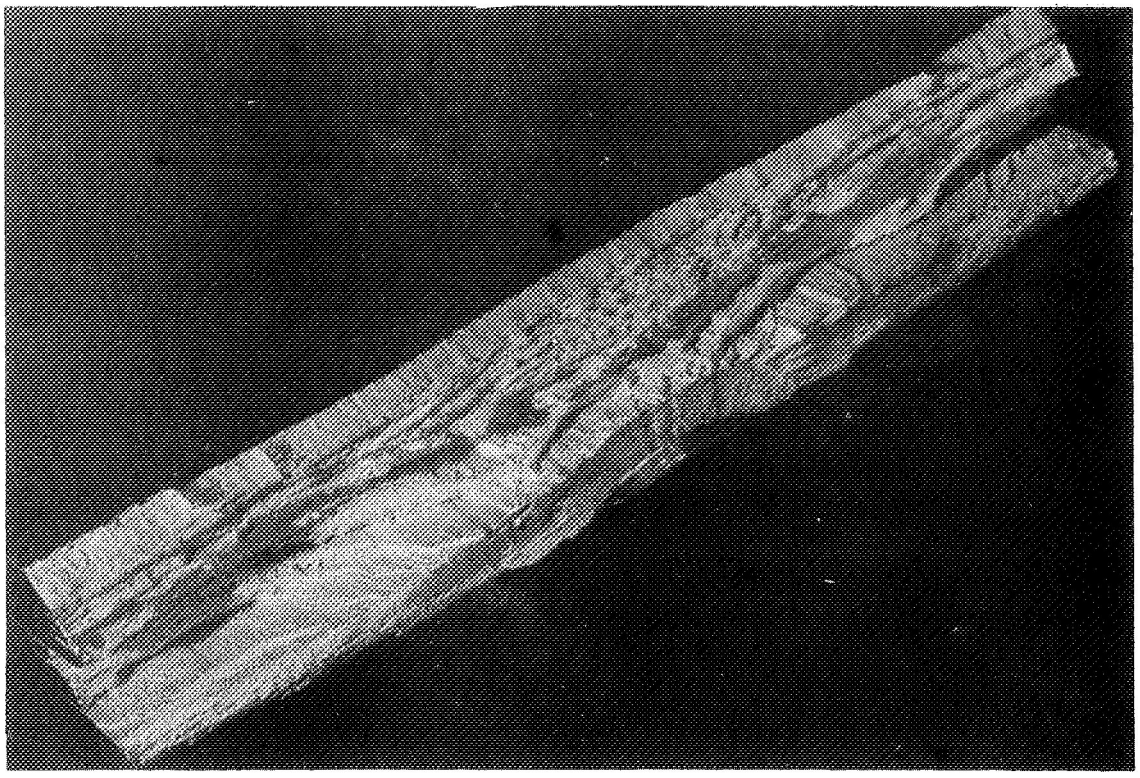

Fig. VI-7 Fracture Face of an Aℓ X7007-T6 Surface-Flawed Specimen, Load Applied in the Longitudinal Direction, Temperature = -423°F

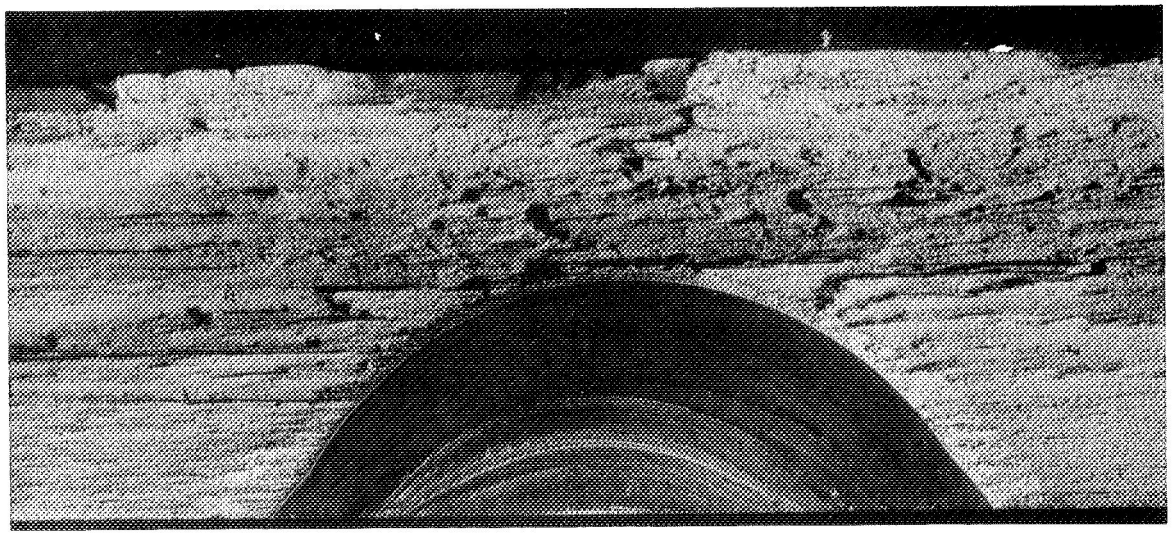

Fig. VI-8 Fracture Face of an Aℓ X7007-T6 Surface-Flawed Specimen, Load Applied in the Transverse Direction, Temperature = 70°F

Fracture-toughness values were calculated for compact-tension specimens that had been tested in the transverse direction. These values are shown below.

Temperature (°F)	Critical Stress Intensity (ksi $\sqrt{in.}$)
70	32
-320	23
-423	28

In these cases, the direction in which the cracks extended was normal to the direction of the laminations, and blunting did not appear to occur. Figure VI-9 shows the fracture face of a typical compact-tension specimen.

Fracture-toughness test data for parent-metal specimens of Aℓ X7007-T6 are included in Fig. VI-10.

b. Welded-Metal Tests/Effect of Temperature*

Fracture-toughness tests (in the longitudinal direction only) were performed on welded surface-cracked and compact-tension specimens of X7007-T6 and 2021-T81 at 70, -320, and -423°F to characterize the effect of temperature on toughness.

As shown below, the toughness of the Aℓ 2021-T81 surface-flawed specimens is higher at cryogenic temperatures than at room temperature. The one-in. thickness of the welded plates proved inadequate for obtaining fracture data for the through-cracked compact tension specimen, except at -423°F.

	Critical Stress Intensity (ksi $\sqrt{in.}$)	
Temperature (°F)	Surface-Cracked Specimens	Compact-Tension Specimens
70	29	
-320	35	
-423	31	28

The date for -423°F show relatively good agreement. (Although this type of comparison could not be made for wrought material, the directionality effects in a cast structure are limited enough so that the data for the two types of specimens can be compared.)

*These tests were conducted as part of Task III.

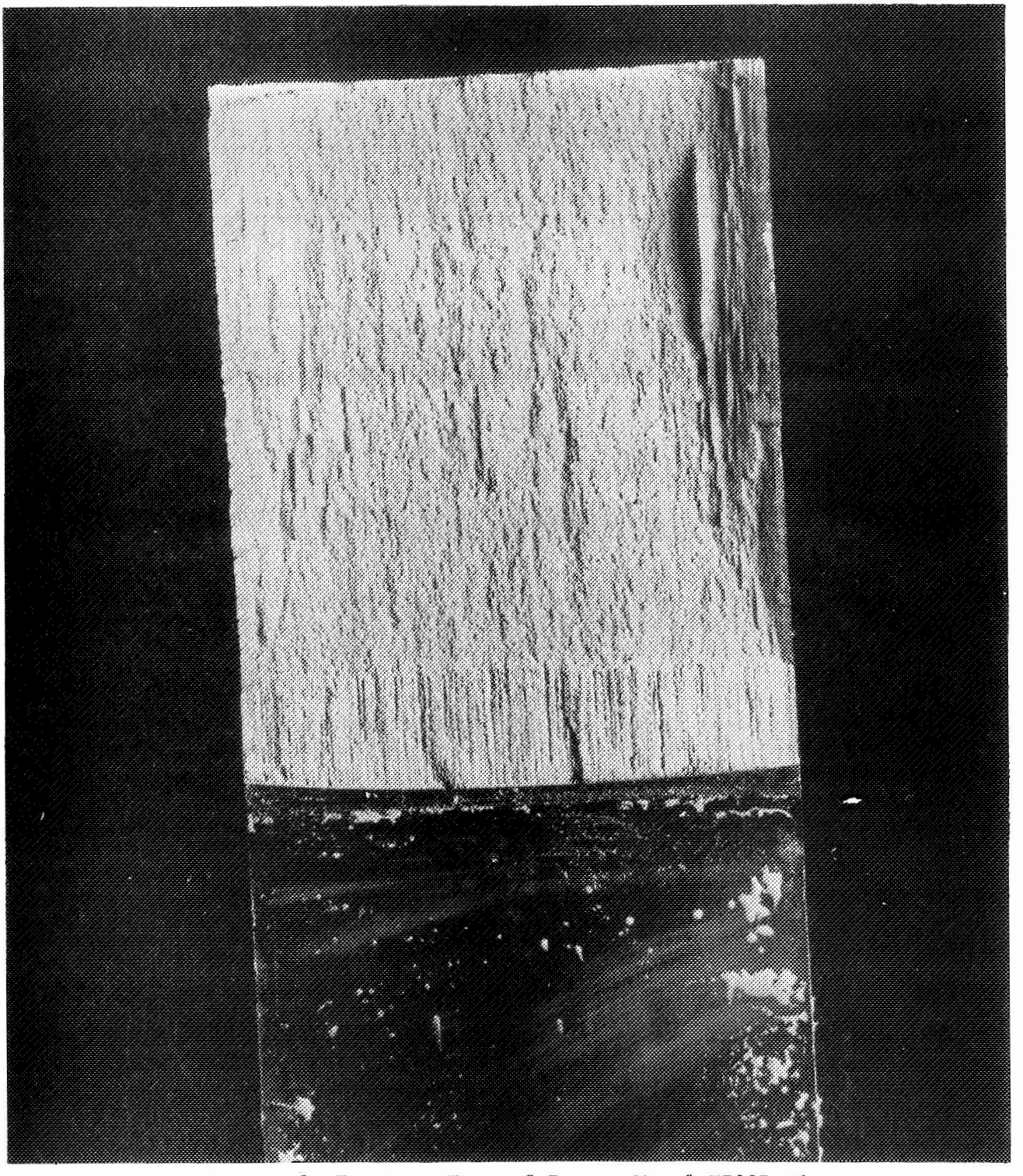

Fig. VI-9 Fracture Face of Parent-Metal X7007-T6 Compact-Tension Specimen

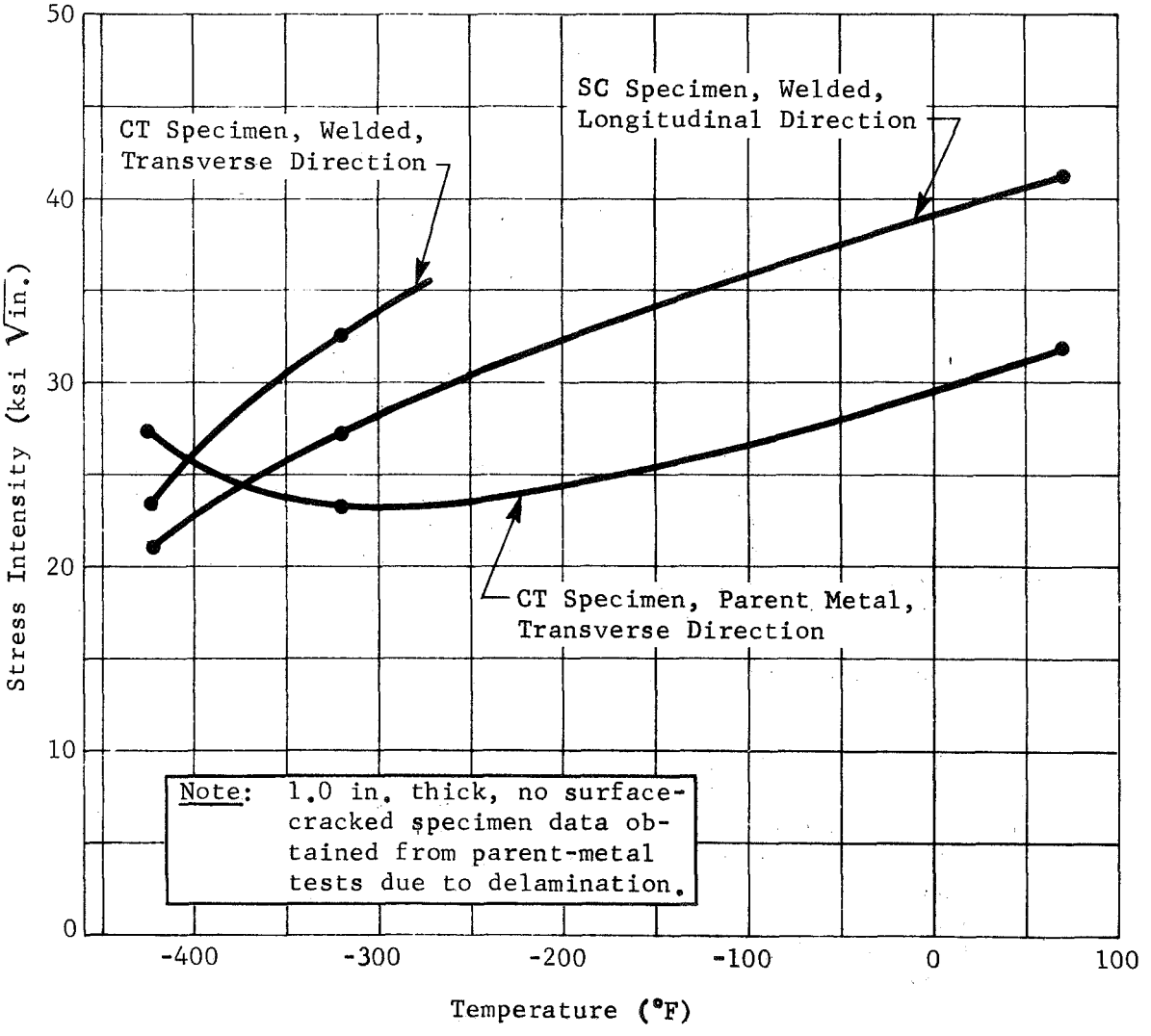

Fig. VI-10 Static Fracture Toughness of X7007-T6 Aluminum Alloy

The fracture stress/yield stress ratio was well above 1.0 for all surface-cracked specimens, and was typically between 1.2 and 1.4. Normally, such a high fracture stress/yield stress ratio would tend to invalidate the test results. However, in this case the welded material had not been stress-relieved, and the behavior can be readily explained.

When making a multipass weld on wide plates (our plates were two ft wide), the residual stresses at right angles to the weld can become significant. Although these residual stresses exist as tension stresses at the surface of the material, equilibrium requirements tell us that there should be transverse compressive stresses in the central portion of the weld zone. Now, if there is a crack approximately halfway through the plate, there may be rather high residual compression forces on the nose of the crack. Because these must be overcome during loading, the nominal stress can be greater than the local stress in the center of the weld, and the fracture stress/yield stress ratio may suggest that yielding has occurred even though the center of the weld is still elastic. No program was conducted for determining the extent of residual stress variations in multiple-pass weld joints. However, for full use of fracture mechanics principles in fail-safe design approaches, such a program would be essential.

Test data for the welded Aℓ 2021-T81 specimens are presented in Fig. VI-4.

Because of the location of the failures in the 70°F, unnotched Aℓ 2021-T81 welded tension specimens and of reports of possible low toughness in the heat-affected zone, several specimens that had defects as close as possible to the fusion line were prepared and tested. In two samples, the tip of the defect was actually in the heat-affected zone, very close to the fusion line. Cross-sectional examinations of the failed specimens showed that the path of the fracture was not in the plane of the defect, but jumped to the fusion line and followed it for some distance. The toughness values for two replicate specimens were 27 and 28 ksi $\sqrt{\text{in.}}$. A third specimen failed at a slightly lower level (22 ksi $\sqrt{\text{in.}}$); subsequent examination showed that the defect was in the cast material very close to the fusion line and followed the fusion line during fracture.

The welded Aℓ X7007-T6 exhibited the decrease in toughness with reductions in temperature that is characteristic of 7000-Series alloys. However, at room temperature, the toughness (41 ksi $\sqrt{\text{in.}}$) was quite high. The stress-intensity data for the two types of specimens follow and are also shown in Fig. VI-10.

Temperature (°F)	Critical Stress Intensity (ksi $\sqrt{in.}$)	
	Surface-Cracked Specimens	Compact-Tension Specimens
70	41	
-320	28	33
-423	21	24

At 70°F, there was not enough "pop-in" in the compact-tension welded specimens for us to determine the fracture toughness, but the cryogenic toughness levels obtained from the two types of specimens were in reasonably good agreement.

The fracture faces of the welded Aℓ X7007-T6 specimens had several interesting features. The fatigued precrack did not exhibit the smooth, fine-grained appearance that is characteristic of aluminum alloys; instead, the surface patterns (see Fig. VI-11) matched the distribution of second-phase particles found in the macro- and micro-sections that were taken through the weld. These same patterns were apparent in the area of rapid fracture.

c. Welded-Metal Tests/Effect of Weld Parameters*

As a result of the initial findings on the fracture toughness characteristics of welded joints, it was decided to perform a variety of additional surface-flawed specimen tests at room temperature in order to characterize weldment condition and defect location.

For all three aluminum alloys (2021, X7007, and 2014), evaluation was performed for the as-welded (AW), overheated weld (OW), and repaired weld (WR) conditions. In addition, 2021 was aged after welding (WA), after repairing (WRA), and after overheating (OWA) to provide three additional conditions.

The effect of defect location was characterized by placing the surface flaw in the following locations:

1) Weld centerline;

2) Heat-affected zone;

3) Fusion line.

*These tests were conducted as part of Tasks IV and V.

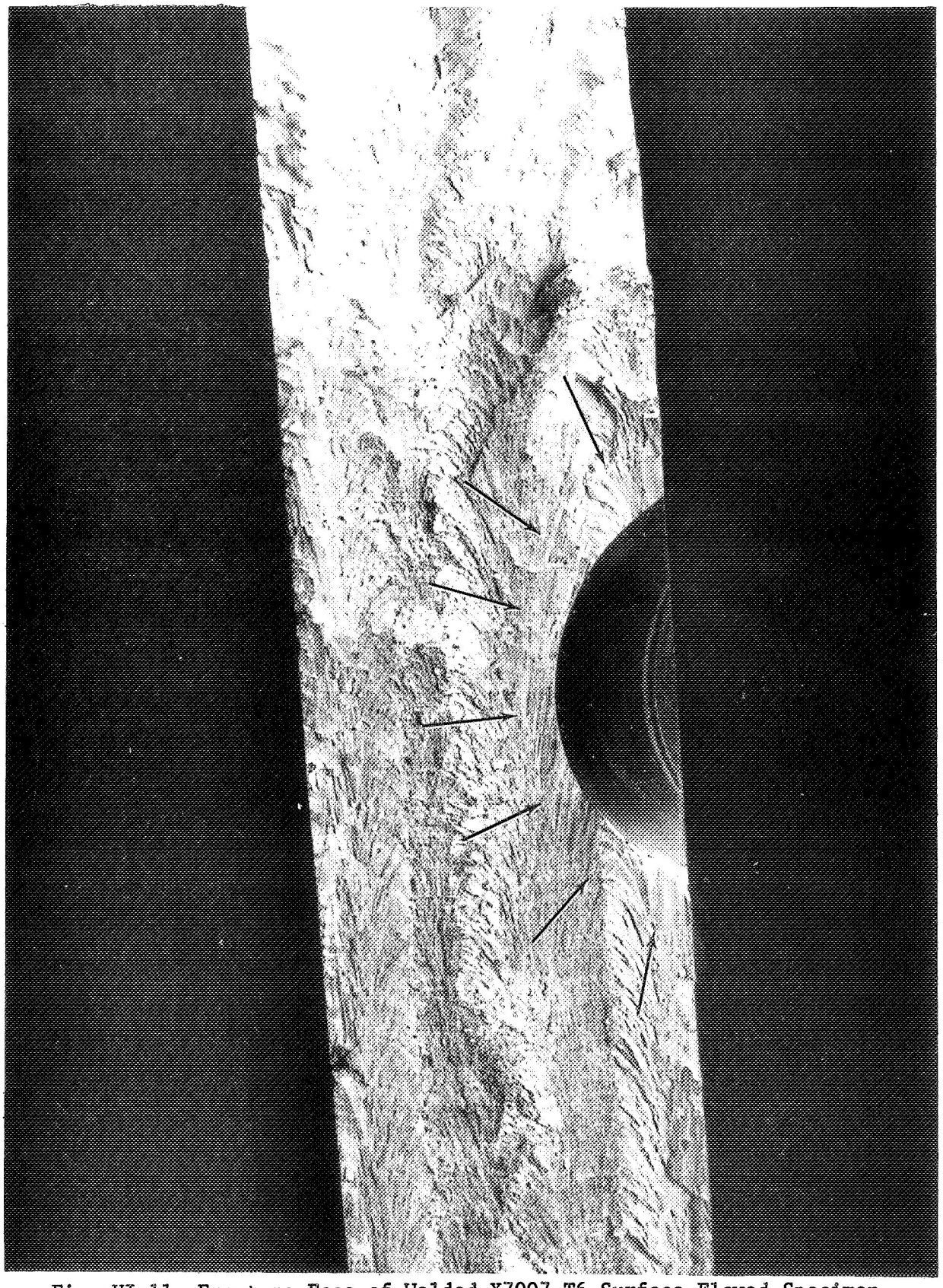

Fig. VI-11 Fracture Face of Welded X7007-T6 Surface-Flawed Specimen (Arrows Indicate Extent of Fatigue Advanced Flaw)

Because of the unknown internal shape of the weld at a specific location, it is virtually impossible to locate the nose of the defect exactly on the fusion line. However, attempts were made to come as close as possible. From prior experience with one alloy, 2021, we learned that if flaws were placed sufficiently close to the fusion line, the fracture would progress to the fusion line and then continue.

The experimental data are summarized in Table VI-6. The data show a general tendency for subcritical crack growth to be most pronounced for the fusion line and heat-affected zone conditions. In the weld centerline, subcritical growth appeared in a few cases for welds which were subjected to excessive heating. More detailed descriptions of behavior are presented in the following paragraphs.

Table VI-6 Summary of Fracture Toughness Data Showing Effect of Weldment Condition and Defect Location

Alloy	Weldment Condition	Average Critical Stress Intensity ($ksi\sqrt{in.}$) for Indicated Defect Location		
		Weld Centerline	Fusion Line	Heat-Affected Zone
2021-T81	AW	24.5	26.1 LBV, SCG	33.8 LBV, SCG
	WA	30.6	27.7 LBV, SCG	37.9 LBV, SCG
	OW	25.1	23.8 LBV, SCG	30.9 LBV, SCG
	OWA	22.8	26.4 LBV, SCG	36.7 LBV, SCG
	WR	26.9	24.0 LBV, SCG	
	WRA	23.0*	26.3 LBV, SCG	
X7007-T6	AW	42.0*	42.2 LBV, SCG	38.8 LBV, SCG
	OW	35.1 LBV, SCG	40.0 LBV, SCG	36.2 LBV, SCG
	WR	40.9 LBV, SCG	42.2 LBV, SCG	
2014-T6	AW	20.2	27.2 LBV, SCG	32.6 LBV, SCG
	OW	22.5*	24.8 LBV, SCG	30.0 LBV, SCG
	WR	25.6 LBV, SCG	26.5 LBV, SCG	

*One specimen exhibited subcritical crack growth.

Legend:

AW	As-welded	WR	Repaired weld
WA	Welded plus aged	WRA	Repaired weld plus aged
OW	Overheated weld	LBV	Lower bound value
OWA	Overheated weld plus aged	SCG	Subcritical crack growth

The 2021-T81 alloy data show that postweld aging can provide improved fracture toughness. This was true for all defect locations but not all weld conditions. The most dramatic increase occurred in the weld centerline where an increase of 25% over the as-welded condition occurred.

However, it was noted that aging of either an overheated or a repaired weld caused a reduction in toughness. No effect on toughness was detected for overheated or repaired welds when postweld aging was not performed. These observations suggest that excessive heat during the weld process affects subsequent postweld aging in a manner that is deleterious to toughness. Postweld aging produced a modest increase in thoughness for flaws located in the heat-affected zone and fusion line areas. In these cases, toughness increased (modestly) for all weld conditions (i.e., normal weld, overheated weld, repaired weld). No explanation for the apparent greater sensitivity of the weld centerline to thermal effects can be made without additional study.

Subcritical flaw growth was observed in 2021-T81 tests conducted with the defect located in the heat-affected zone and fusion line regions. As a result, the toughness level reported is a lower bound value because it is calculated based on the fracture stress and initial flaw size, not on the flaw size at instability. Subcritical flaw growth was detected for only one of the weld centerline specimens; this was a weld repaired and post-weld aged specimen.

A comparison of the toughness of the three regions indicated that the heat affected zone was markedly tougher than the weld centerline or fusion line. As a result of the superior toughness achieved from aged specimens, it was decided that the threshold testing should be performed using welded and aged material.

The X7007-T6 alloy exhibited extremely high weld centerline fracture toughness, quite similar to that observed for the earlier heat. The overheated and repaired welds showed a modest loss of toughness. The highest overall toughness for the three weldment conditions was achieved in the fusion line.

The X7007-T6 composition exhibited subcritical growth in all the regions evaluated. Of the three alloys tested, X7007-T6 showed the greatest susceptibility to subcritical growth in the weld centerline location.

The 2014-T6 composition exhibited a modest increase in fracture toughness for the two overheated conditions (OW and WR) when defects were located in the weld centerline. Essentially the opposite trend was evident for fusion line and heat affected zone defects. Similar to the other two alloys, all fusion line and heat-affected zone specimens exhibited subcritical crack growth. The weld centerline defect location only showed subcritical growth for overheated or repaired welds.

A comparison of the fracture toughness of three alloys shows X7007-T6 to be the toughest, followed in order by 2021-T81 and 2014-T6.

Application of the acoustical monitoring technique on the Aℓ X7007-T6 alloy permitted us to prove that the explanation for formation of the small triangular fracture advances near the front face (see Fig. VI-5) was correct. This was accomplished by loading a heat affected zone specimen until several distinct acoustical emissions were detected. The specimen was then unloaded and stained with a dye-penetrant and baked at a low temperature (~150°F) to achieve drying. The specimen was then reloaded until failure occurred. Examination of the fracture showed the same type of crack blunting around the nose of the crack and the small triangular fracture advance areas near the front face. It was noted that the stain had penetrated into the delamination around the crack front. However, the small triangular zones did not show staining (Fig. VI-12). This indicates that the crack blunting occurs during monotonic loading and that the pop-in does not occur until a higher load is reached.

Staining of other specimens (after loading until acoustical emissions were obtained, and then reloading to failure) showed varying amounts of subcritical growth. In some cases, as much as 0.050-in. crack extension was noted. Figure VI-13 shows a 2021 weld centerline specimen that exhibited 0.020 to 0.030-in. uniform crack growth around the periphery of the crack.

d. Welded-Metal Tests/Baseline Data for Threshold Testing

To perform the threshold testing using the compact tension specimens, it was necessary to characterize the static fracture toughness behavior for each weld condition and flaw location. A summary of the static test results is given in Table VI-7.

The CTS data shows lower critical stress intensity values for the 2021 alloy than those values obtained using surface-flawed specimens. However, this is characteristic of results obtained with compact tension specimens. For calculation of the critical stress intensity, the slope change and displacement shift of the load vs displacement curve was used. The displacement shift in multiple pass welds is not as extensive as that obtained when testing parent metal or single pass welded coupons. The reason for the less pronounced shift can be attributed to the surface fill pass layers of the weld, which are under residual tension stresses, and tend to plastically deform readily when the interior reaches elastic instability. As a result, crack extension in the interior is inhibited.

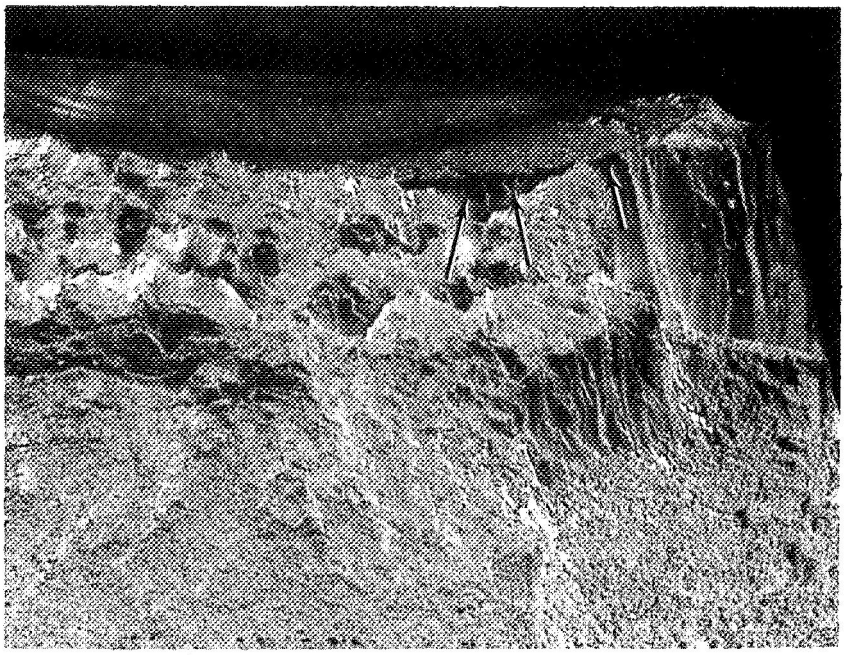

Fig. VI-12 Fracture Face of Aℓ X7007-T6 Surface-Flawed Specimen Showing Staining along Delaminated Crack Front

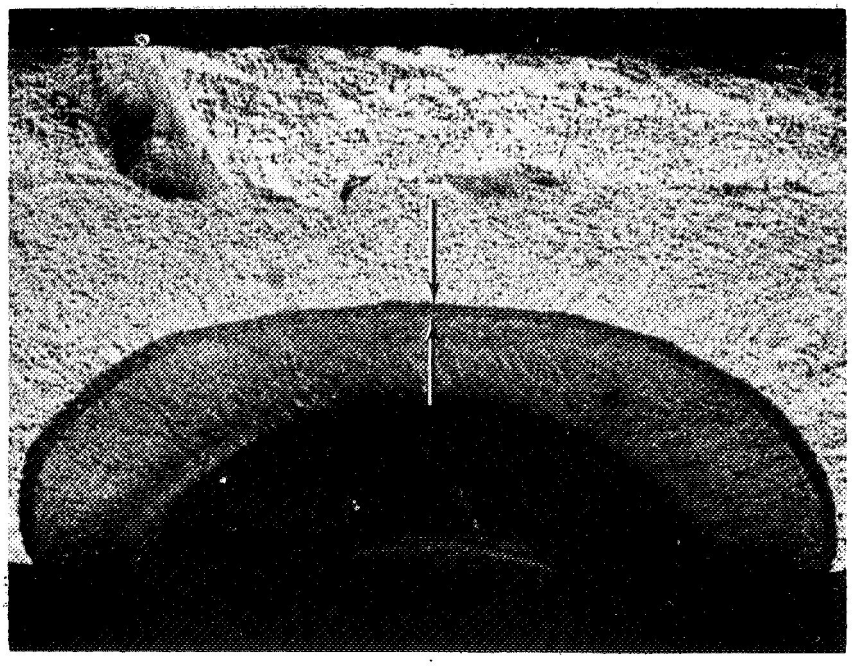

Fig. VI-13 Fracture Face of Aℓ 2021-T81 Surface-Flawed Specimen Showing Slow Crack Extension after Monotonic Loading

Table VI-7 Summary of Compact Tension Specimen Baseline Fracture Toughness Data

Alloy	Weldment Condition	Defect Location		
		Weld Centerline	Fusion Line	Heat Affected Zone
2021-T81	WA	17.9	17.4	22.9
	OW	20.7		
	WRA	16.1	15.4	*
X7007-T6	AW	*	*	*
	OW	*		
	WR	*	*	*

*No K_{Ic}; specimens did not exhibit pop-in behavior.

Legend:

WA	Welded plus aged	WR	Repaired weld
OW	Overheated weld	WRA	Repaired weld plus aged

In the X7007 alloy, we found incremental crack growth and no significant slope change or displacement shift. In addition, cracking occurred out of plane. As a result of these factors, no critical stress intensity could be determined.

2. Cryogenically Stretched Type 301 Stainless Steel

a. Parent-Metal Tests

Room-temperature tests performed using surface-flawed specimens showed that the fracture toughness was slightly higher than 100 ksi $\sqrt{in}$. In the longitudinal direction, one specimen was loaded to 108 ksi $\sqrt{in}$. $\left(\sigma / \sigma_{ys} = 1.00\right)$ without failing. The remaining specimens were cracked to create deeper flaws and failed at 102 ksi $\sqrt{in}$. The transverse specimens failed at an average stress intensity of 103 ksi $\sqrt{in}$., showing no directionality effects.

At cryogenic temperatures, the fracture toughness decreased significantly and was lower in the transverse direction. The fracture-toughness data are shown below and in Fig. VI-14.

Temperature (°F)	Critical Stress Intensity (ksi $\sqrt{in.}$)	
	Longitudinal Direction	Transverse Direction
70	102	103
-320	66	52
-423	55	44

Even though the toughness of the stainless steel decreased about 50% as the temperature went from 70 to -423°F, this was still a high level of toughness, considering that the tensile strength was so high (350 ksi). However, at -423°F the critical flaw size, at normal working stresses, can be extremely small.

b. Welded-Metal Tests

At room temperature, the fracture toughness of surface-cracked welded specimens (80 ksi $\sqrt{in.}$) was approximately 78% of that for the parent metal. At cryogenic temperatures, the fracture toughness decreases further: at -320 and -423°F, the toughness was 42 and 37 ksi $\sqrt{in.}$, respectively, or only about 65% as tough as the parent metal. These test data are presented in Fig. VI-14.

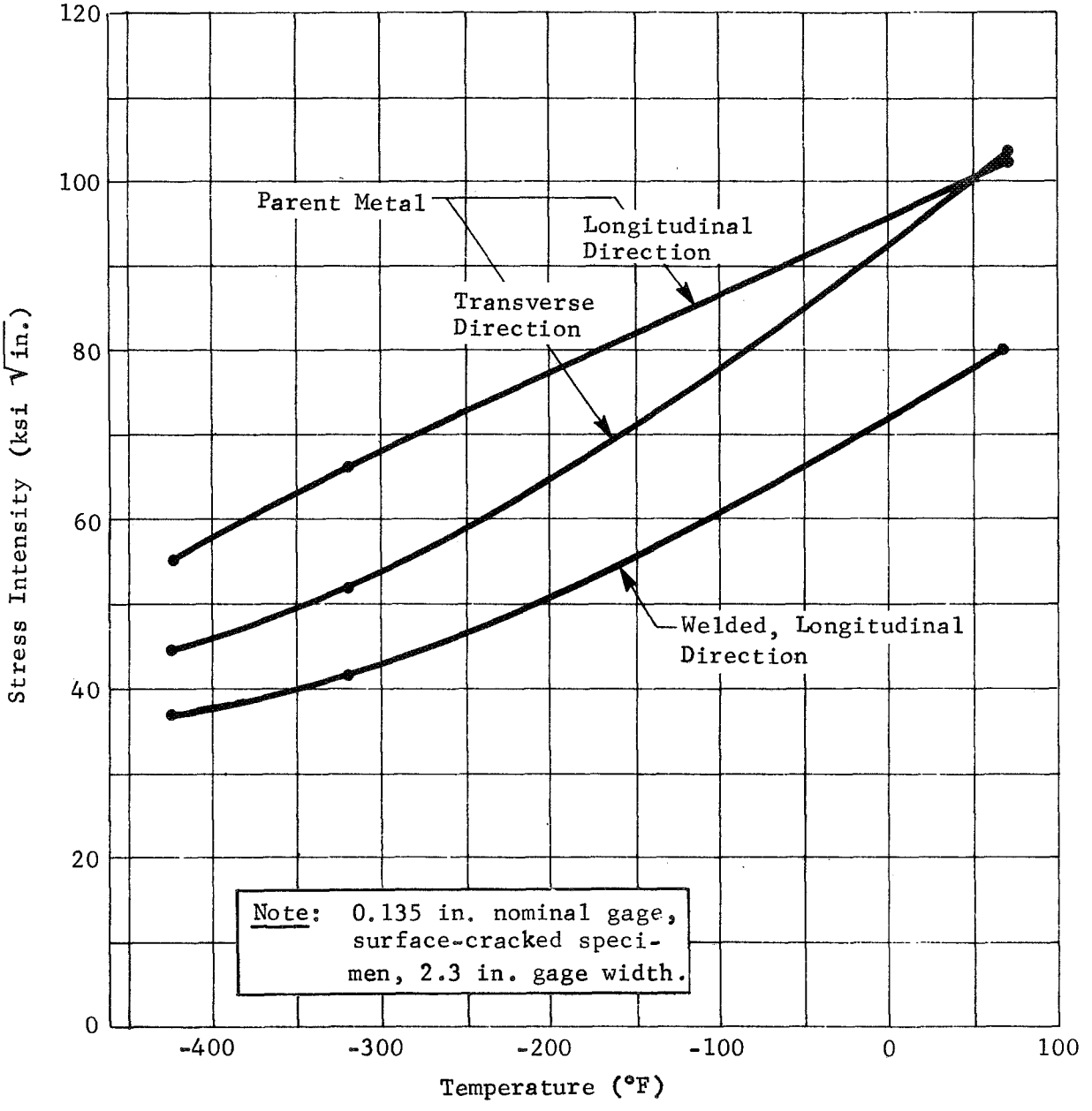

Fig. VI-14 Static Fracture Toughness of Cryogenically Stretched Type 301 Stainless Steel

C. CYCLIC-LOAD FLAW-ENLARGEMENT TESTS

In most cases, only three tests were performed to characterize crack-growth behavior. From this limited amount of testing, we can obtain only a crude idea of this process (the exponential crack-growth function, for example, cannot be calculated with such limited information). Therefore, the prime purpose for conducting these tests was to compare our results with available data.

In all cyclic tests, the stress ratio, R*, was less than 0.05. In most cases R was about 0.02. As a result, the data are treated as though R = 0. Instead of using $\Delta K = K_{max} - K_{min}$, we have presented the test data as K_{max}; but for convenience, we have called the stress intensity K rather than K_{max} in order to indicate that we are using the average maximum stress intensity, not the initial stress intensity.

In these tests, we tried to keep the difference between the initial stress intensity and the final stress intensity small. By doing so, we were able to obtain a more accurate linear interpolation of the crack-growth rate.

1. Aluminum Alloys

a. Parent-Metal Tests

Test data for compact-tension specimens are presented in Fig. VI-15 and IV-16.†

---

*R = minimum stress/maximum stress.

†Detailed tabular data for all cyclic tests were presented in the interim report.

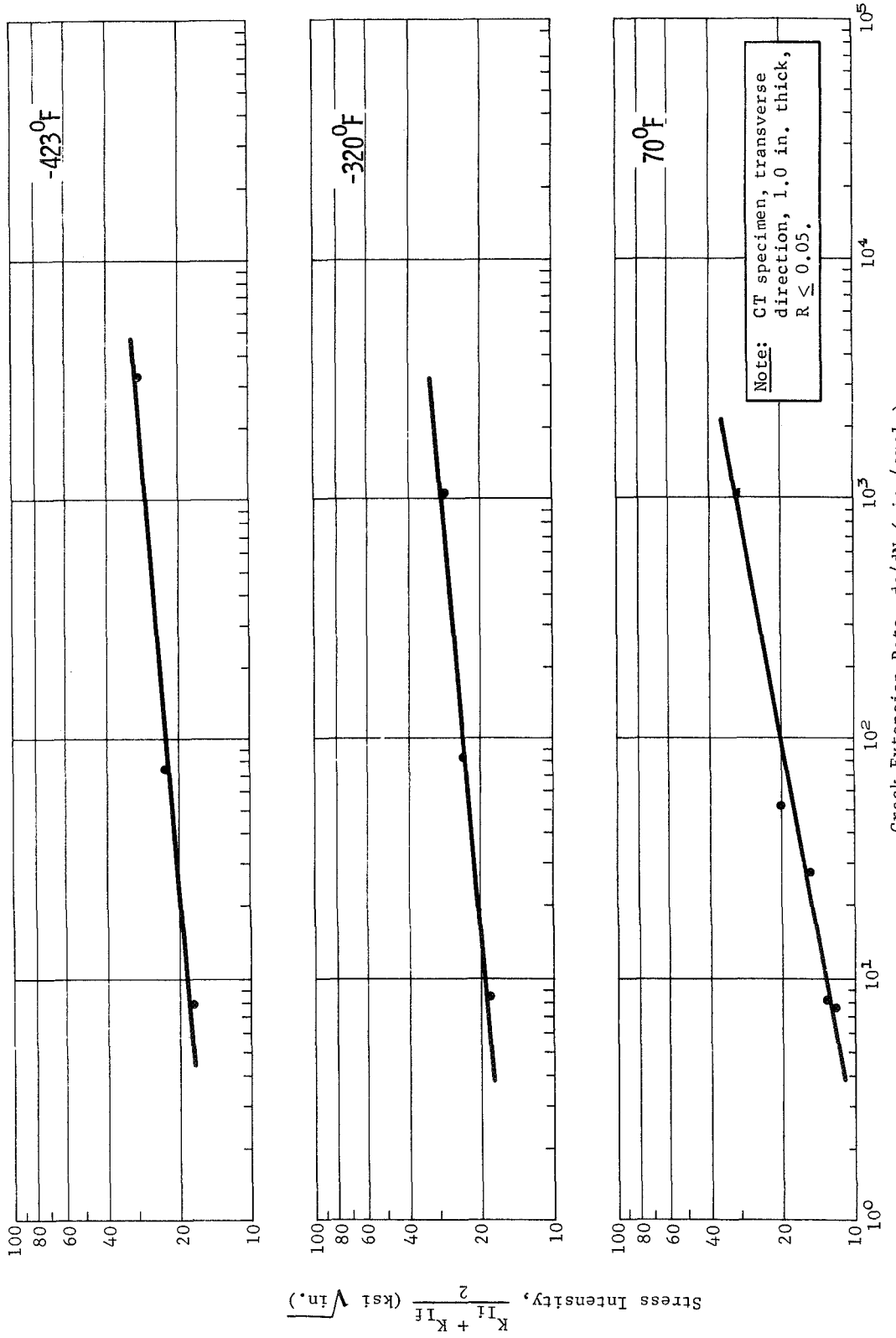

Fig. VI-15 Cyclic Crack-Extension Rates for Parent Metal (2021-T81 Aluminum Alloy)

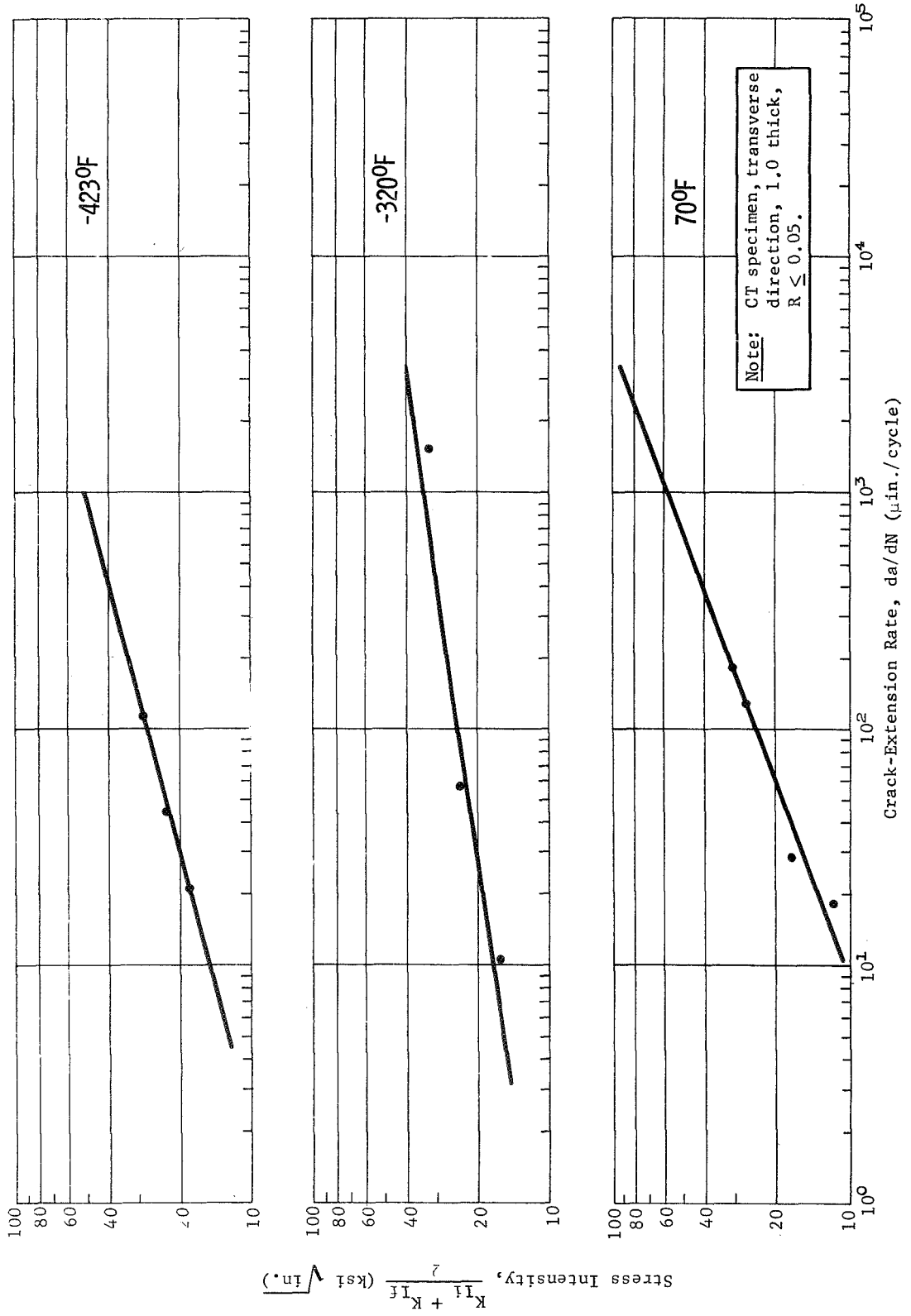

Fig. VI-16 Cyclic Crack-Extension Rates for Parent Metal (X7007-T6 Aluminum Alloy)

b. Welded-Metal Tests

Surface-cracked specimens were used to obtain the data presented in Fig. VI-17 and VI-18. In some cases, multiple data were obtained by periodically fatigue-marking the specimens. Figure VI-19 shows the fracture face of a typical, fatigue-marked, Aℓ 2021-T81 welded specimen.

Surface-flawed specimens were not intentionally cycled to failure. Had we attempted to induce fractures at stresses below the yield strength, the end of the semiminor crack axis would have been so close to the back face that the stress intensity would be meaningless.

2. Cyrogenically Stretched Type 301 Stainless Steel

Surface-cracked specimens were tested to determine the crack-growth rates for parent-metal and welded specimens. The data from these tests (see Fig. VI-20) show that, at 70 and -320°F, cracks in welded material grew at a faster rate than those in parent material (compared at the same stress intensity). However, at -423°F, no difference in the crack growth rates was observed. This behavior is understandable since the welded material exhibits a lower K_{Ic} than the parent metal. Therefore, for a given stress intensity, the K_{Ii}/K_{Ic} ratio would be higher for welded material.

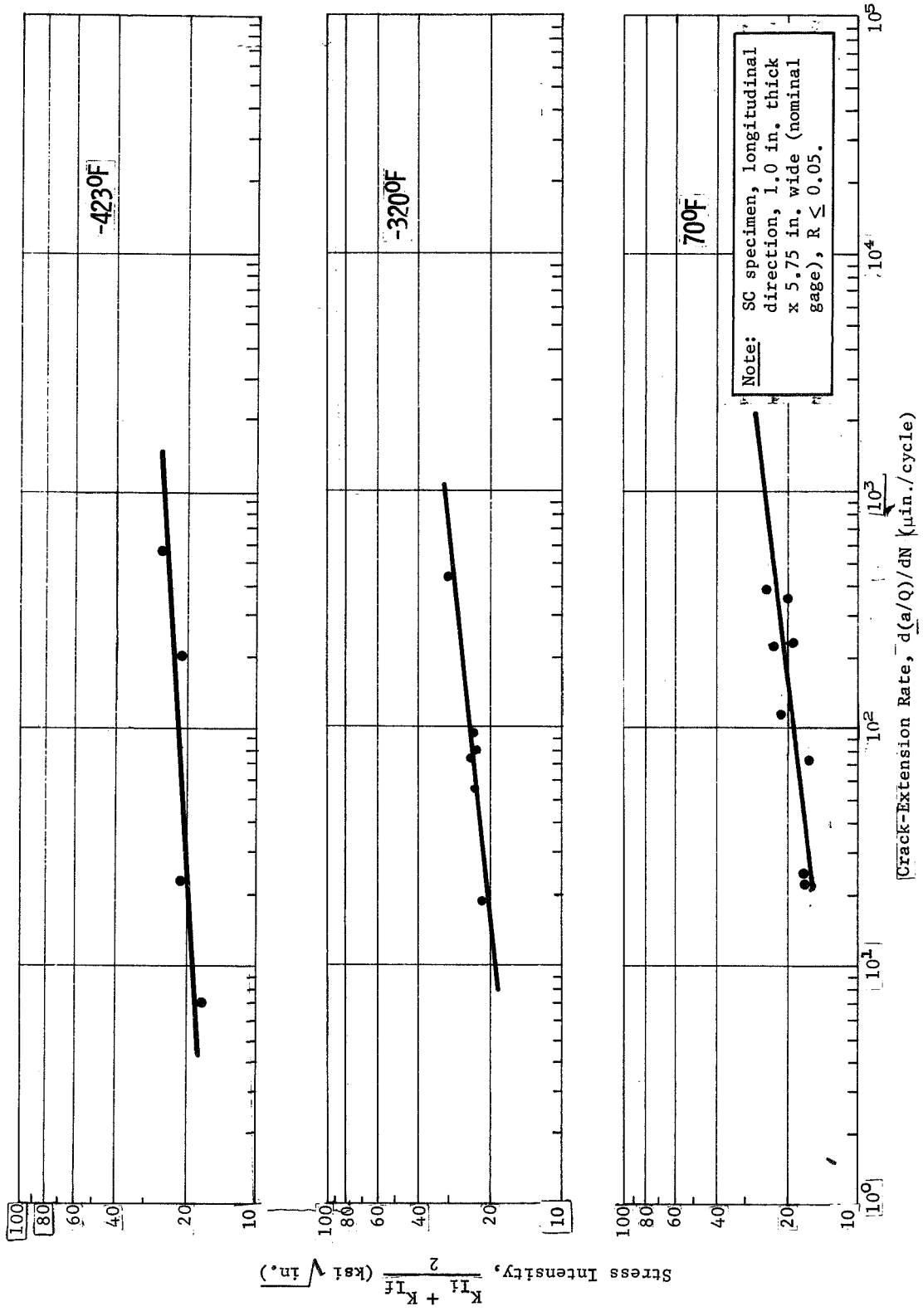

Fig. VI-17 Cyclic Crack-Extension Rates for Welded 2021-T81 Aluminum Alloy

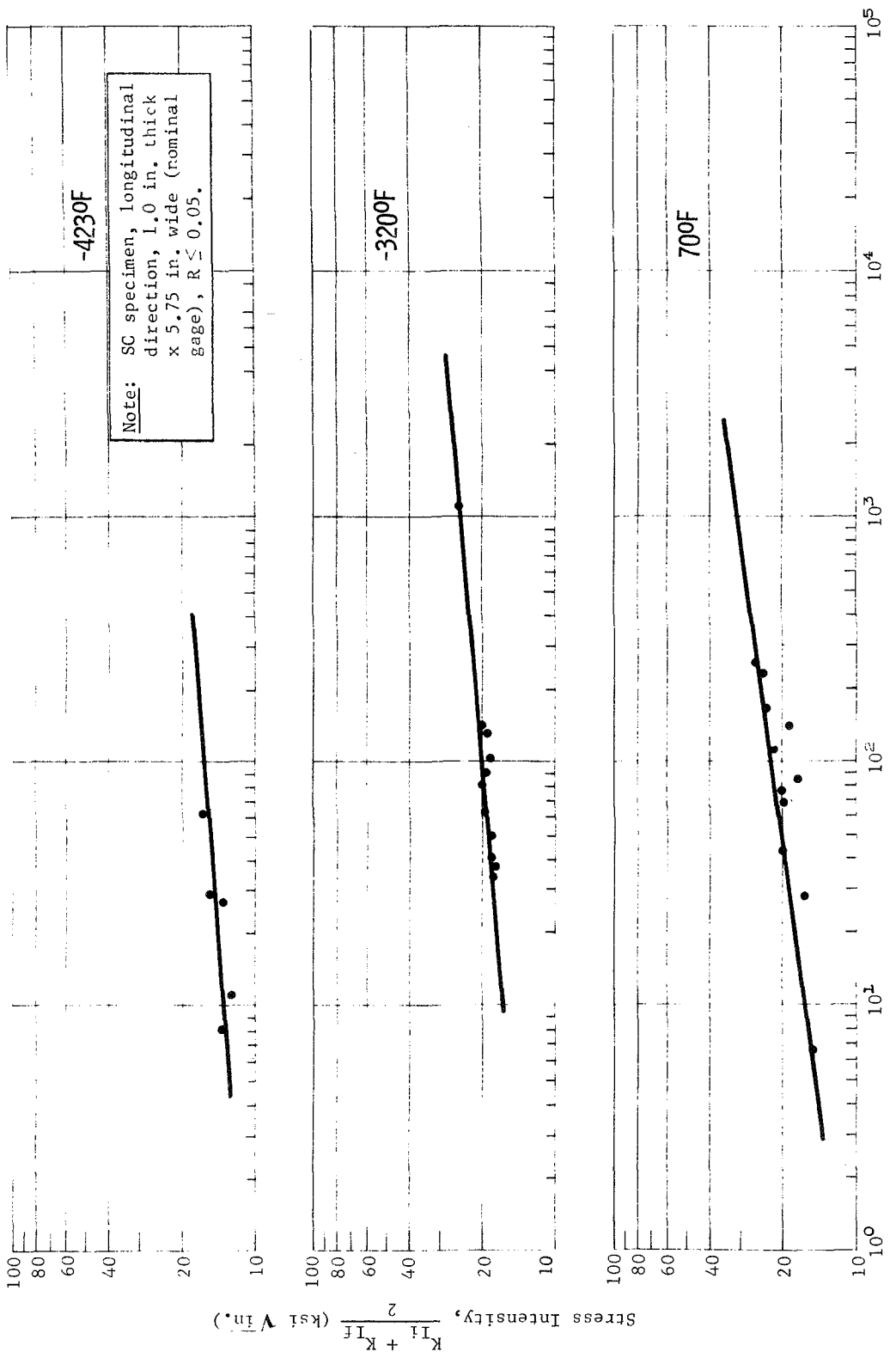

Fig. VI-18 Cyclic Crack-Extension Rates for Welded X7007-T6 Aluminum Alloy

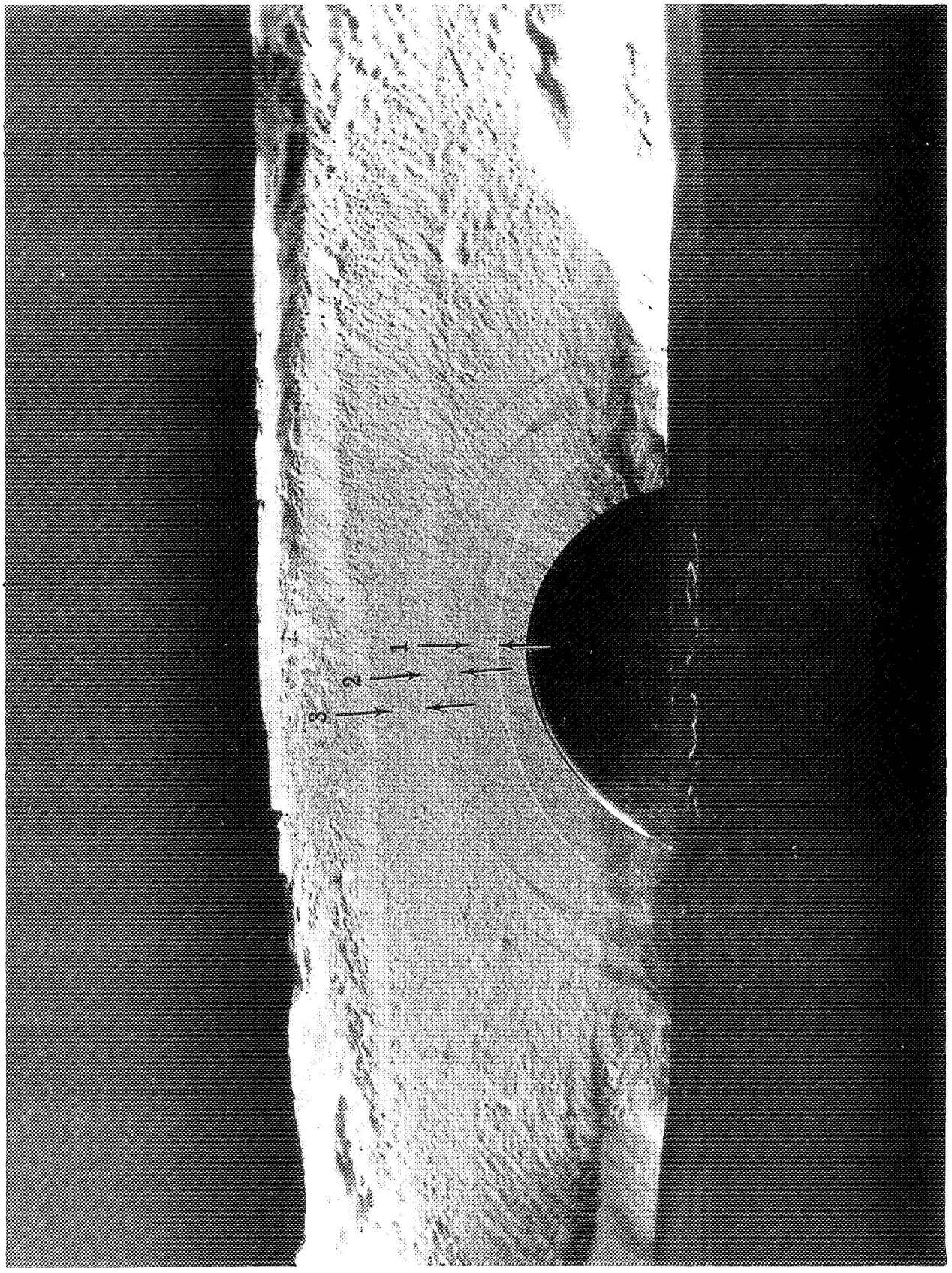

Fig. VI-19 Fracture Face of Fatigue - Marked 2021-T81 Cyclic Fracture-Toughness Specimen
(Arrows indicate width of cyclic flaw growth zones)

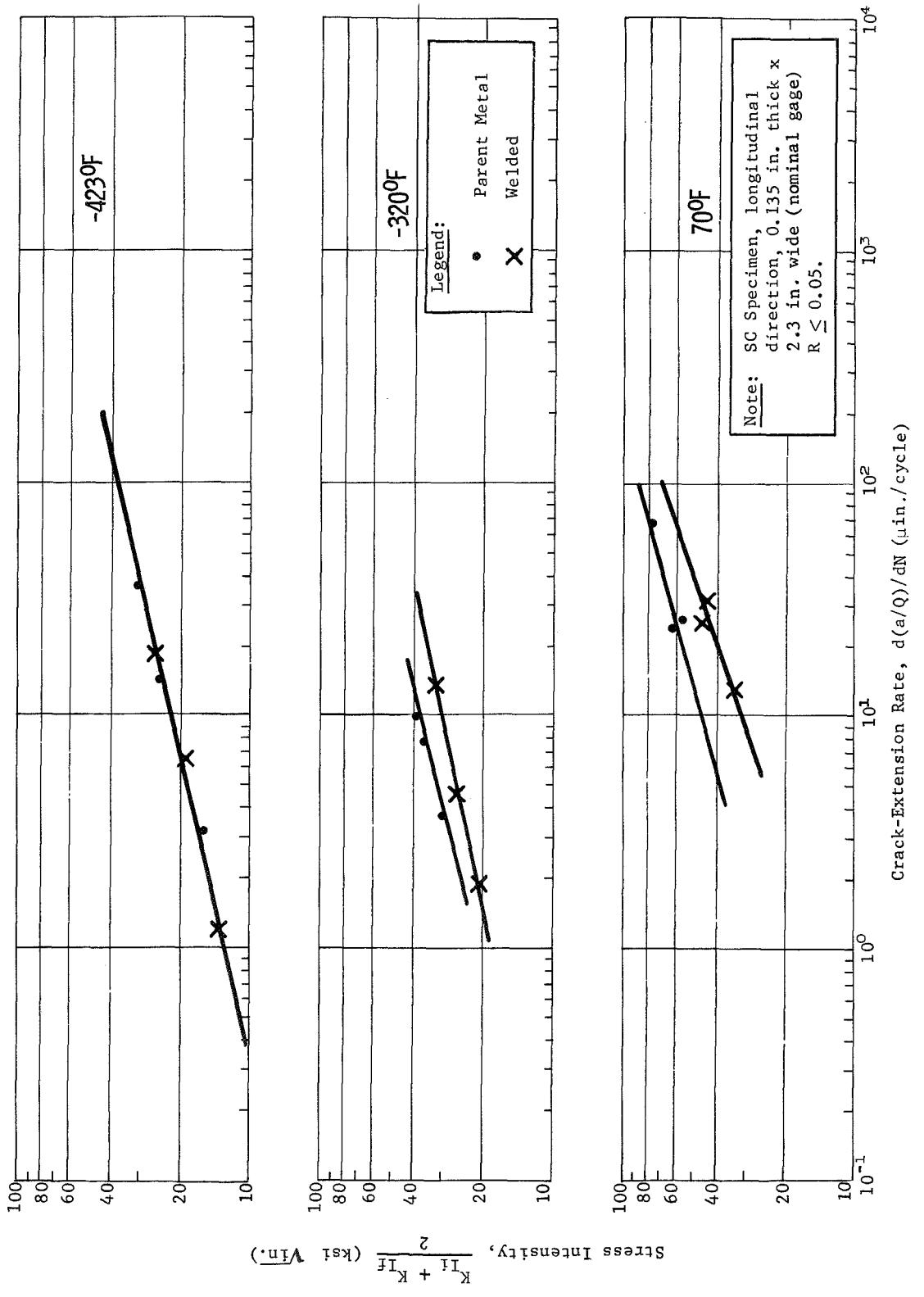

Fig. VI-20 Cyclic Crack-Extension Rates for Parent Metal and Welded Cryogenically Stretched 301 Stainless Steel

D. SUSTAINED-LOAD FLAW-ENLARGEMENT TESTS

These tests were performed to determine the minimum stress intensity that would produce subcritical flaw growth in the various alloy specimens to show the effects of temperature, weldment condition, defect location, and environment. In general, three specimens were used to bracket the threshold level, but in some cases, it was necessary to use extra specimens. Because time and funds did not permit us to confirm the exact levels, these data are only approximate.

1. Aluminum Alloys

a. Parent-Metal Tests/Effect of Temperature*

The threshold data for Aℓ 2021-T81 and Aℓ X7007-T6 are summarized in the following table.

Aluminum Alloy	Threshold Level, K_{TH}/K_{Ic}		
	70°F	-320°F	-423°F
2021-T81	$0.77 < K_{TH}/K_{Ic} < 0.82$	$K_{TH}/K_{Ic} = 0.82$	$K_{TH}/K_{Ic} < 0.76$
X7007-T6	$0.38 < K_{TH}/K_{Ic} < 0.48$	$0.73 < K_{TH}/K_{Ic} < 0.82$	$0.71 < K_{TH}/K_{Ic} < 0.80$

Detailed data showing the behavior found for each specimen tested are given in the following table.

* This work was performed as part of Task II.

Aluminum Alloy	Temperature (°F)	Stress-Intensity Ratio, K_{Ii}/K_{Ic}	Crack Growth
2021-T81	70	0.77	No
2021-T81	70	0.77	No
2021-T81	70	0.82	Yes
2021-T81	70	0.83	Yes
2021-T81	-320	0.73	No
2021-T81	-320	0.82	No
2021-T81	-320	0.82	Yes
2021-T81	-320	0.88	Yes
2021-T81	-423	0.76	Yes*
2021-T81	-423	0.79	Yes
2021-T81	-423	0.90	Yes
2021-T81	-423	0.91	Yes
X7007-T6	70	0.36	No
X7007-T6	70	0.48	Yes†
X7007-T6	70	0.53	Yes†
X7007-T6	70	0.64	Yes
X7007-T6	70	0.71	Yes
X7007-T6	-320	0.73	No
X7007-T6	-320	0.82	Yes
X7007-T6	-320	0.96	Yes
X7007-T6	-320	1.04	Yes
X7007-T6	-320	1.07	Yes
X7007-T6	-423	0.71	No
X7007-T6	-423	0.80	Yes

*Very slight.

†Slight.

The data for Aℓ 2021-T81 are typical of aluminum alloys in an inert environment. X7007-T6 has a very low threshold at room temperature, but at cryogenic temperatures, the threshold level is more typical.

b. Welded Metal Tests/Effect of Temperature*

The threshold data for welded specimens of both aluminum alloys are summarized below.

Aluminum Alloy	Threshold Level, K_{TH}/K_{Ic}		
	70°F	-320°F	-423°F
2021-T81	$0.58 < K_{TH}/K_{Ic} < 0.61$	$0.62 < K_{TH}/K_{Ic} < 0.69$	$0.69 < K_{TH}/K_{Ic} < 0.72$
X7007-T6	$0.85 < K_{TH}/K_{Ic} < 0.90$	$0.59 < K_{TH}/K_{Ic} < 0.74$	$0.50 < K_{TH}/K_{Ic} < 0.62$

Detailed data showing the behavior found for each specimen tested are given in the following table.

Aluminum Alloy	Temperature (°F)	Stress-Intensity Ratio, K_{Ii}/K_{Ic}	Crack Growth
2021-T81	70	0.50	No
2021-T81	70	0.58	Yes*
2021-T81	70	0.61	No
2021-T81	70	0.63	Yes
2021-T81	70	0.65	Yes
2021-T81	-320	0.62	No
2021-T81	-320	0.69	Yes
2021-T81	-320	0.73	Yes
2021-T81	-423	0.69	No
2021-T81	-423	0.72	Yes
2021-T81	-423	0.79	Yes
X7007-T6	70	0.81	No
X7007-T6	70	0.85	No
X7007-T6	70	0.90	Yes
X7007-T6	70	0.90	Yes
X7007-T6	70	0.91	Yes
X7007-T6	70	1.01	Yes
X7007-T6	-320	0.59	No
X7007-T6	-320	0.74	Yes
X7007-T6	-320	0.79	Yes
X7007-T6	-423	0.50	No
X7007-T6	-423	0.62	Yes*

*Very slight.

*This work was performed as part of Task III.

The data suggest that welded Aℓ 2021-T81 has a rather low threshold at room temperature with a slight increase at cryogenic temperatures.

The data for welded Aℓ X7007-T6 specimens are more difficult to interpret. Examinations of the surfaces showed that the fatigue precrack was not smooth and that the surface was faceted with numerous cracks (see Fig. VI-21). In addition, the crack front was usually quite irregular, which made it extremely diffcult to tell whether crack growth had occurred. As a result, we feel that the stress intensity could not be calculated accurately.

c. Welded-Metal Tests/Effect of Welding Parameters*

Data for both alloys are summarized in Table VI-8. Detailed data are contained in Appendix Tables A-6 and A-7.

The 2021-T81 composition exhibited satisfactory threshold levels. Although the threshold levels could not be precisely determined with the minimal level of testing performed, a good deal of very valuable information was obtained.

In many cases the 2021-T81 alloy exhibited localized growth. Figure VI-22 shows a typical fracture face for a welded plus aged weld centerline specimen where the growth was localized at the intersection of the surface weld pass with the second penetration pass. This localized growth occasionally made detection of the threshold level rather difficult. When growth is uniform, detection of the threshold is greatly simplified. Figure VI-23 shows the three specimens of the overheated (OW), weld centerline (WC) series. In this photo, the slim band between the initial fatigue precrack and the posttest fatigue zone is the sustaned load growth. In the third specimen, no differentiation between the initial and final fatigue zone can determined.

Evaluation of the X7007-T6 welds was quite difficult because of the unusual shear faceting that makes it difficult to identify sustained load growth as different from fatigue extension. The weld centerline clearly exhibited the lowest threshold. The lowest threshold level was for the as-welded (AW) condition. Figure VI-24 shows extensive growth in a specimen tested at 29 ksi $\sqrt{in}$. The OW and weld repaired (WR) conditions that exhibited reduced critical stress intensities in the surface flawed tests had a higher threshold than the tougher AW condition.

*This work was performed as part of Task VI.

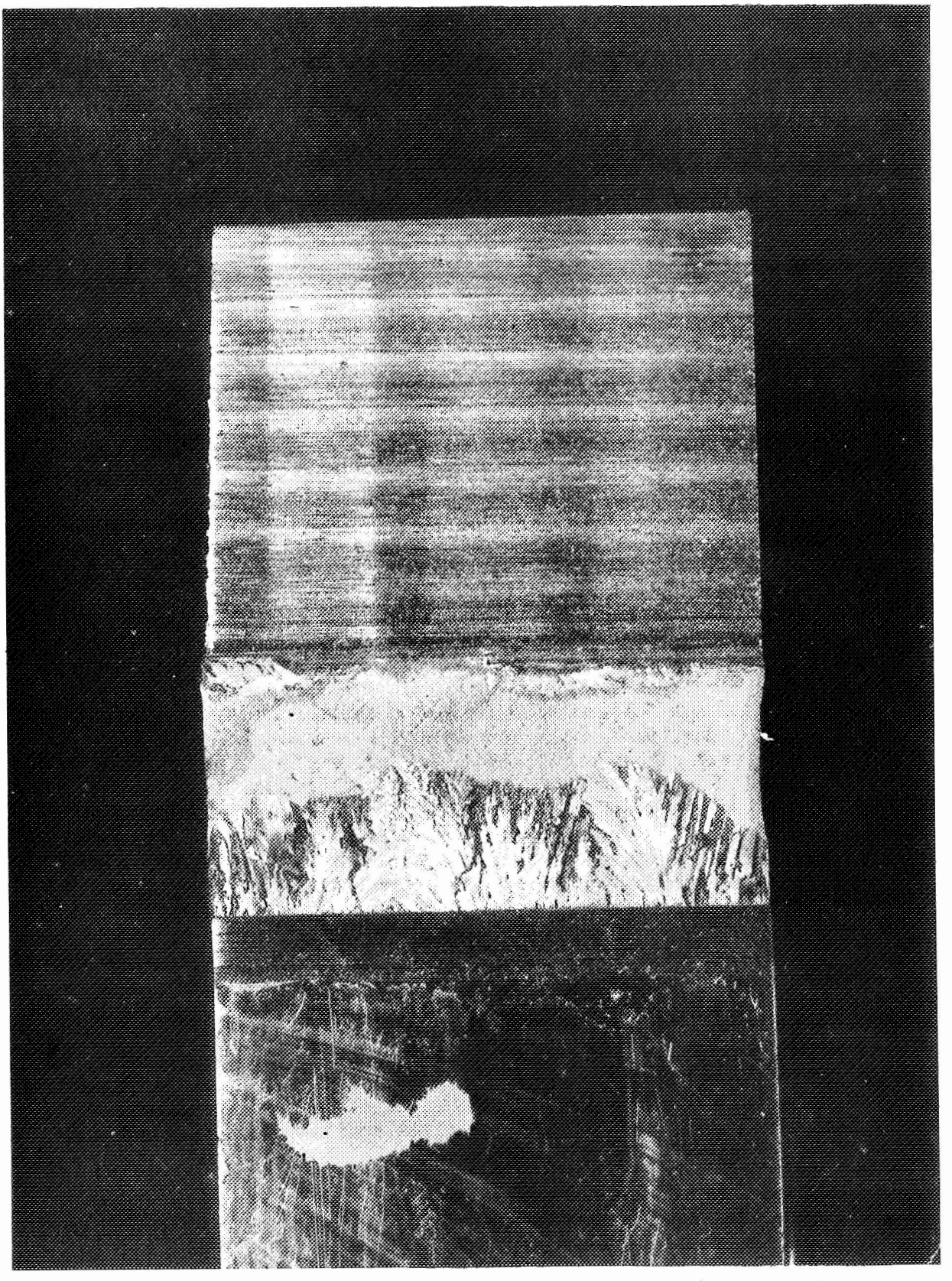

Fig. VI-21 Fracture Surface of Sustained-Load, Welded X7007-T6 Specimen

Table VI-8 Summary of Sustained Load Flaw Enlargement Tests for Weld Specimens in Air

Alloy	Weldment Condition	Defect Location	Threshold Level, K_{TH}/K_{Ic} or K_{TH}	Comments
2021-T81	WA	WC	$0.60 < K_{TH}/K_{Ic} < 0.69$	Localized Growth
	WA	FL	$0.50 < K_{TH}/K_{Ic} < 0.58$	Uniform growth
	WA	HAZ	$0.58 < K_{TH}/K_{Ic} < 0.70$	Uniform growth
	OW	WC	$0.67 < K_{TH}/K_{Ic} < 0.77$	Uniform growth
	WRA	WC	$0.73 < K_{TH}/K_{Ic} < 0.80$	Localized growth not as extensive as WA/WC
	WRA	FL	$0.76 < K_{TH}/K_{Ic} < 0.89$	Localized growth, very small amount
	WRA	HAZ	$K_{TH} \sim$ 11-12 ksi $\sqrt{in.}$	Uniform growth, tendency for laminar cracking
X7007-T6	AW	WC	$K_{TH} <$ 11 ksi $\sqrt{in.}$	Much shear faceting; not much growth at 11 ksi $\sqrt{in.}$
	AW	FL	$16 < K_{TH} <$ 31 ksi $\sqrt{in.}$	Very irregular growth; one specimen had defect outside FL region.
	AW	HAZ	$18 < K_{TH} <$ 20 ksi $\sqrt{in.}$	Growth uniform along crack front; generally slight growth
	OW	WC	$K_{TH} \ll 18$	Growth significant at 18 ksi $\sqrt{in}$; threshold probably significantly lower.
	WR	WC	$16 < K_{TH} <$ 20 ksi $\sqrt{in.}$	Uniform growth at higher stress intensities
	WR	FL	$K_{TH} <$ 12 ksi $\sqrt{in.}$	Very slight growth at 12 ksi $\sqrt{in.}$; K_{TH} probably very close to 12 ksi $\sqrt{in.}$
	WR	HAZ	$17 < K_{TH} <$ 21 ksi $\sqrt{in.}$	Growth above K_{TH} uniform

Legend:

WA Welded plus aged
WC Weld centerline
OW Overheated Weld
HAZ Heat-affected zone
FL Fusion line
WRA Repaired weld plus aged
AW As-welded
WR Repaired weld

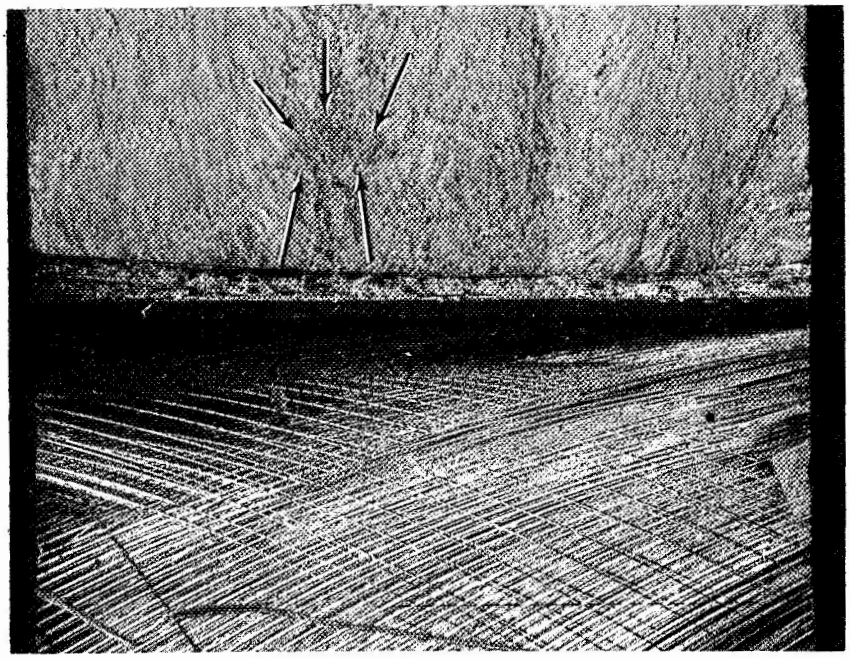

Fig. VI-22 Fracture Face of Aℓ 2021-T81 Compact Tension Specimen Showing Localized Growth during Sustained Load Exposure

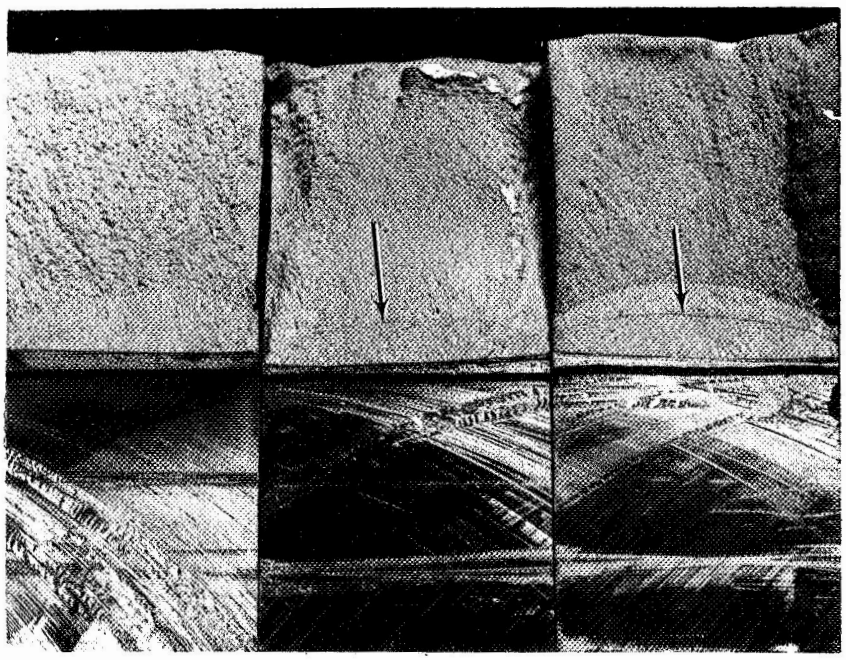

Fig. VI-23 Fracture Face of Three Aℓ 2021-T81 Compact Tension Specimens Showing No Growth (left) and Slight Growth (center and right) during Sustained Load Exposure

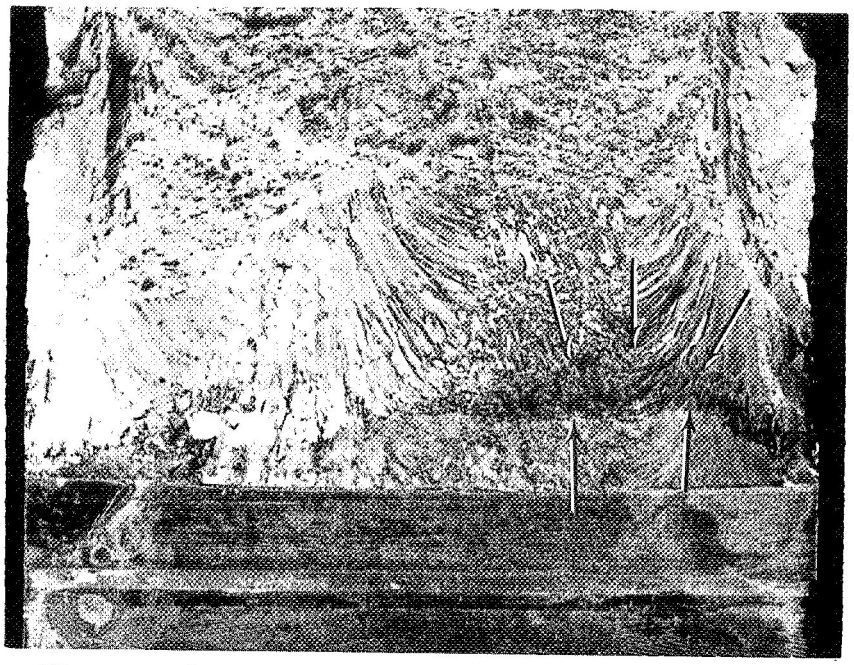

Fig. VI-24 Fracture Face of Aℓ X7007-T6 Compact Tension Specimen Showing Faceted Appearance and Area of Extensive Sustained Load Crack Growth

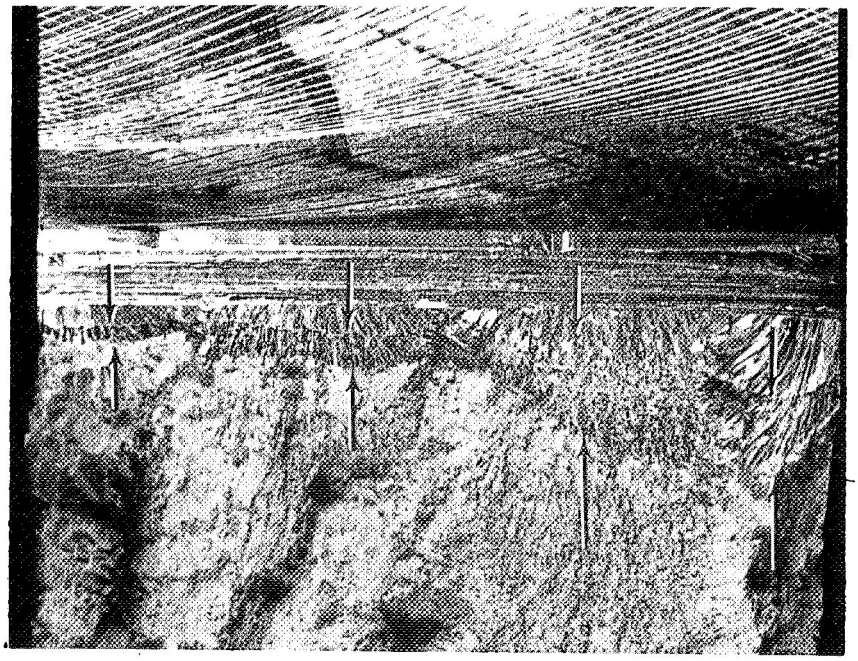

Fig. VI-25 Fracture Face of Aℓ X7007-T6 Compact Tension Specimen Showing Sustained Load Crack Growth along Entire Crack Front

The fusion line tests showed improved threshold levels compared to the weld centerline. Based on the amount of growth, it is estimated that the AW level was close to 16 ksi $\sqrt{in.}$ The weld repaired condition exhibited a level closer to 12 ksi $\sqrt{in.}$

The heat affected zone tests clearly showed that this region exhibited the highest threshold data. Weldment condition had little effect on the threshold level. Figure VI-25 shows a typical frature face exhibiting slow growth along the entire crack front.

d. Welded-Metal Tests/Effect of Corrosive Environment*

Tests to show the effect of a deleterious environment were performed in a 3 1/2% NaCℓ solution. Experimental data for both alloys are summarized in Table VI-9. Detailed data are presented in Appendix Tables A-8 and A-9.

The 2021-T81 composition appeared to exhibit a decrease in threshold that was most sinificant for the weld centerline region, as shown in the following tabulation.

Weldment Condition	Threshold Level, K_{TH}/K_{Ic}	
	Air	Salt
WA	$0.60 < K_{TH}/K_{Ic} < 0.67$	$0.40 < K_{TH}/K_{Ic} < 0.45$
OW	$0.67 < K_{TH}/K_{Ic} < 0.77$	$0.54 < K_{TH}/K_{Ic} < 0.62$
WRA	$0.73 < K_{TH}/K_{Ic} < 0.80$	$K_{TH}/K_{Ic} < 0.63$

In the fusion line tests, no decrease in threshold was found for the welded plus aged condition. A significant decrease was noted for the weld repaired and aged condition.

Heat affected zone tests exhibited no decrease in threshold due to the corrosive environment.

The X7007-T6 showed a significant reduction threshold for the weld centerline condition. In the as-welded material, where the air test showed very slight growth at 11 ksi $\sqrt{in.}$, the salt tests showed extensive growth at 12 ksi $\sqrt{in.}$, thereby suggesting the threshold level was actually much lower. For the other two conditions, OW and WR, threshold levels also decreased significantly.

*This work was performed as part of Task VI.

Table VI-9 Summary of Sustained Load Flaw Enlargement Tests for Welded Specimens in 3-1/2% NaCl Solution

Alloy	Weldment Condition	Defect Location	Threshold Level, K_{TH}/K_{Ic} or K_{TH}	Comments
2021-T81	WA	WC	$0.40 < K_{TH}/K_{Ic} < 0.45$	Generally uniform growth along crack front
	WA	FL	$0.50 < K_{TH}/K_{Ic} < 0.58$	Generally uniform growth along crack front
	WA	HAZ	$0.58 < K_{TH}/K_{Ic} < 0.70$	
	OW	WC	$0.54 < K_{TH}/K_{Ic} < 0.62$	Localized growth
	WRA	WC	$K_{TH}/K_{Ic} < 0.63$	
	WRA	FL	$0.50 < K_{TH}/K_{Ic} < 0.59$	Localized growth
	WRA	HAZ	$K_{TH} \sim$ 12-13 ksi $\sqrt{in.}$	
X7007-T6	AW	WC	$K_{TH} <<$ 12 ksi $\sqrt{in.}$	Extensive growth at 12 ksi $\sqrt{in.}$
	AW	FL	$K_{TH} <$ 11 ksi $\sqrt{in.}$	Local growth
	AW	HAZ	$K_{TH} >$ 15 ksi $\sqrt{in.}$	No growth detected
	OW	WC	$K_{TH} <$ 11 ksi $\sqrt{in.}$	All specimens exhibited extensive local growth
	WR	WC	$11 < K_{TH} <$ 13 ksi $\sqrt{in.}$	
	WR	FL	$9 < K_{TH} <$ 12 ksi $\sqrt{in.}$	Local growth
	WR	HAZ	$19 < K_{TH} <$ 20 ksi $\sqrt{in.}$	Local growth, very limited growth at 20 ksi $\sqrt{in.}$

Legend:

WA	Welded plus aged	HAZ	Heat-affected zone	AW	As-welded
WC	Weld centerline	OW	Overheated weld	WR	Repaired weld
FL	Fusion lined	WRA	Repaired weld plus aged		

In the fusion line area, a significant decrease in threshold occurred for the as-welded condition and to a lesser degree for the WR tests.

The heat affected zone region that showed the least effect of weldment condition also showed the least affect of corrosive environment.

2. Type 301 Stainless Steel

a. Parent Metal Tests

The threshold data for cryogenically-stretched Type 301 stainless steel specimens are summarized in the following table.

Threshold Level, K_{TH} K_{Ic}		
70°F	-320°F	-423°F
$0.67 < K_{TH}$ $K_{Ic} < 0.79$	$0.58 < K_{TH}$ $K_{Ic} < 0.68$	$0.55 < K_{TH}$ $K_{Ic} < 0.65$

Detailed data showing the behavior found for each specimen test are given in the following table.

Temperature (°F)	Stress-Intensity Ratio, K_{Ii}/K_c	Crack Growth
70	0.67	No
70	0.79	Yes*
70	0.80	Yes*
70	0.88	Yes
-320	0.42	No
-320	0.46	No
-320	0.58	No
-320	0.68	Yes*
-423	0.55	No
-423	0.65	Yes
-423	0.76	Yes

*Slight.

The threshold level at 70°F is probably close to the upper-limit value since the amount of crack growth at values of 0.79 and 0.80 was slight. The cryogenic threshold levels are approximately 60% of the cirtical stress intensity.

b. Welded Metal Tests

The threshold data for welded Type 301 stainless steel specimens are sumarized below.

Threshold Level, K_{TH}/K_{Ic}		
70°F	-320°F	-423°F
$0.58 < K_{TH}/K_{Ic} < 0.64$	$0.88 < K_{TH}/K_{Ic} < 0.90$	$0.65 < K_{TH}/I_{Ic} < 0.72$

Detailed data showing the behavior found for each specimen test are given in the following table.

Temperature (°F)	Stress-Intensity Ratio, K_{Ii}/K_{Ic}	Crack Growth
70	0.58	No
70	0.64	Yes
70	0.77	Yes
-320	0.72	No
-320	0.88	No
-320	0.90	Yes
-423	0.65	No
-423	0.72	Yes*
-423	0.79	Yes
-423	0.91	Yes†

*Slight.
†Failed.

At room temperature, the threshold level for the welded specimens appears to be slightly lower than that for the parent metal, which is not surprising. The cryogenic behavior is somewhat confusing as a result of the rather high level indicated at -320°F.

E. CORROSION TESTS*

Aluminum alloy corrosion test data are presented in Appendix A. Table itemization is given by the following guide:

Appendix Guide - Corrosion Tests	
Alloy	Appendix Table
Aℓ 2021-T81	A-10
Aℓ X7007-T6	A-11
Aℓ 2014-T6	A-12
Aℓ 2219-T87	A-13
Aℓ 7075-T6	A-14

A summary of the behavior of general and stress corrosion test results is given in Table VI-10.† The table shows that the Kure Beach seacoast exposure was less severe than the laboratory exposure. The 90-day Kure Beach exposure was insufficient to show stress corrosion in the 7075 alloy used as a control. Although a minimum exposure of 180 days at Kure Beach would have been preferred, insufficient time was available during the contract for that exposure period. The surface corrosion effect resulting from the laboratory exposure (30 days) was more severe than the 90-day seacoast exposure (Fig. VI-26). This is not surprising since the laboratory exposure is considered to be equivalent to 5 to 6 times the standard seacoast exposure, and, therefore, the 30-day exposure is equivalent to almost twice the Kure Beach exposure.

The 2021 alloy exhibited an improved corrosion resistance in the welded plus aged condition compared to the as-welded material, as determined by laboratory tests. No stress corrosion cracking was found in either case; however, the as-welded material exhibited a greater tendency toward intergranular attack, particularly in the fusion line and heat-affected zone areas. Shallow stress corrosion cracking was found in the heat-affected zone of the overheated, overheated plus aged, and repaired weld specimens tested in the laboratory environment.

---

*Data presented in this section was obtained in Task VII testing.

†General corrosion testing in the laboratory used the 20% salt fog method. Stress corrosion testing in the laboratory used alternate immersion in 3½% NaCℓ solution

Table VI-10 Summary of Aluminum Corrosion Test Results

Alloy	Condition	Laboratory Exposure		Kure Beach Exposure	
		General Corrosion	Stress Corrosion	General Corrosion	Stress Corrosion
2021-T81	PM	L	N	L	N
	AW	L	N	L	N
	WA	L	N	L	N
	OW	M	S (HAZ)	M	N
	OWA	L	S (HAZ)	L	N
	WR	L	S (HAZ)	L	N
	WRA	L	N	L	N
X7007-T6	PM	L	N	L	N
	AW	L	N	L	N
	OW	L	N	L	N
	WR	L	N	L	N
2014-T6	PM	M	N	L	N
	AW	M	I	L	N
	OW	L-D	N	L	N
	WR	L	N	L	N
2219-T87	PM		N	L	N
	AW	L	N	L	N
	WR	L	N	L	N
7075-T6	PM	L	N	L	N

Legend:

PM	Parent metal	L	Light surface pitting
AW	As-welded	M	Moderate surface pitting
WA	Welded plus aged	D	Deep surface pitting or stress corrosion cracking
OW	Overheated weld		
OWA	Overheated weld plus aged	N	No stress corrosion
WR	Repaired weld	S	Shallow stress corrosion
WRA	Repaired weld plus aged	I	Intermediate stress corrosion

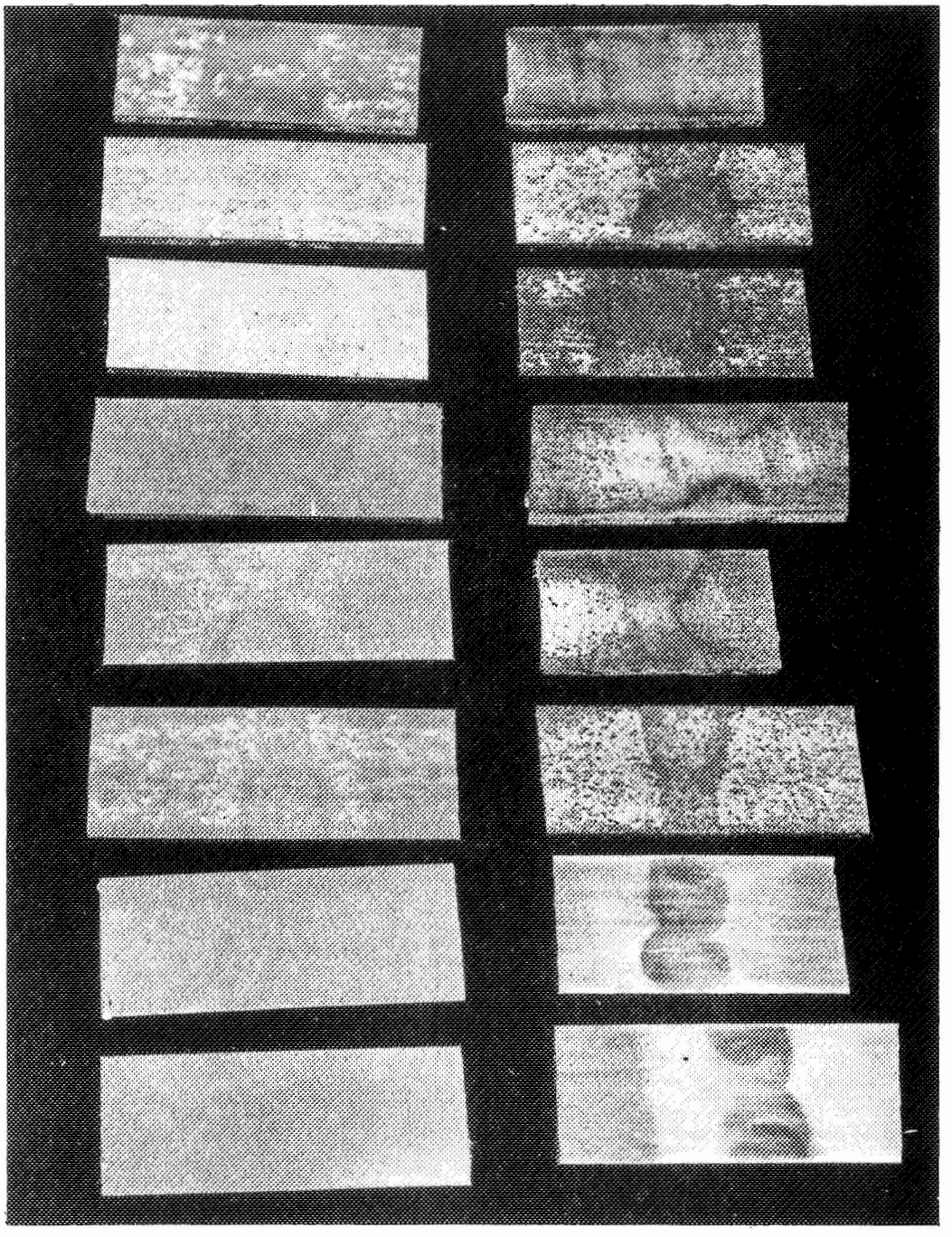

Fig. VI-26 Sections from Stress Corrosion Specimens Tested at Kure Beach (left) and Laboratory Exposure (right) Showing Difference in Surface Attack

No evidence of stress corrosion cracking was found during examination of the specimens exposed at Kure Beach.

Alloy X7007 exhibited light surface pitting in the general corrosion tests. No evidence of stress corrosion cracking was found for either exposure condition. It is quite probable that a longer time of exposure would have indicated severe attack once initiation had occurred. This behavior is not surprising because the surface oxide is quite different from that of 2000 series alloys and initially is quite resistant to attack.

The 2014-T6 composition showed the anticipated behavior. General corrosion tests exhibited light surface pitting. Under stress, pitting increased significantly and stress corrosion cracking was detected in several cases.

The behavior of alloy 2219-T87 was also typical. Light surface pitting was found; no stress corrosion cracking was observed.

Parent metal 7075-T6 alloy exhibited no stress corrosion cracking and light surface pitting.

In addition to the effect of exposure time, another factor must be considered to account for the rather insignificant corrosion effects. This is grain direction; although the "bacon slice" sectioning technique exposes short transverse material, the stress is actually applied in the long transverse direction. It is well known that stress corrosion resistance is considerably greater in the long transverse direction.

VII. DATA COMPARISON, CONCLUSIONS, AND RECOMMENDATIONS FOR FUTURE WORK

This chapter compares the experimental data for Aℓ X7007-T6, Aℓ 2021-T81, and Type 301 stainless steel obtained during this program with data for materials currently used in liquid propellant systems, discusses the overall suitability of these new compositions for potential applications, and presents recommendations for additional work, based on the present state of behavioral knowledge.

A. MECHANICAL PROPERTIES

The Aℓ 2021-T81 and Aℓ X7007-T6 alloys were developed as high-strength, cryogenic alloys. A comparison of the parent-metal strength properties of these two alloys with those of the currently-used high-strength compositions (see Fig. VII-1) illustrates that Aℓ 2021-T81 and Aℓ X7007-T6 are slightly stronger. The data for the high-strength compositions now in use are taken from the *Cryogenic Materials Data Handbook* (Ref 9) and represent typical properties for a variety of gages, and therefore may not clearly show the superiority of the two new alloys, since the inclusion of sheet-gage property data in the typical properties presumably raises the average value. Actually the room temperature strength of the 1-inch thick 2014-T6 plate was greater than that of both heats of the 2021-T81 alloy.

The weld strengths of Aℓ 2021-T81 and Aℓ X7007-T6 appear to be at least as high as those of the currently-used high-strength alloys.

As a candidate for high-strength applications, cryogenically-stretched Type 301 stainless steel can best be compared to titanium alloys. For cryogenic service, the only titanium alloys that can be considered are 5Aℓ-2.5Sn (ELI) and 6Aℓ-4V (ELI, annealed) titanium. As shown in Fig. VII-2, the stainless steel is significantly stronger than the titanium alloys. However, on a strenth-density basis, the stainless steel is comparable only with the 6Aℓ-4V titanium and only at 70°F; below room temperature, the titanium is clearly superior. The strength-density value for the stainless steel in the cryogenic range is slightly lower than that of the 5Aℓ-2.5Sn composition.

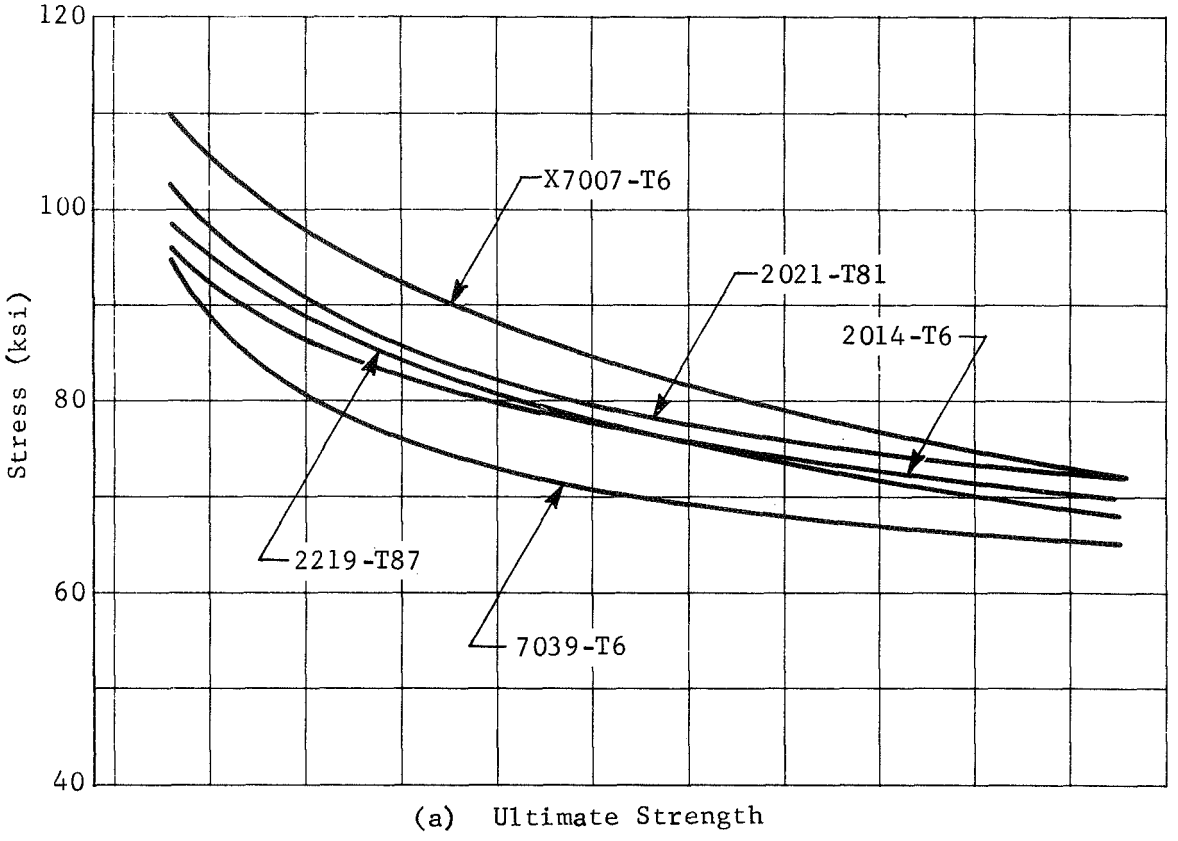

(a) Ultimate Strength

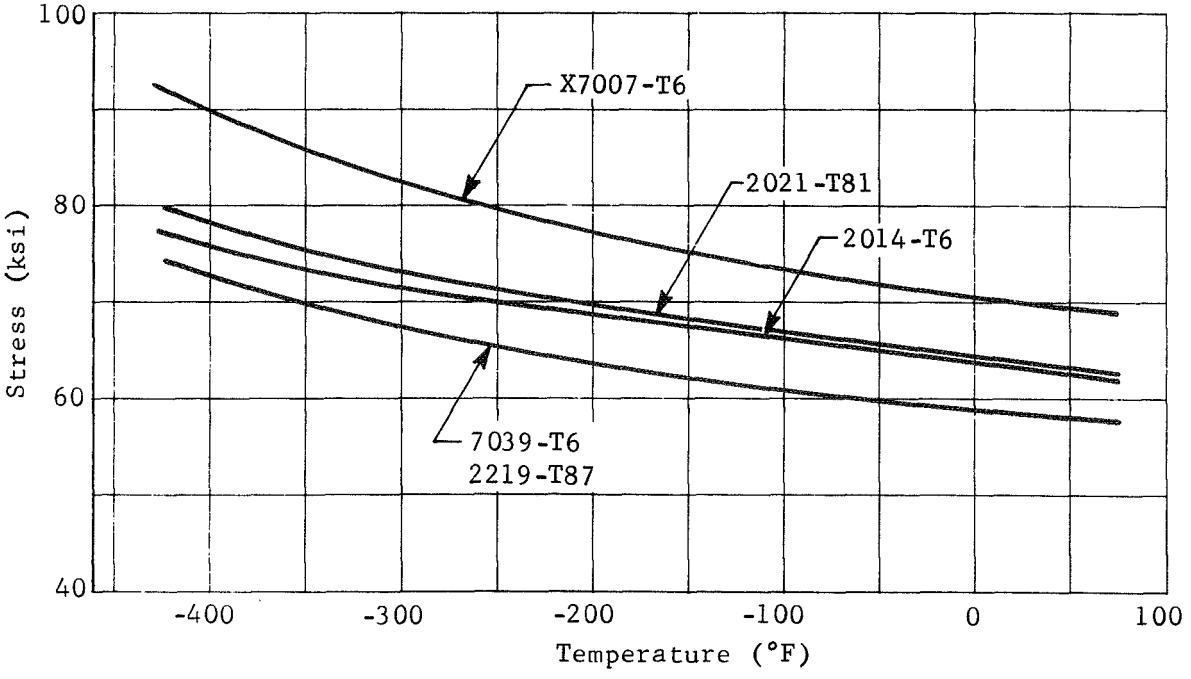

(b) Yield Strength

Fig. VII-1 Ultimate Strength and Yield Strength of Various Aluminum Alloys

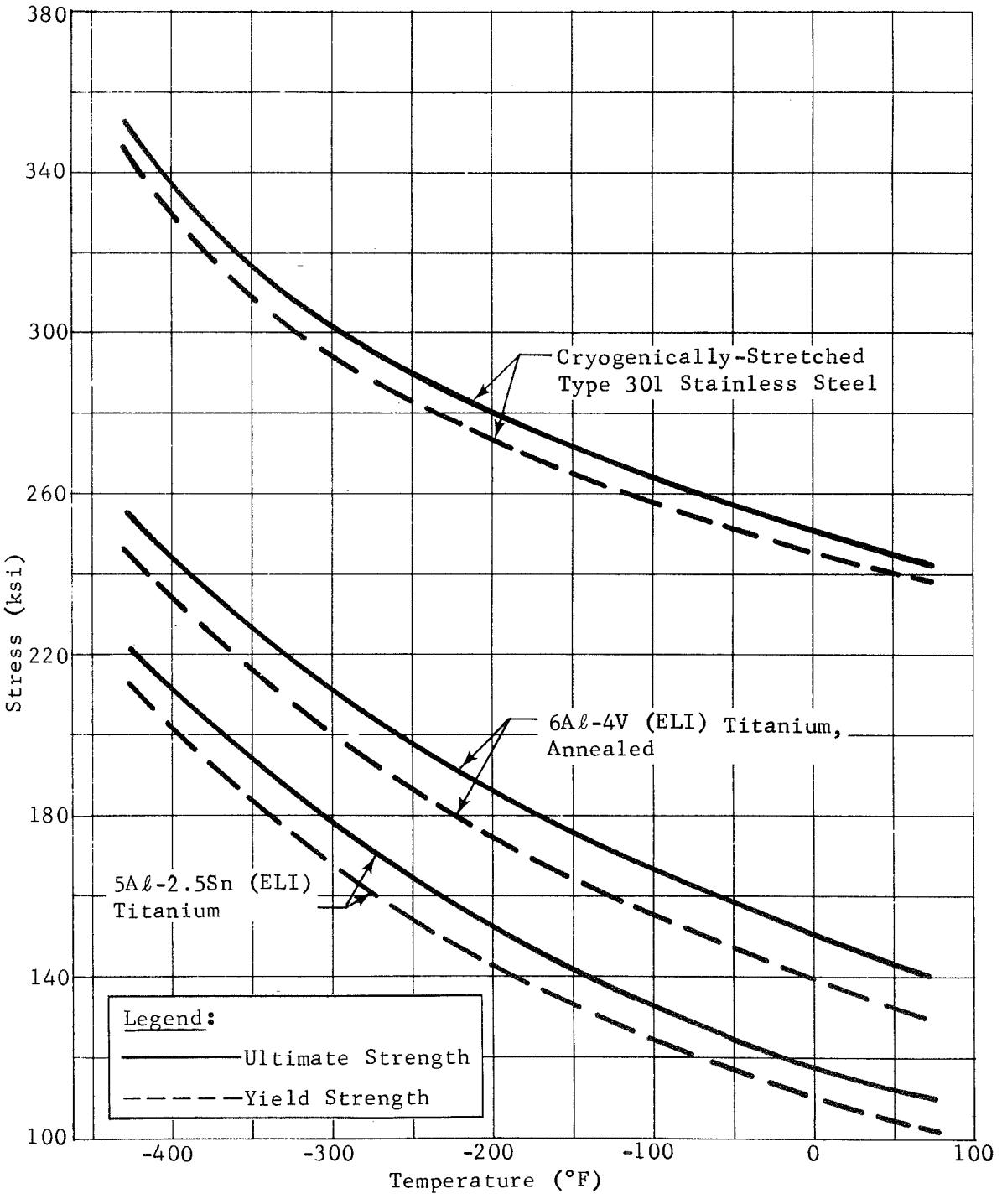

Fig. VII-2 Ultimate Strength and Yield Strength of Various Titanium Alloys and Cryogenically Stretched Type 301 Stainless Steel

The weld-joint efficiency for the stainless steel, 95%, is approximately that obtained using titanium alloys. Therefore, the strength of the various welded specimens will exhibit the same relationship as that shown for the various parent-metal specimens.

The rather peculiar behavior of Poisson's ratio of aluminum and stainless steel as a function of temperature (i.e., the sharp increase between -320 and -423°F)* was also noted by Boeing during an investigation of deep flaws in thin-walled 2219-T87 aluminum alloy and 5Aℓ-2.5Sn titanium tanks (Ref 11). Although no logical explanation for this behavior is apparent, two independent investigations have shown similar behavioral trends.

B. STATIC FRACTURE TOUGHNESS

The comparison of the static fracture-toughness of the two candidate aluminum alloys with that of those alloys now in use must be a qualitative one because the bulk of our parent-metal tests and those reported in the literature were made using different types of specimens.

The static fracture-toughness of parent-metal 2021-T81 is similar to that of other 2000-series compositions, such as 2014-T6 and 2219-T87. The significant increase in toughness with decreasing temperature found for the as-welded 2021-T81 alloy is similar to that noted by Hall (Ref 8) for 2014-T6, and somewhat greater than observed for 2219-T87 (Ref 7 and 11).

It is difficult to compare the static fracture toughness of parent-metal specimens of X7007-T6 with that of other aluminum alloys because only compact-tension-specimen data were obtained. However, it appears that the room-temperature toughness is at least comparable with that of the 2000-series alloys. Unlike the 2000-series alloys, however, the toughness of the X7007-T6 composition decreases with decreasing temperature.

The static fracture toughness of welded 2021-T81 clearly shows that aging of a normal weld is beneficial. Slow crack extension occurs in the fusion line and heat affected zone regions of this composition, as well as X7007-T6 and 2014-T6. The highest toughness region of the 2021 weld is the heat affected zone; toughness of the fusion line and weld centerline were quite similar and up to 1/3 lower than the heat affected zone.

*See interim report for detailed data.

The static facture toughness of the welded X7007-T6 is extremely high (more than 40 ksi $\sqrt{in.}$) at 70°F, but decreases sharply as the temperature decreases. However, even at -423°F, the X7007 is still tough enough to be considered a candidate composition. Weld repairing was not deleterious; overheating during weld did decrease toughness, but the resultant level was still quite high. Defect location had little effect on toughness. Slow crack growth was found for most weld centerline tests, in addition to that already noted for the other defect locations.

Tests performed on 2014-T6 for comparison purposes clearly showed the superior toughness of both 2021-T81 and X7007-T6.

The parent-metal stainless steel exhibits tough behavior at 70°F. According to the ASTM recommendations for the thickness required to obtain valid plane-strain fracture-toughness data, our room-temperature specimens were not sufficiently thick. However, there is no doubt that the apparent toughness, more than 100 ksi $\sqrt{in.}$, is outstanding for such high-strength material. By comparison with titanium, we found that the toughness of the parent-metal 301 stainless steel is below that of 5Aℓ-2.5Sn (ELI) titanium, but above that of 6Aℓ-4V (ELI) titanium. As noted earlier, although the toughness of 301 stainless steel decreases markedly with temperature reductions, its toughness at -423°F is remarkably high, considering that its strength is about 350 ksi. This toughness at -423°F is comparable to that of 6Aℓ-4V (solution-treated and aged) titanium at ambient temperature. The welded specimens of 301 stainless showed less fracture toughness than we had expected. Although as-welded 6Aℓ-4V (ELI) titanium exhibits a lower fracture toughness efficiency (ratio of parent-metal/welded fracture toughness) than the 301 stainless steel (Ref 9), the titanium can be stress-relieved to increase the efficiency to a level higher than that of the stainless steel. The limited data available on the fracture toughness of welded 5Aℓ-2.5Sn (ELI) titanium (Ref 8) indicate that its efficiency ratio exceeds unity even down to cryogenic temperatures.

C. CYCLIC-LOAD FLAW ENLARGEMENT

In any analysis of cyclic crack-growth data, one of the first considerations to be made is whether the data truly follow a power-function relationship. For the plane-stress condition, using through-cracked specimens, Paris (Ref 13) has shown that the behavior can be characterized by the equation

$$\frac{da}{dN} = C\ \Delta K^n,$$

where:

$\frac{da}{dN}$ = the cyclic crack-growth rate;

C = a coefficient that takes into effect material and condition, stress ratio, loading conditions, etc;

ΔK = the difference between the maximum and minimum stress intensities $\left(K_{max} - K_{min}\right)$ that occur during a loading cycle.

The exponent n was found to be approximately equal to four for a variety of materials. However, recent work seems to question the validity of the functional relationship, and particularly the value commonly accepted.

An evaluation of our limited data showed a wide variation of the exponent n. Our values varied from approximately three to 10. Other data for surface-flawed specimens, such as those reported by Hall (Ref 8) showed a similar variation in the value of n. However, his predictions of cyclic-load flaw enlargement behavior were based on the assumption that $n \simeq 4$ did typify the experimental data.

Since the amount of data generated in this program and that available from previous work were too limited to confidently establish the power-function relationship, we decided to compare the cyclic-load flaw-enlargement behavior of the three materials studied in this program with that of other materials on a graphical basis. The behavior of 2021-T81 and X7007-T6 was compared with that of 2219 and 2014, and the behavior of high-strength, cryo-stretched 301 stainless steel was compared with that of 6Aℓ-4V and 5Aℓ-2.5Sn titanium alloys.

A comparision of the data available for parent-metal aluminum with our data was made difficult by the fact that surface-flawed specimens were used by other researchers, whereas our tests were performed using compact-tension specimens. Figure VII-3 shows that there is a similar crack-growth tendency for surface-flawed specimens, but a significantly lower tendency toward crack growth for compact-tension specimens, as evidenced by the greater slope. However, since the direction of crack growth is different for the two types of specimens we feel that there is no real basis for comparision.

On the other hand, a comparison can be made for the welded material. In this case, all the data were obtained using similar surface-flawed specimens. The data, plotted in Fig. VII-4, show surprisingly similar behavior. The 70°F data are interesting to note: the six sets of data that are plotted fall into a rather narrow band. At -320°F, similar behavior is noted.

The data for 301 stainless steel are compared with available data for titanium in Fig. VII-5. At 70°F, the parent-metal 301 exhibits the greatest resistance to crack growth, i.e., shows the lowest crack-growth rate for a given stress intensity. The behavior of welded stainless steel is similar to that for 6Aℓ-4V ELI (parent-metal and welded) titanium at the higher stress intensities. The 5Aℓ-2.5Sn (ELI) parent metal exhibited the least resistance to crack growth. The data compared at -320°F were not for overlapping stress intensities and are not exactly comparable. The titanium curves appear flatter than those for 301 stainless steel. The -423°F data are limited but suggest that there is slightly less crack growth for the 6Aℓ-4V titanium than for the 301 stainless steel.

It appears from the available data that the cyclic growth behavior of the 2021-T81 and X7007-T6 is similar to that observed for currently-used aluminum alloys. The amount of cyclic growth observed in the cryogenically-stretched stainless steel is similar in magnitude to that reported for titanium alloys.

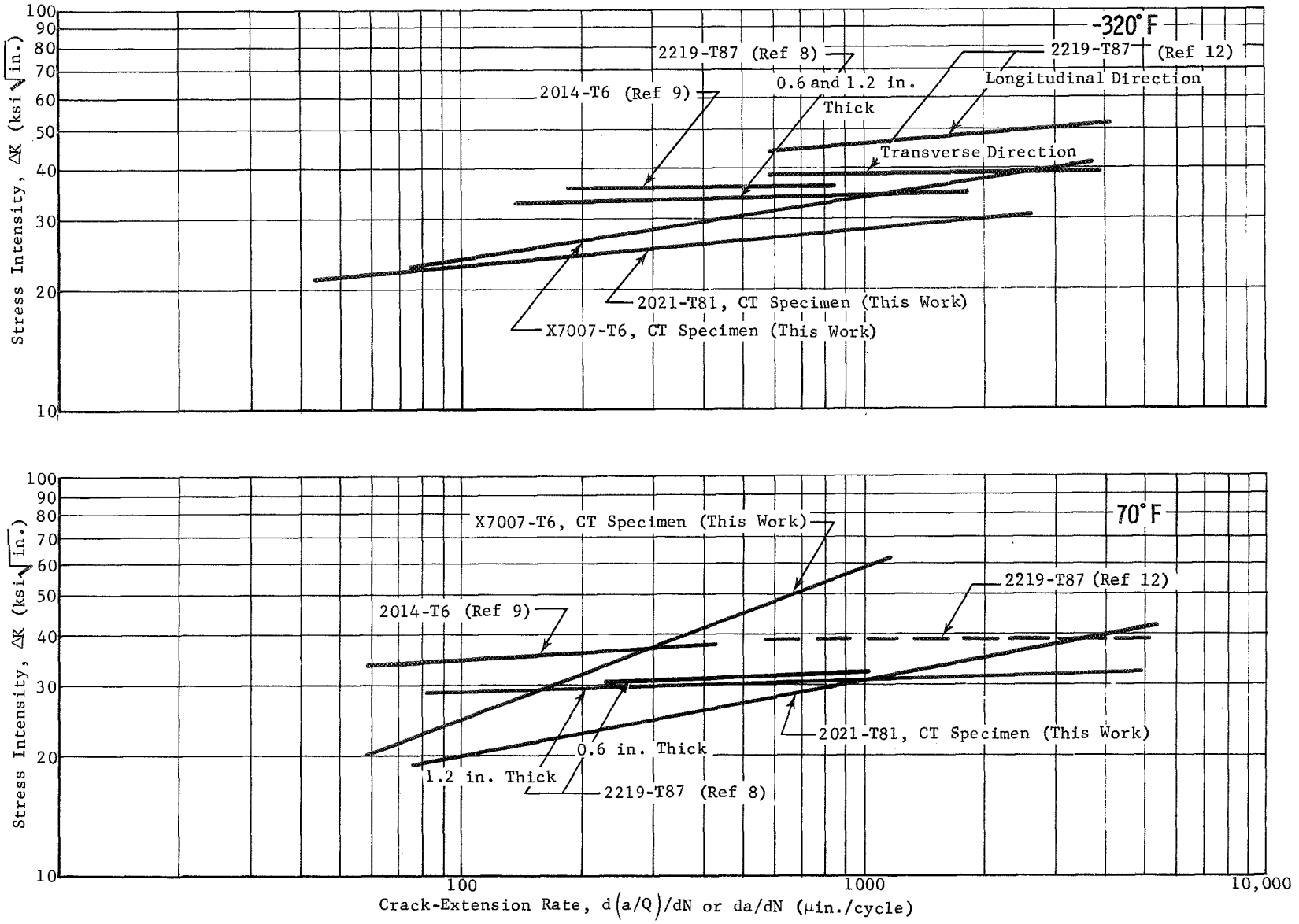

Fig. VII-3 Cyclic Crack-Extension Rates for Various Parent-Metal Specimens (Aluminum Alloys)

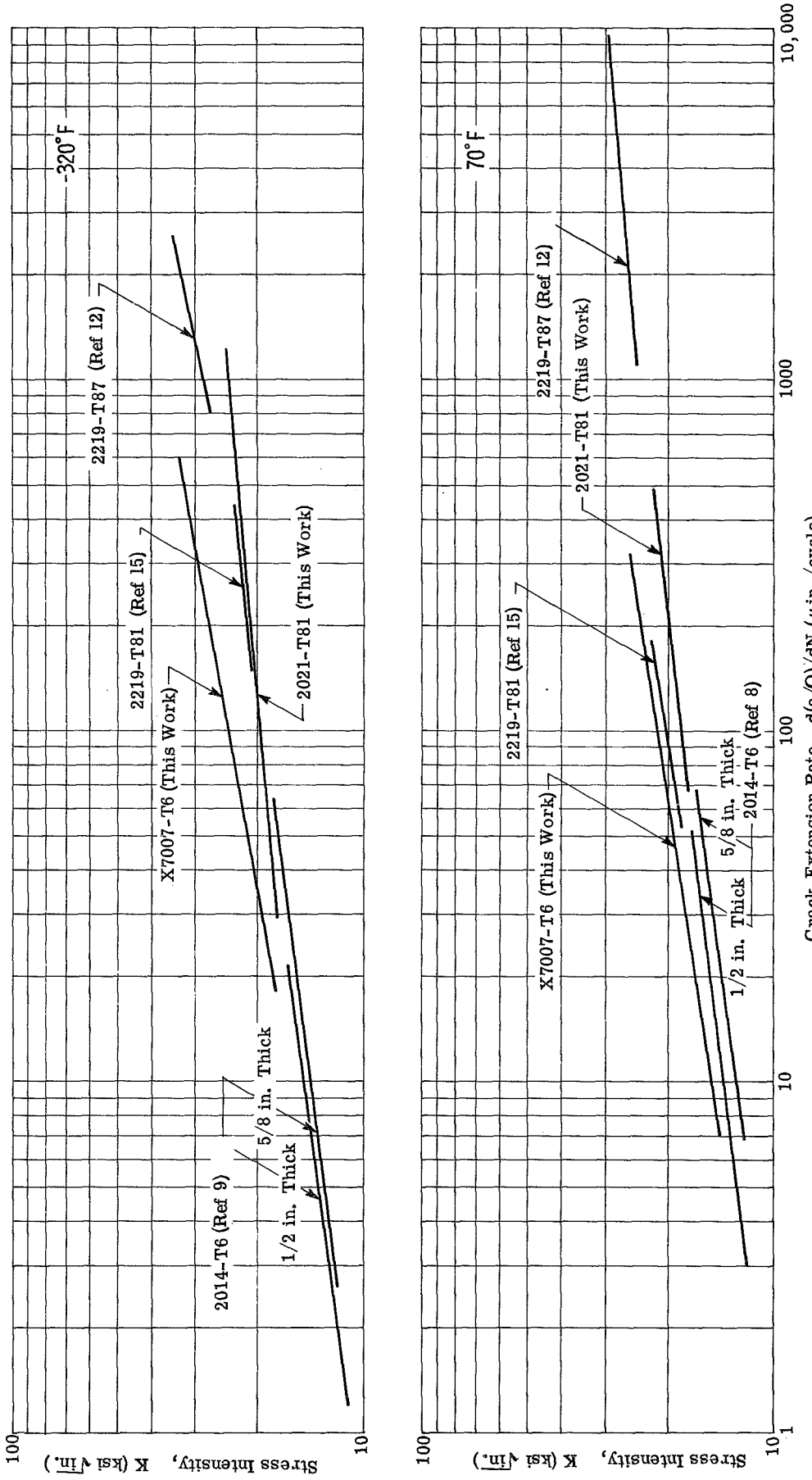

Fig. VII-4 Cyclic Crack-Extension Rates for Various Welded Specimens (Aluminum Alloys)

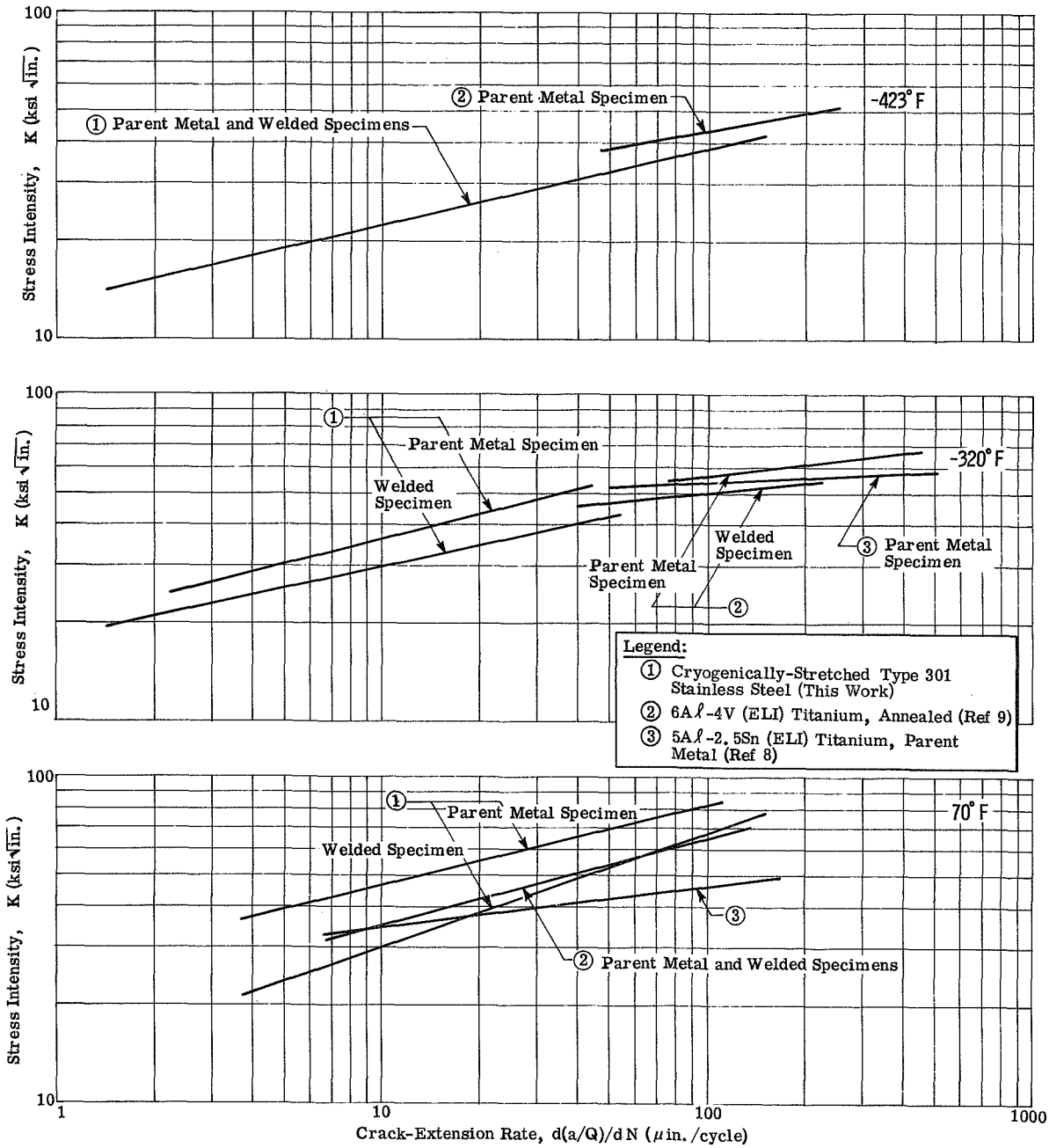

Fig. VII-5 Cyclic Crack-Extension Rates for Various Titanium Alloys and Cryogenically Stretched Type 301 Stainless Steel

D. SUSTAINED-LOAD FLAW ENLARGEMENT

The sustained-load flaw growth behavior of the two aluminum alloys screened in this program must be compared with that of 2219-T81, the only aluminum alloy for which adequate data have been generated. Tiffany (Ref 16) has reported that two distinct threshold values can be established for surface-flawed aluminum alloys: a no-growth threshold, and a growth-no failure threshold. The following table summarizes his results for 2219-T81 parent metal.

Temperature (°F)	Threshold Level, K_{TH}/K_{Ic}*	
	No Growth	Growth-No Failure
70	0.63	0.90
-320	0.73	0.82
-423	0.75	0.87
*Time - approximately 10 hours.		

Previous data obtained by Tiffany (Ref 12) reported a parent-metal no-failure threshold at 70°F of approximately 95%. The threshold at -320°F decreased to less than 90%. These no-failure data are in substantial agreement with the later work in which the two thresholds were reported. The no-failure thresholds for welded material at 70 and -320°F appear to be slightly over 80% in 24 hr. No data for the no-growth threshold are available.

In our tests using compact-tension specimens, only a no-growth threshold was established. Therefore, we can only compare the parent metal on the no-growth criterion. Our comparisons of the welded metal must be more qualitative. However, since the entire comparison is being made using different types of specimens, it should be obvious that all of the remarks with respect to threshold are, at best, qualitative.

The parent-metal 2021-T81 appears to exhibit threshold data similar to those of the 2219-T81 at all temperatures. The X7007-T6 alloy exhibits a significantly, and quite disturbing, low level for the room-temperature threshold. However, at cryogenic temperatures, the level is restored to that of 2021 and 2219. Since the same low threshold in air at room temperature does not occur at cryogenic temperatures, it is quite possible that a stress-corrosion mechanism in air may be operative.

Welded material showed generally lower threshold values than the parent material. With 2219 aluminum, welding is performed using parent-metal composition filler, 2319, and, hence, the observance of a slightly decreased threshold is attributable primarily to material structure and condition. However, with the 2021 and X7007, welding is performed using dissimilar filler material, and therefore, threshold behavior is also a function of composition.

The threshold levels for welded 2021-T81 in various conditions and defect locations were generally in the 50 to 70% range for welded plus aged material. As-welded material (weld centerline only) exhibited an apparent threshold level slightly lower than the welded plus aged material. For those conditions involving weld repair or overheating, the threshold level appeared to be slightly greater than the welded plus aged condition.

Some of the threshold levels are based on very localized growth behavior. Although this growth can be significant in the depth direction, the width is often quite small. Tests have not been performed for sufficient duration to determine whether these zones subsequently become arrested. It appears that the tendency for growth is strongly linked with location in the weld, welding procedure, and residual stresses. Therefore, the characterization of the four-pass weld used in this work does not necessarily characterize welded joints in general. Much additional work will have to be performed to determine how welding variables affect the threshold for slow crack growth under sustained loading.

Evaluation of as-welded, weld centerline material at cryogenic temperature showed a modest increase in threshold level.

The threshold level for welded X7007-T6 presents a bit of a dilemma. In the original work described in Chapter VI, a rather high threshold $\left(85\text{-}90\%\ K_{Ic}\right)$ was found. In the succeeding work on welding parameters, a very low threshold was determined. This is due partially to the great difficulty in interpretation of the fracture faces when the faceting previously described occurs. It is currently not known whether this significant difference in threshold is associated with the difficulty of interpretation or is a real effect. However, since a great deal of threshold testing was performed in the second portion of this program and general agreement was found in the 14 groups of welded X7007-T6 specimens evaluated, it is likely that the initial work must be suspect.

Threshold testing performed in 3½% NaCℓ solution clearly showed the deleterious effects in the presence of a sharp notch. In the 2021-T81 alloy, the greatest decrease in threshold was associated with the weld centerline; the fusion line and heat-affected zones showed slightly less of an effect. The X7007-T6 alloy also showed the greatest environmental effect for the weld centerline and the least for the heat-affected zone.

The 301 stainless steel exhibits a threshold level that is clearly lower than that reported for titanium alloys.

E. GENERAL AND STRESS CORROSION

The laboratory and Kure Beach exposure tests showed that the 2021-T81 alloy is no worse than the 2014-T6 composition currently used for aerospace structures. As expected, it appears to be inferior to 2219 alloy.

The tests performed on the X7007-T6 alloy showed no evidence of stress corrosion. However, based upon the significant deterioration of the slow-growth threshold level in the presence of a deleterious environment, it is probable that the stress corrosion data would have showed an effect during a longer exposure.

F. GENERAL CONCLUSIONS

Considering all of the available data, it appears that all three compositions are worthy of further consideration as candidates for structural service. The following paragraphs present a summary of the behavior for each alloy.

1. Aℓ 2021-T81

This composition exhibits good strength. Although somewhat superior to 2014-T6, the parent-metal tensile and yield strengths for the two heats evaluated in this study are not sufficiently greater to justify selection of this alloy on the basis of strength alone. However, its strength is superior to that of 2219-T87. The strength of the welded specimens are typical of those for 2000-series alloys. The static fracture toughness of the parent metal

is comparable to that of other 2000-series alloys. The tendency toward delamination in this alloy does not have to be considered a detriment, but in fact may be valuable in reducing the tendency toward premature fracture. The fracture toughness in the as-welded condition is between that of 2014-T6 and 2219-T87, and since both of these alloys are deemed adequate for structural service, 2021-T81 should also be satisfactory. In the welded plus aged condition, 2021-T81 exhibits higher toughness than in the as-welded condition. However, adequate toughness is developed in the as-welded condition.

Under cyclic-loading conditions, the behavior of 2021 is typical of aluminum alloys.

Under sustained loading, the threshold for the onset of subcritical crack growth is sufficiently low in the as-welded and welded plus aged conditions so that a rather low operating stress in the weld region would be required. However, weld lands in the structure can compensate for this. The parent metal threshold is similar to that of 2219 alloy and quite satisfactory for engineering structures.

The environmental effects, as determined by corrosion testing and threshold testing, do not show effects that appear to be any more deleterious than observed for 2014-T6 alloy.

One of the key reasons for the possible application of this composition revolves around the question of its weldability. Our experience has shown that 2014-T6 is moderately difficult to weld, and that 2219-T87 is easier to weld because it has a reduced tendency toward hot shortness cracking. Although the amount of welding performed in this program was insufficient to evaluate the weldability rating of 2021-T81, there is general agreement that it is readily weldable. Therefore, the reason for the candidacy of 2021-T81 is that it is easier to weld than 2014-T6 and much stronger than 2219-T87. Postweld aging is recommended in order to improve its stress-corrosion resistance but is not necessary. However, postweld aging increases the difficulty of fabrication, particularly for large structures. On the basis of the available data, it appears that as-welded 2021-T81 would be adequate when postweld aging is not performed.

2. Aℓ X7007-T6

The tensile strength of X7007-T6 is clearly so superior to that of other weldable aluminum alloys that it must be considered a candidate for structural service. The high-yield strength of welded joints is particularly significant. The static fracture toughness of both parent-metal and welded material is excellent at 70°F; and despite the normal decrease in toughness with decreasing temperature, the level at -423°F is deemed adequate for structural consideration. The severe delamination problem should not be troublesome in most applications; however, care should be taken to avoid stresses in the short transverse direction since our characterization of properties in that direction has been only for the unnotched tension specimens.

Cyclic crack-growth rates appear to be similar to those found for other aluminum alloys. The most significant handicap for X7007 is its generally low threshold under sustained loading. Environmental effects further reduce threshold stress intensity. Although our corrosion tests were not conclusive, the threshold test confirms the suspicion that the material is sensitive to a salt environment. As a result of this environmental sensitivity, it is probable that great caution would be exercised in application of this alloy.

3. Cryogenically Stretched Type 301 Stainless Steel

This material appears to be an excellent high-strength candidate for cryogenic service. The ease of fabrication and the resultant integrity of the finished product makes this alloy very attractive for aerospace applications. This composition can be considered competitive with titanium alloys on the basis of strength. Since its tensile strength can be varied over a significant range as a result of cryogenic prestress, some versatility in design can be achieved with the cryogenically stretched steel. The static fracture toughness of this alloy is quite outstanding at all temperatures, both for the parent metal and for welded specimens.

Its subcritical crack-growth behavior under cyclic loading is similar to that observed for titanium alloys. Under sustained-load conditions, crack growth begins at a lower threshold ratio than that in titanium. Since its static toughness is between that of the two titanium candidate alloys, an operational stress based on the threshold-proof test approach could be higher or lower than that obtained using titanium.

The principal question with respect to application of the 301 stainless steel is that of adequate characterization of its threshold behavior in a variety of environments. Titanium was considered to be an outstanding material until premature failures occurred in many environments previously deemed to be nondeleterious. As a result, titanium alloys are now being thoroughly characterized for new environments as new applications arise. Although we expect austenitic stainless steel to exhibit excellent sustained-load behavior in many environments, the transformation processing takes this material out of the austenitic category. It is therefore necessary to scrutinize this composition as we do for martensitic, high-strength, precipitation-hardened stainless steels and to carefully evaluate environmental effects.

G. RECOMMENDATIONS FOR FUTURE WORK

The aluminum evaluation has shown that slow crack growth during monotonic loading occurs in welded material. It is recommended that additional work be performed to study this behavior in more detail and in other alloys such as 2219. In some cases, the indications of crack extension were found at very low-stress intensities, below the sustained-load threshold. It would be interesting to determine whether extensive growth would occur under cyclic loading conditions. The cyclic work reported in this document was for weld centerline defects; the observations of slow crack growth were primarily found in the fusion line and heat-affected zone. Therefore, we have not sufficiently evaluated this effect.

The threshold behavior of multiple-pass welded specimens has raised questions which suggest additional study. The localized nature of growth, the significance of residual stresses, and the correlation between threshold data obtained from compact-tension specimens and surface-flawed specimens should be studied further.

The application of cryogenically stretched 301 stainless steel in aerospace service has raised many questions in recent months. Most of these deal with adequate fracture mechanics characterization of the material with respect to grade (low silicone vs normal grade), thermal condition (aged vs unaged), strength level, condition (parent metal vs aged), and threshold level. The latter is particularly significant. With continuing interest in this material because of its outstanding combination of strength and toughness, additional characterization is imperative.

VIII. REFERENCES

1. F. R. Schwartzberg, R. D. Keys, and T. F. Kiefer: Interim Report, Cryogenic Alloy Screening. NASA CR-72617, Martin Marietta Corporation, Denver, Colorado, February 1970.

2. G. R. Irwin: "Crack-Extension Force for a Part-Through Crack in a Plate." Journal of Applied Mechanics, Vol 84E, No. 4, December 1962, pp 651 thru 654.

3. A. S. Kobayashi: On the Magnification Factors of Deep Surface Flaws. Structural Development Research Memorandum No. 16. The Boeing Company, December 1965.

4. F. W. Smith: Stress-Intensity Factors for a Semielliptical Flaw. Structural Development Research Memorandum No. 17. The Boeing Company, August 1966.

5. L. J. Larson: Depth Effect for Semielliptical Surface Flaws. R-69-14. Martin Marietta Corporation, Denver, Colorado, October 1969.

6. F. W. Smith: Stress-Intensity Factors for Surface-Flawed Fracture Specimens. R-69-15. Martin Marietta Corporation, Denver, Colorado, October 1969.

7. E. T. Wessel: "State-of-the-Art of the WOL Specimen for K_{Ic} Fracture-Toughness Testing." Engineering Fracture Mechanics, Vol I, No. 1, June 1968, p 77.

8. C. F. Tiffany, P. M. Lorenz, and L. R. Hall: Investigation of Plane-Strain Flaw Growth in Thick-Walled Tanks. NASA CR-54837. The Boeing Company, February 1966.

9. L. R. Hall: Plane-Strain Cyclic Flaw Growth in 2014-T62 Aluminum and 6Al-4V (ELI) Titanium. NASA CR-72396. The Boeing Company, November 1968.

10. F. R. Schwartzberg, S. H. Osgood, and R. G. Herzog: Cryogenic Materials Data Handbook. AFML-TDR-64-280 and Supplements. Martin Marietta Corporation, Denver, Colorado, August 1968.

11. J. N. Masters, W. P. Haese, and R. W. Finger: Investigation of Deep Flaws in Thin Wall Tanks. NASA CR 72606. The Boeing Company, December, 1969.

12. C. F. Tiffany and P. M. Lorenz: Fracture-Toughness and Sub-critical-Flaw-Growth Characteristics of Saturn SI-C Tankage Materials. D2-22802 (Contract NAS8-5608). The Boeing Company, April 1964.

13. Personal Communications with E. Willner of Lockheed Missile and Space Company, 1968 and 1969.

14. P. C. Paris, M. P. Gomez, and W. E. Anderson: "A Rational Analytic Theory of Fatigue." Trends in Engineering (University of Washington), Vol 13, No. 1, 1961.

15. W. E. Witzell and C. J. Kropp: Weldment Flaw-Growth Characteristics of 2219-T81 Aluminum Alloy. NASA CR-72288. General Dynamics/Convair, San Diego, California, September 1967.

16. C. F. Tiffany, P. M. Lorenz, and R. C. Shah: Extended Loading of Cryogenic Tanks. NASA CR 72252. The Boeing Company, July 1967.

APPENDIX A

TABULATED EXPERIMENTAL DATA

Table A-1 Static Fracture Toughness Properties of Welded 2021-T81 Aluminum Alloy (Surface-Flawed Specimen*; Room Temperature)

Weldment Condition	Defect Location	Flaw Size: Depth, a (in.)	Flaw Size: Length, 2c (in.)	Flaw Size: Shape, a/Q	Fracture Stress (ksi)	Fracture Stress/ Yield Stress Ratio	Critical Stress Intensity (ksi $\sqrt{in.}$)	Comments
AW	WC	0.455	1.41	0.303	22.2	1.14	23.8	
		0.480	1.48	0.320	21.1	1.09	23.3	
		0.410	1.30	0.277	25.7	1.33	26.4	
	FL	0.460	1.36	0.295	25.4	1.23	27.0 (LBV)	SCG @ 10.3 ksi $\sqrt{in.}$
		0.435	1.46	0.308	23.3	1.15	25.2 (LBV)	SCG @ 25 ksi $\sqrt{in.}$
	HAZ	0.380	1.19	0.231	34.2	1.55	33.9 (LBV)	SCG @ 6 ksi $\sqrt{in.}$
		0.390	1.21	0.261	33.8	1.53	33.7 (LBV)	SCG @ 8.7 ksi $\sqrt{in.}$
WA	WC	0.480	1.49	0.321	30.0	1.28	33.1	
		0.450	1.48	0.315	28.7	1.22	31.4	
		0.420	1.39	0.281	27.1	1.16	28.0	
		0.410	1.42	0.297	27.9	1.19	29.7	
	FL	0.455	1.37	0.297	27.6	1.14	29.3 (LBV)	SCG @ 20.9 ksi $\sqrt{in.}$
		0.330	1.38	0.271	29.4	1.22	29.9 (LBV)	SCG @ 11.0 ksi $\sqrt{in.}$
		0.420	1.29	0.279	24.3	1.	25.0 (LBV)	SCG @ 19.3 ksi $\sqrt{in.}$
		0.390	1.30	0.276	26.0	1.	26.7	
	HAZ	0.440	1.36	0.295	35.8	1.43	37.9 (LBV)	SCG @ 20.2 ksi $\sqrt{in.}$
		0.430	1.42	0.302	35.4	1.42	37.9 (LBV)	SCG
OW	WC	0.440	1.40	0.299	21.7	1.19	23.2	
		0.490	1.64	0.349	22.1	1.21	25.4	
		0.430	1.52	0.316	24.4	1.33	26.8	
		0.410	1.38	0.290	24.4	1.33	25.6	
		0.435	1.36	0.293	24.3	1.33	25.7	
		0.410	1.34	0.285	25.4	1.39	26.4	
	FL	0.390	1.21	0.281	24.2	1.33	24.1 (LBV)	SCG @ 19.9 ksi $\sqrt{in.}$
		0.400	1.23	0.266	23.4	1.28	23.5 (LBV)	SCG @ 12.4 ksi $\sqrt{in.}$
	HAZ	0.300	1.06	0.222	34.8	1.86	32.0 (LBV)	SCG @ 13.5 ksi $\sqrt{in.}$
		0.410	1.27	0.274	27.7	1.48	29.3 (LBV)	SCG @ 7.9 ksi $\sqrt{in.}$
		0.440	1.35	0.291	30.7	1.65	32.3 (LBV)	SCG @ 32 ksi $\sqrt{in.}$
OWA	WC	0.400	1.33	0.275	22.1	0.90	22.6	
		0.480	1.36	0.291	21.9	0.89	23.0	
	FL	0.420	1.35	0.277	22.3	0.84	22.9 (LBV)	SCG @ 15.4 ksi $\sqrt{in.}$
		0.440	1.36	0.293	28.4	1.07	30.0 (LBV)	SCG @ 4.4 ksi $\sqrt{in.}$
	HAZ	0.443	1.39	0.298	35.2	1.24	37.5 (LBV)	SCG @ 14.4 ksi $\sqrt{in.}$
		0.452	1.38	0.298	33.9	1.20	36.1 (LBV)	SCG @ 10.7 ksi $\sqrt{in.}$
WR	WC	0.460	1.37	0.298	25.4	1.32	27.0	
		0.400	1.20	0.262	26.8	1.39	26.7	
	FL	0.480	1.46	0.321	24.8	1.29	27.4 (LBV)	SCG @ 23.8 ksi $\sqrt{in.}$
		0.360	1.14	0.245	26.3	1.37	25.4 (LBV)	SCG @ 24.1 ksi $\sqrt{in.}$
WRA	WC	0.450	1.35	0.293	21.8	0.88	23.0 (LBV)	SCG @ 9.7 ksi $\sqrt{in.}$
		0.475	1.51	0.324	20.7	0.84	22.9	
	FL	0.445	1.27	0.278	26.1	1.06	26.6 (LBV)	SCG @ 12.6 ksi $\sqrt{in.}$
		0.410	1.31	0.281	25.8	1.04	26.0 (LBV)	SCG @ 24.3 ksi $\sqrt{in.}$

*1.0 in. thick x 5.75 in. wide (nominal) cross section; longitudinal direction.

Legend:

AW	As welded	WC	Weld centerline
WA	Welded plus aged	FL	Fusion line
OW	Overheated weld	HAZ	Heat-affected zone
OWA	Overheated weld plus aged	LBV	Lower bound value
WR	Repaired weld	SCG	Subcritical crack growth (lowest detectable level as indicated)
WRA	Repaired weld plus aged		

Table A-2 Static Fracture Toughness Properties of Welded X7007-T6 Aluminum Alloy (Surface-Flawed Specimen*; Room Temperature)

Weldment Condition	Defect Location	Flaw Size			Fracture Stress (ksi)	Fracture Stress/ Yield Stress Ratio	Critical Stress Intensity ($ksi\sqrt{in.}$)	Comments
		Depth, a (in.)	Length, 2c (in.)	Shape a/Q				
AW	WC	0.450	1.38	0.292	36.2	0.91	42.6	
		0.415	1.32	0.255	41.9	1.05	41.3 (LBV)	SCG @ 15.3 ksi in.
	FL	0.422	1.31	0.282	41.6	1.04	43.1 (LBV)	SCG
		0.370	1.27	0.267	41.1	1.02	41.4 (LBV)	SCG
	HAZ	0.350	1.19	0.252	>42.0	>1.00	>41.2 (LBV)	SCG; pinhole failure
		0.380	1.34	0.274	38.0	0.94	38.8 (LBV)	SCG
OW	WC	0.540	1.39	0.301	32.9	0.88	35.2 (LBV)	SCG
		0.530	1.40	0.302	32.7	0.88	35.0 (LBV)	SCG
	FL	0.350	1.17	0.248	40.4	1.06	39.2 (LBV)	SCG @ 8.6 $ksi\sqrt{in.}$
		0.420	1.35	0.289	38.4	1.03	40.4 (LBV)	SCG @ 29.3 $ksi\sqrt{in.}$
		0.390	1.29	0.273	38.8	1.04	39.7 (LBV)	SCG @ 37.0 $ksi\sqrt{in.}$
	HAZ	0.370	1.49	0.267	>39.9	1.03	>40.2 (LBV)	SCG @ 31.3 $ksi\sqrt{in.}$
		0.400	1.37	0.264	39.3	1.12	41.2 (LBV)	SCG @ 22.9 $ksi\sqrt{in.}$
WR	WC	0.460	1.37	0.298	39.0	1.07	41.5 (LBV)	SCG @ 24.9 $ksi\sqrt{in.}$
		0.400	1.20	0.261	40.4	1.11	40.3 (LBV)	SCG @ 17.4 $ksi\sqrt{in.}$
	FL	0.375	1.21	0.259	42.9	1.18	42.5 (LBV)	SCG @ 25.0 $ksi\sqrt{in.}$
		0.430	1.35	0.289	39.6	1.08	41.5 (LBV)	SCG @ 27.8 $ksi\sqrt{in.}$

*1.0 in. thick × 5.75 in. wide (nominal) cross section; longitudinal direction.

Legend:

AW	As-welded	FL	Fusion line
OW	Overheated weld	HAZ	Heat affected zone
WR	Repaired weld	LBV	Lower bound value
WC	Weld centerline	SCG	Subcritical crack growth (lowest detectable level as indicated)

Table A-3 Static Fracture Toughness Properties of Welded 2014-T6 Aluminum Alloy (Surface-Flawed Specimen*; Room Temperature)

Weldment Condition	Defect Location	Flaw Size			Fracture Stress (ksi)	Fracture Stress/ Yield Stress Ratio	Critical Stress Intensity (ksi $\sqrt{in.}$)	Comments
		Depth, a (in.)	Length, 2c (in.)	Shape, a/Q				
AW	WC	0.435	1.50	0.291	17.0	0.69	17.9	
		0.460	1.48	0.305	20.8	0.84	22.4	
	FL	0.435	1.36	0.292	26.1	0.99	27.5	
		0.415	1.40	0.292	25.4	0.96	26.8	
	HAZ	0.405	1.34	0.285	32.1	1.14	33.5 (LBV)	SCG
		0.425	1.38	0.294	30.1	1.06	31.8 (LBV)	SCG @ 21.0 ksi$\sqrt{in.}$
OW	WC	0.390	1.38	0.285	20.7	0.99	21.5	
		0.390	1.48	0.291	18.8	0.89	19.7	
		0.360	1.35	0.277	20.7	0.99	21.2 (LBV)	SCG @ 20.5 ksi$\sqrt{in.}$
		0.370	1.37	0.281	23.0	1.10	23.8	
	FL	0.390	1.37	0.255	23.9	1.14	25.0 (LBV)	SCG @ 22.2 ksi$\sqrt{in.}$
		0.430	1.39	0.269	25.7	1.22	27.3 (LBV)	SCG @ 5.0 ksi$\sqrt{in.}$
	HAZ	0.425	1.36	0.292	28.0	1.02	29.5 (LBV)	SCG @ 17.8 ksi$\sqrt{in.}$
		0.425	1.34	0.288	29.2	1.07	30.5 (LBV)	SCG @ 24.8 ksi$\sqrt{in.}$
WR	WC	0.405	1.22	0.264	25.1	1.22	25.1 (LBV)	SCG @ 25.0 ksi$\sqrt{in.}$
		0.410	1.28	0.275	25.6	1.25	26.1 (LBV)	SCG @ 25.9 ksi$\sqrt{in.}$
	FL	0.420	1.24	0.240	27.1	1.32	25.9 (LBV)	SCG @ 25.8 ksi$\sqrt{in.}$
		0.375	1.28	0.270	26.9	1.29	27.2 (LBV)	SCG @ 27.0 ksi$\sqrt{in.}$

*1.0 in. thick × 5.75 in. wide (nominal) cross section; longitudinal direction.

Legend:

AW	As-welded	FL	Fusion line
OW	Overheated weld	HAZ	Heat affected zone
WR	Repaired weld	LBV	Lower bound value
WC	Weld Centerline	SCG	Subcritical crack growth (lowest detectable level as indicated)

Table A-4 Static Fracture Toughness Properties of Welded 2021-T81 Aluminum Alloy (Compact Tension Specimen,* Room Temperature)

Weldment Condition	Defect Location	Flaw Size		Stress-Intensity Parameter, Y	Pop-in Load (lb)	Critical Stress Intensity (ksi $\sqrt{in.}$)	Comments
		a_{avg} (in.)	a/W				
WA	WC	1.03	0.515	14.1	2540	18.4	
		0.99	0.500	13.5	2420	16.4	
		1.08	0.540	15.0	2300	18.9	
	FL	1.04	0.520	14.3	2345	17.5	
		1.04	0.520	14.3	2370	17.6	
		1.04	0.520	14.3	2320	17.2	
	HAZ	1.01	0.505	13.8	3290	22.6	
		1.05	0.525	14.4	3110	23.2	
		1.02	0.510	13.9	3200	22.9	
OW	WC	0.99	0.495	13.5	2970	20.1	
		0.98	0.490	13.3	3130	20.7	
		1.01	0.505	13.8	3050	21.4	
WRA	WC	1.04	0.520	14.2	2075	15.2	
		1.02	0.510	13.9	2400	17.0	
		1.03	0.515	14.1	2130	16.0	
	FL	0.99	0.495	13.5	2225	15.2	
		1.00	0.500	13.6	2330	15.9	
		1.01	0.505	13.8	2170	15.2	
	HAZ	1.00	0.500	13.6	>2005	>14.1	No pop-in
		1.02	0.510	13.9	>2010	>14.4	No pop-in
		1.01	0.505	13.8	>2860	>20.4	No pop-in

*1.0 in. thick.

Legend:

WA	Welded Plus Aged
OW	Overheated Weld
WRA	Repaired Weld Plus Aged
WC	Weld Centerline
FL	Fusion Line
HAZ	Heat Affected Zone

Table A-5 Static Fracture Toughness Properties of Welded X7007-T6 Aluminum Alloy (Compact Tension Specimen,* Room Temperature)

Weldment Condition	Defect Location	Flaw Size		Stress-Intensity Parameter, Y	Pop-in Load (lb)	Critical Stress Intensity (ksi $\sqrt{in.}$)	Comments
		a_{avg} (in.)	a/W				
AW	WC	1.02	0.510	13.9	>5775	>39.4	No pop-in
		1.02	0.510	13.9	>5120	>34.9	No pop-in
		1.04	0.520	14.2	>5000	>34.6	No pop-in
	FL	1.14	0.570	16.2	>4490	>38.7	No pop-in
		1.01	0.505	13.8	>4720	>32.5	No pop-in
		1.02	0.510	13.9	>5240	>36.5	No pop-in
	HAZ	0.98	0.490	13.3	>3800	>24.8	No pop-in
		1.05	0.525	14.4	>3600	>26.5	No pop-in
		0.99	0.495	13.5	>3700	>25.7	No pop-in
OW	WC	0.99	0.495	13.3	>7400	>49.6	No pop-in
		0.98	0.490	13.3	>7920	>52.2	No pop-in
		0.98	0.490	13.5	>7890	>52.3	No pop-in
WR	WC	1.05	0.525	14.4	>4600	>36.6	No pop-in
		1.02	0.510	13.9	>4850	>33.9	No pop-in
		1.02	0.510	13.9	>4590	>32.2	No pop-in
	FL	1.04	0.520	14.2	>5030	>36.4	No pop-in
		1.06	0.530	14.6	>5000	>37.5	No pop-in
		1.04	0.520	14.2	>4800	>34.8	No pop-in
	HAZ	1.02	0.510	13.9	4380	30.6	
		1.00	0.500	13.6	3850	26.0	
		1.00	0.500	13.6	3780	25.8	

*1.0 in. thick.

Legend:

AW	As-Welded
OW	Overheated Weld
WR	Repaired Weld
WC	Weld Centerline
FL	Fusion Line
HAZ	Heat Affected Zone

Table A-6 Sustained-Load Crack-Growth Threshold Properties of Welded 2021-T81 Tested in Air*

Weldment Condition	Defect Location	Flaw Size a_{avg} (in.)	Load (lb)	Initial Stress Intensity (ksi $\sqrt{in.}$)	Stress Intensity Ratio, K_{Ii}/K_{Ic}	Time (hr)	Description of Crack Behavior
WA	WC	1.03	2173	15.4	0.86	96	G, L, E
		1.01	2080	14.4	0.80	143	G, L, E
		1.11	1520	12.5	0.69	73	G, L, S
		1.03	1490	10.8	0.60	71	N
	FL	1.07	1845	14.6	0.86	70	G, U, E
		1.02	1613	11.8	0.69	72	G, U, E
		1.06	1356	10.4	0.61	71	N
	HAZ	1.06	2900	22.3	0.98	70	G, U, S
		1.03	2440	17.4	0.77	113	G, U, S
		1.00	2400	16.6	0.73	68	N
OW	WC	1.01	2776	19.1	0.92	114	G, U, S
		1.01	2348	16.0	0.77	120	G, U, S
		1.02	1965	13.9	0.67	72	N
WRA	WC	1.06	2040	15.0	0.93	118	G, L, S
		1.03	1788	12.8	0.80	95	G, L, S
		1.04	1615	11.8	0.73	70	N
	FL	1.01	2020	14.2	0.92	76	G, L, S
		1.03	1879	13.7	0.89	72	G, L, S
		1.03	1626	11.7	0.76	96	N
	HAZ	1.01	1740	12.5	--	113	G, U, S
		1.03	1526	11.2	--	89	N
		1.03	1382	10.2	--	70	N

*Compact tension specimen; longitudinal direction, 1-in. thick.

Legend:

WA	Welded Plus Aged	G	Crack Growth
OW	Overheated Weld	N	No Crack Growth
WRA	Repaired Weld Plus Aged	U	Crack Growth Along Entire Front
WC	Weld Centerline	L	Localized Crack Growth
FL	Fusion Line	E	Extensive Growth (>0.01 in.)
HAZ	Heat Affected Zone	S	Slight Growth (<0.01 in.)

Table A-7 Sustained-Load Crack-Growth Threshold Properties of Welded X7007-T6 Tested in Air*

Weldment Condition	Defect Location	Flaw Size a_{avg} (in.)	Load (lb)	Initial Stress Intensity (ksi $\sqrt{in.}$)	Stress Intensity Ratio, K_{Ii}/K_{Ic}	Time (hr)	Description of Crack Behavior
AW	WC	1.00	4374	29.7	--	96	G, U, E
		1.00	3720	25.2	--	88	G, U, E
		1.00	1627	11.1	--	70	G, L, S
	FL	0.97	4720	30.6	--	71	G, U, S
		0.98	2616	17.3	--	132	G, L, S†
		0.99	2095	15.8	--	72	G, L, S
	HAZ	0.98	3252	21.3	--	67	G, U, E
		1.01	3066	20.2	--	91	G, L, S§
		1.00	2829	17.5	--	78	N
		0.97	2865	16.8	--	89	N§
OW	WC	1.03	3586	25.7	--	70	G, L, E
		1.06	2760	19.9	--	73	G, L, S
		1.10	2166	17.5	--	72	G, U, E
WR	WC	1.04	4144	29.9	--	66	G, U, E
		1.03	3479	24.5	--	71	G, U, S
		1.03	2850	20.0	--	72	G, L, S
		1.00	2298	15.5	--	74	N
	FL	1.02	3436	24.1	--	96	G, U, S
		1.06	2110	15.8	--	115	G, L, S
		1.06	1694	12.4	--	74	G, L, S
	HAZ	0.99	3150	21.0	--	72	G, U, S
		0.97	2628	17.1	--	70	N
		1.00	2292	15.6	--	72	N

*Compact tension specimen; longitudinal direction; 1 in. thick.

†Defect outside of FL zone.

§Defect very close to HAZ.

Legend:

AW	As-welded	G	Crack Growth
OW	Overheated Weld	N	No Crack Growth
WR	Repaired Weld	U	Crack Growth Along Enter Front
WC	Weld Centerline	L	Localized Crack Growth
FL	Fusion Line	E	Extensive Growth (>0.01 in.)
HAZ	Heat Affected Zone	S	Slight Growth (<0.01 in.)

Table A-8 Sustained-Load Crack-Growth Threshold Properties of Welded 2021-T81 Tested in 3½% NaCℓ Solution

Weldment Condition	Defect Location	Flaw Size a_{avg} (in.)	Load (lb)	Initial Stress Intensity (ksi $\sqrt{in.}$)	Stress Intensity Ratio, K_{Ii}/K_{Ic}	Time (hr)	Description of Crack Behavior
WA	WC	1.02	1599	12.4	0.69	72	G, U, E
		1.07	1440	10.6	0.59	74	G, U, E
		1.01	1140	8.1	0.45	68	G, L, S
		1.06	943	7.2	0.40	72	N
	FL	1.03	1673	12.1	0.71	72	N†
		1.03	1364	9.9	0.58	70	G, U, S
		1.02	1182	8.5	0.50	72	N
	HAZ	1.00	1920	13.3	0.58	76	N
		1.02	2260	16.0	0.70	72	G, L, S
		1.02	2496	17.5	0.76	72	G, U, S
OW	WC	1.17	1920	15.7	0.75	72	G, L, E
		1.02	1820	13.0	0.62	72	G, L, S
		1.02	1585	11.3	0.54	72	N
WRA	WC	1.06	1330	10.2	0.63	72	N
		1.04	1270	9.3	0.58	69	N
		1.04	1040	7.7	0.48	69	N
		1.03	934	6.8	0.43	72	N
	FL	1.01	1780	13.0	0.84	70	G, L, S
		1.06	1460	11.1	0.72	68	G, L, S
		1.01	1290	9.1	0.59	69	G, L, S
		1.03	1084	7.7	0.50	72	N
	HAZ	1.02	1840	13.1	--	72	G, U, S
		1.01	1477	11.9	--	72	N
		1.01	1270	9.1	--	72	N

*Compact tension specimen; longitudinal direction; 1-in. thick.

†Defect outside of FL zone.

Legend:

WA	Welded Plus Aged	G	Crack Growth
OW	Overheated Weld	N	No Crack Growth
WRA	Repaired Weld Plus Aged	U	Crack Growth Along Entire Front
WC	Weld Centerline	L	Localized Crack Growth
FL	Fusion Line	E	Extensive Growth (>0.01 in.)
HAZ	Heat Affected Zone	S	Slight Growth (<0.01 in.)

Table A-9 Sustained-Load Crack-Growth Threshold Properties of Welded X7007-T6 Tested in 3½% NaCℓ Solution*

Weldment Condition	Defect Location	Flaw Size a_{avg} (in.)	Load (lb)	Initial Stress Intensity (ksi $\sqrt{in.}$)	Stress Intensity Ratio, K_{Ii}/K_{Ic}	Time (hr)	Description of Crack Behavior
AW	WC	1.06	2618	27.6	--	71	G, L, E
		0.99	2960	19.6	--	72	G, L, S
		1.08	2251	16.6	--	72	G, L, S
		1.04	1680	11.9	--	72	G, L, E
	FL	1.02	3168	22.1	--	70	G, L, S
		1.01	2576	17.6	--	76	G, L, E
		0.97	2153	14.1	--	72	G, L, S
		1.03	1625	11.2	--	72	G, L, S
	HAZ	0.99	2420	15.2	--	70	N
		0.97	2100	13.9	--	72	N
		0.98	1663	10.9	--	72	N
OW	WC	1.04	2940	21.5	--	70	G, L, E
		1.02	2200	15.6	--	72	G, L, E
		1.08	1423	11.0	--	72	G, L, E
WR	WC	1.03	2840	20.1	--		G, L, E
		1.04	1818	13.1	--	72	G, L, S
		1.06	1393	10.6	--	72	N
	FL	0.97	2595	15.8	--	72	G, L, S
		1.07	1614	12.0	--	71	G, L, S
		1.05	1210	8.7	--	72	N
	HAZ	1.03	2800	19.6	--	70	G, L, S
		1.00	2415	16.3	--	72	N
		0.97	2874	18.6	--	72	N

*Compact tension specimen; longitudinal direction, 1-in. thick.

Legend:

AW	As-welded	G	Crack Growth
OW	Overheated Weld	N	No Crack Growth
WR	Repaired Weld	L	Localized Crack Growth
WC	Weld Centerline	E	Extensive Growth (>0.01 in.)
FL	Fusion Line	S	Slight Growth (<0.01 in.)
HAZ	Heat Affected Zone		

Table A-10 Corrosion Behavior of 2021-T81 Aluminum Alloy

Condition	Stress Level (% Yield Strength)	Severity of Corrosion at Indicated Location					
		Location	Surface Pitting	Intergranular Attack (in.)	Stress Corrosion Cracking	Volume Loss (%)	Stress Loss (ksi)
Laboratory Exposure							
PM	90	PM	L	0.015	None	3	3.3
	80	PM	L	0.013	None	3	1.1
	70	PM	L	0.009	None	2	1.2
	65	PM	L	0.005	None	2	<1
	0	PM	L	Nil		2	
AW	90						
	80	All	D	0.010	None	4	
	65	All	D	0.010	None	5	
	0	All	L	Nil			
WA	90	HAZ	M	0.005	None	3	
	80	FL,HAZ	M	0.020	None	3	1.2
	70	HAZ	M	0.005	None	3	2.0
	65	FL,HAZ	L	0.002	None	<2	
	0	All	L	Nil		<1	
OW	90	FL,HAZ	M	0.020	None	6	3.3
	80	FL,HAZ	M	0.015	None	6	4.4
	65	FL,HAZ	M	0.016	Shallow (HAZ)	6	2.6
	0	All	M	Nil		2	
OWA	80	FL,HAZ	M	0.004	None		
	70	FL,HAZ	M	0.004	None		
	65	FL,HAZ	M	0.012	Shallow (HAZ)	5	
	0	All	L	Nil		<1	
WR	90						
	80	FL,HAZ	M	0.016	Shallow	5	
	70	WC,HAZ	M	0.010	Shallow (HAZ)	3	2.3
	0	All	L	Nil		<1	
WRA	90	WC,HAZ	M	0.012	None	8	2.2
	80	WC,HAZ	D	0.009	None	8	2.2
	70	WC,HAZ	D	0.012	None	8	1.9
	0	All	L	Nil		<1	
Kure Beach Exposure							
PM	90	PM	M	0.005	None	<1	1.4
	80	PM	M	0.010	None	<1	1.2
	65	PM	L	0.005	None	<1	1.2
	0	PM	L	Nil		<1	
AW	90	HAZ	L	0.005	None	1	2.8
	80	HAZ	L	0.003	None	<1	3.3
	65	HAZ	L	0.003	None	<1	1.8
	--	All	L	Nil		<1	
WA	90	WC	L	0.004	None	1	4
	90	HAZ	L	0.011	None	1	4
	70	FL	L	0.007	None	<1	2.8
	70	HAZ	L	0.002	None	<1	2.8
	65	All	L	0.005	None	<1	2.6
	0	All	L	Nil		<1	
OW	90	HAZ	L	0.005	None	1	2.8
	80	HAZ	L	0.003	None	<1	3.3
	65	HAZ	L	0.003	None	<1	1.8
	0	All	M	Nil		2	
OWA	80	HAZ	L	0.007	None	2	1.8
	70	FL,HAZ	L	0.004	None	1	1.6
	65	FL,HAZ	L	0.003	None	2	2.1
	0	All	L	Nil		<1	
WR	90	FL,HAZ	M	0.004	None	1	4.2
	80	FL,HAZ	M	0.004	None	<1	1.6
	65	WC,HAZ	L	0.002	None	<1	<1
	0	All	L	Nil		<1	
WRA	90	HAZ	L	0.003	None	<1	2.9
	80	HAZ	L	0.003	None	<1	4.3
	65	FL,HAZ	L	0.002	None	<1	
	0	All	L	Nil		<1	

Legend:

PM	Parent Metal	WC	Weld centerline
AW	As-welded	FL	Fusion line
WA	Welded plus aged	HAZ	Heat affected zone
OW	Overheated weld	L	Light surface pitting
OWA	Overheated weld plus aged	M	Moderate surface pitting
WR	Repaired weld	D	Deep surface pitting
WRA	Repaired weld plus aged	Shallow cracking = ≤0.010 in.	

Table A-11 Corrosion Behavior of X7007-T6 Aluminum Alloy

Condition	Stress Level (% Yield Strength)	Severity of Corrosion at Indicated Location					
		Location	Surface Pitting	Intergranular Attack (in.)	Stress Corrosion Cracking	Volume Loss (%)	Stress Loss (ksi)
Laboratory Exposure							
PM	80	PM	L	Nil	None	<1	
	70	PM	L	Nil	None	<1	
	65	PM	L	Nil	None	<1	
	0	PM	L	Nil			
AW	90	HAZ	L	0.003	None	1	
	90	FL,WC	L	Nil	None	<1	
	80	All	L	Nil	None	<1	
	65	All	L	0.002	None	<1	
	0	All	L	Nil		<1	
OW	90	All	L	Nil	None	<1	
	80	All	L	Nil	None	<1	
	65	All	L	Nil	None	<1	
	0	All	L	Nil		<1	
WR	90	All	L	0.003	None	<1	
	80	HAZ	L	0.005	None	<1	
	65	HAZ	L	0.007	None	<1	
	65	FL,WC	L	0.003	None	<1	
	0	All	L	Nil		<1	
Kure Beach Exposure							
PM	90	PM	L	0.002	None	2	2.3
	80	PM	L	0.002	None	<1	<1
	65	PM	L	Nil	None	<1	<1
	0	PM	L	Nil		<1	
AW	90	WC	L	0.004	None	<1	3.6
	80	All	L	Nil	None	<1	1
	65	All	L	Nil	None	<1	1
OW	90	All	L	0.002	None	<1	2.9
	80	All	L	Nil	None	<1	2.7
	65	All	L	Nil	None	<1	<1
	0	All	L	Nil		<1	
WR	90	FL	L	0.004	None	<1	2.0
	80	FL	L	0.002	None	<1	<1
	65	HAZ	L	0.003	None	<1	<1
	0	All	L	Nil		<1	

Legend:

PM	Parent Weld	WC	Weld centerline
AW	As-welded	FL	Fusion line
OW	Overheated weld	HAZ	Heat affected zone
WR	Repaired weld	L	Light surface pitting

Table A-12 Corrosion Behavior of 2014-T6 Aluminum Alloy

Condition	Stress Level (% Yield Strength)	Severity of Corrosion at Indicated Location					
		Location	Surface Pitting	Intergranular Attack (in.)	Stress Corrosion Cracking	Volume Loss (%)	Stress Loss (ksi)
Laboratory Exposure							
PM	90	PM	M	0.007	None	4	
	80	PM	M	0.010	None	3	
	65	PM	M	0.006	None	3	
	0	PM	M	Nil		2	
AW	90	FL,HAZ	M	0.007	Intermediate	<1	
	80	HAZ	L	0.006	Intermediate	1	
	65	FL	D	0.006	Intermediate	2	
	65	WC,HAZ	D	0.016	Intermediate	2	
	0	All	M	Nil		2	
OW	90	FL,HAZ	L	0.006	None	3	
	80	FL	L	0.008	None		
	65	FL,HAZ	M	0.007	None	2	
	0	HAZ	D	0.010		1	
	0	FL,WC	L	Nil		<1	
WR	90	FL,HAZ	M	0.010	None	3	
	80	FL,HAZ	L	0.008	None		
	65	FL,HAZ	L	0.008	None	5	<1
	0	All	L	Nil			
Kure Beach Exposure							
PM	90	PM	L	0.004	None	<1	2.0
	80	PM	L	0.009	None	<1	<1
	65	PM	L	0.008	None	<1	1.4
	0	PM	L	Nil		<1	
AW	90	HAZ	L	0.003	None	<1	5.8
	80	HAZ	L	0.004	None	<1	4.1
	65	HAZ	L	0.003	None	<1	1.9
	0						
OW	90	HAZ	L	0.004	None	<1	2.8
	80	HAZ	L	0.004	None	<1	2.3
	65	HAZ	L	0.002	None	<1	1.3
	0						
WR	90	WC,HAZ	L	0.002	None	<1	2.6
	80	WC,HAZ	L	0.002	None	<1	1.6
	65	WC,HAZ	L	0.002	None	<1	<1
	0	All	L	Nil		<1	

Legend:

PM	Parent metal	FL	Fusion Line
AW	As-welded	HAZ	Heat-affected zone
OW	Overheated weld	L	Light surface pitting
WR	Repaired wled	M	Moderate surface pitting
WC	Weld centerline	D	Deep surface pitting

Shallow cracking = <0.010 in. Intermediate cracking = 0.010 - 0.015 in.

Table A-13 Corrosion Behavior of 2219-T87 Aluminum Alloy

Condition	Stress Level (% Yield Strength)	Severity of Corrosion at Indicated Location					
		Location	Surface Pitting	Intergranular Attack (in.)	Stress Corrosion Cracking	Volume Loss (%)	Stress Loss (ksi)
Laboratory Exposure							
PM	80	PM	D	0.005	None	4	3.3
	70	PM	D	0.006	None	3	<1
	65	PM	D	0.008	None	4	
	0	PM	M	0.005		2	
AW	90	FL,HAZ	M	0.012	None	4	3.5
	80	FL,HAZ	M	0.012	None	3	<1
	65	FL,HAZ	M	0.010	None	3	
	0	All	L	Nil		1	
WR	90	WC	D	0.006	None	5	<1
	90	HAZ	D	0.011	None	4	<1
	80	WC	D	0.010	None	4	1.6
	80	HAZ	D	0.015	None	4	1.6
	65	HAZ	D	0.012	None	5	2.2
	0	All	L	Nil		<1	
Kure Beach Exposure							
PM	90	PM	L	0.005	None	<1	2.3
	80	PM	L	0.003	None	<1	<1
	65	PM	L	0.002	None	<1	1.7
	0	PM	L	Nil		<1	
AW	90	HAZ	L	0.005	None	<1	1.6
	80	HAZ	L	0.006	None	<1	<1
	65	HAZ	L	0.004	None	<1	<1
	0	All	L	Nil			
WR	90	WC,HAZ	L	0.006	None	<1	1.6
	80	FL,HAZ	L	0.004	None	<1	<1
	65	WC	L	0.002	None	<1	<1
	65	HAZ	L	0.005	None	<1	<1
	0	All	L	Nil		<1	

Legend:

PM	Parent metal	HAZ	Heat-affected zone
AW	As-welded	L	Light surface pitting
WR	Repaired weld	M	Moderate surface pitting
WC	Weld centerline	D	Deep surface pitting
FL	Fusion line		

Table A-14 Corrosion Behavior of 7075-T6 Aluminum Alloy

Condition	Stress Level (% Yield Strength)	Severity of Corrosion at Indicated Location					
		Location	Surface Pitting	Intergranular Attack (in.)	Stress Corrosion Cracking	Volume Loss (%)	Stress Loss (ksi)
Laboratory Exposure							
PM	80	PM	L	0.005	None	<2	
	70	PM	L	0.005	None	<2	
	65	PM	L	0.005	None	<2	<1
	0	PM	L	Nil		<1	
Kure Beach Exposure							
PM	80	PM	L	0.004	None	<1	1.3
	70	PM	L	0.003	None	<1	<1
	65	PM	L	0.003	None	<1	<1
	0	PM	L	Nil		<1	

Legend:

PM Parent metal
L Light surface pitting

APPENDIX B

SURVEY ON 2021-T81 AND X7007-T6 ALUMINUM ALLOYS

I. INTRODUCTION

High strength-to-weight ratio is one of the basic criteria for structural materials for liquid fueled space boosters. Others include good toughness, fabricability, and compatibility with a variety of environmental conditions. Aluminum alloys exhibit these qualities and, as a result, have been the principal structural materials used for booster construction. The earlier boosters used medium strength 5000 series alloys. More current boosters, starting with the Titan series, graduated to high strength 2000 series alloys. Alloy 2014 has been the principal composition used for booster construction. This alloy was originally considered to be nonweldable, but the need for a high strength-to-weight alloy forced the development of suitable welding techniques. Some construction has used the slightly lower strength, but more readily weldable, 2219 alloy.

In the past decade, a variety of new aluminum compositions has been developed. The bulk of these have been weldable 7000 series compositions. To incorporate weldability and some improvement in stress corrosion resistance, these aluminum-zinc alloys had to be diluted significantly and, as a result, strength properties were somewhat lower than for 2000 series alloys.

To develop higher strength-to-weight ratio aluminum alloys, NASA initiated a program with the Alcoa Research Laboratories to develop a weldable, high-strength aluminum suitable for applications at temperatures to -423°F. This work was performed under contract NAS8-5452 during the period 1963 to 1967 (Ref. 1). As a result of this work, the two aluminum alloys evaluated in the "Cryogenic Alloy Screening" program (2021-T81 and X7007-T6) were developed.

II. ALLOY DEVELOPMENT PROGRAM

The alloy development program undertaken by Alcoa had the following properties and characteristics established as goals:

1) Tensile properties at room temperature -
   a) Tensile strength: 75 ksi (min),
   b) Yield strength: 65 ksi (min),
   c) Elongation: 10% in 2 in. (min);
2) Tensile properties at -423°F not inferior to those specified at room temperature;
3) Notched/unnotched tensile ratio(K_T = 10) at -
   a) Room temperature - 1.0 (min),
   b) At -423°F - 0.9 (min);
4) Weldability by conventional TIG or MIG techniques equivalent to those of 5456 or 2219;
5) Good ductility and fracture toughness at temperatures down to -423°F in both the as-welded and postweld aged conditions;
6) Weld joint efficiencies of 80% minimum at room temperature;
7) Notched/unnotched tensile ratio (K_T = 10) in the as-welded condition - 0.85 minimum at -423°F;
8) Maximum resistance to corrosion and stress-corrosion cracking.

Alloy compositions investigated in the Al-Cu system (2000 series alloys) were modifications of 2219. Although 2219 does not exhibit the high strengths of 2014, the superior weldability was considered to be paramount. The intent of this portion of the development work was to attempt to obtain strengthening by the addition of Mg, Si, Cd, or Sn without sacrificing weldability.

It was determined that Cd and Sn provided the highest level of strengthening. The notched/unnotched tensile ratio tended to decrease with increasing strength and was only slightly lower at -320°F than at room temperature. Strength decreased when the metal was cold worked (stretched) before aging. A short artificial treatment (pre-aging) before stretching partially restored strength.

The addition of both Cd and Sn to 2219 resulted in strengths that met the contact requirements, but only when pre-aged before stretching. The elongation of the alloy approached the desired value of 10%. The notched/unnotched tensile ratio also was close to the room temperature goal, exceeded the -423°F goal, and showed only slight variation with testing temperature.

Stress corrosion tests of the candidate composition showed that the Cd and Sn alloy had superior corrosion resistance, with failure occurring only after an extended time in the accelerated corrosion test.

Weld cracking tests using 2319 filler metal and an inverted T-joint showed little cracking, indicating good commercial weldability.

It was found that MIG and TIG welds could be made without difficulty for the Cd and Sn variation. Weld joint efficiencies were 60% for the as-welded condition and 65% for the post-weld aged condition. This is below the desired goal of 80%, but was superior to 2219 alloy. Notch toughness of weldments at both 70 and -320°F was good.

In summary, it was shown that a modification of 2219 with Cd and Sn could meet the strength requirements. This alloy also exhibited good notch toughness, good weldability, and it was indicated that acceptable stress-corrosion resistance could be developed. The one property significantly below the contract goal was weld tensile strength.

This alloy was selected for further development and was first designated M825, and then later designated X2021.

In the 7000 series, emphasis was placed on the Cu-free Aℓ-Zn-Mg compositions. Although the highest strength levels can be attained with those compositions containing Cu, weldability and notch toughness become impaired. It was decided to concentrate alloy development on composition containing only Zn and Mg. Twenty experimental compositions were evaluated. Mechanical property tests of the alloys showed that notch-toughness at room temperature was generally very good, but was much poorer at -320°F. Notch toughness decreased with increasing yield strength. An alloy in the vicinity of 6% Zn and 2% Mg met the desired yield strength of 65 ksi and provided the optimum cryogenic notch-toughness.

Further investigations were conducted on alloys near the desirable 6 Zn-2 Mg composition. These alloys also contained small amounts of Mn, Cr, and Cu. Some compositions contained a small amount of Zr to improve weldability. Detailed evaluation of these alloys showed that one alloy, M793 (6.51% Zn, 1.64% Mg, 0.12% Cu, 0.10% Zr) most nearly met the contact strength and notch-toughness requirements. Although this composition had better stress-corrosion resistance than the other alloys, it was still susceptible to stress corrosion cracking in the short transverse direction. Weldability was acceptable; weld strength approached the contract goals. However, cryogenic notch-toughness was low and susceptibility to stress-corrosion cracking existed in welded joints. A modification was selected for further development. In this alloy, the Mg concentration was increased to 1.8% to provide a slight improvement in strength. This alloy was subsequently registered as X7007.

Subsequent to the identification of the two candidate compositions (X2021 and X7007), additional studies were performed in the following areas:

Variations in major alloying elements;

Quench sensitivity;

Trace elements;

Alloy modification;

Aging studies;

Treatments to improve stress corrosion resistance;

Fabricability.

The two alloys developed in this program (X2021 and X7007) came very close to meeting the overall contract objectives. The estimated average unnotched and notched tension properties of these alloys are summarized in Table B-1 and compared with the contract objectives. Also, listed in Table B-1 are the properties of existing weldable alloys used or considered for aerospace vehicle applications.

The room temperature tensile strengths of both alloys are similar and were slightly below the contract goal of 75 ksi. X7007 exhibits a yield strength slightly above the goal of 65 ksi, while the X2021 yield level is slightly below the target value. Alloy X2021 exhibited lower elongation at room temperature than the other alloys.

Table B-1 Comparison of Tensile Properties of Experimental and Commercial High Strength, Weldable Alloys

Property	Testing Temperature (°F)	2219-T851	2014-T651	X2021-T81	5456-H343	7039-T6351	X7007-T6E136	Contract Goals
Tensile Strength (ksi)	70	66	70	73	56	67	73	75
	-112	71	74	79	59	73	81	--
	-320	83	84	89	73	86	91	--
	-423	99	100	101	81	99	104	--
Yield Strength (ksi)	70	50	63	63	43	57	67	65
	-112	54	68	68	45	63	71	--
	-320	61	74	75	51	70	81	--
	-423	68	81	82	54	77	88	--
Elongation (%)	70	12	13	9	8	12	12	10
	-112	13	13	9	9	12	12	--
	-320	15	14	9	11	12	10	--
	-423	18	12	9	7	12	10	--
Notched/Unnotched Tensile Ratio*	70	1.17	1.15	1.00	--	1.28	1.31	1.00
	-112	1.08	--	1.06	--	1.09	1.15	--
	-320	1.06	0.98	1.02	--	0.94	0.95	--
	-423	0.99	0.96	1.00	--	0.89	0.90	0.90

*Round notched specimens - K_t = 10.

The notch tension properties of X2021 met the contract goal. Although the room temperature toughness was lower than that of the other alloys, the toughness ratio remained constant with decreasing temperature so that at -423°F it was higher than that of the other compositions. Alloy X7007 exhibited the typical high room temperature toughness with decreasing temperature characteristic for 7000 series alloys. However, the contractual goals were met, even at -423°F.

Stress corrosion testing showed that the resistance of X2021 approached that of 2219, which is excellent and shows no failures at 0.75 σ ys. The resistance of X7007 was somewhat lower, being similar similar to that of 7039. Susceptibility to cracking was noted in the short-transverse direction, which is quite characteristic for 7000 series alloys.

Weldability studies showed that the X2021 alloy welded with 2319 filler metal provided weldability similar to that of 2219/2319 and better than that of the 2014/2319 parent/filler combination. The X7007/5356 combination was found to be similar to that of 7039/5356; it was, therefore, deemed commercially weldable, but with somewhat more difficulty than X2021.

Mechanical property studies of weldments showed that X2021 strength levels were intermediate between the high strength 2014 and the lower strength 2219. Strength level was well below the ambitious target of 60 ksi. The X7007 weld strength values approached the contract goal and were among the highest observed for aluminum alloys.

Limited stress corrosion testing of weldments showed that post-weld aged X2021 was resistant to corrosion, whereas as-welded material was susceptible. X7007 weldments were susceptible to stress corrosion cracking.

Alloy X2021 was found to be an improvement in high strength weldable alloys. The alloy was found to be superior to 2219 in most respects. A comparison with 2014 showed that X2021 exhibited similar parent metal strength properties, but superior stress-corrosion resistance and weldability. Weld strength was not as great as 2014.

Alloy X7007 was found to have an outstanding combination of mechanical properties, but was found to be susceptible to stress corrosion cracking in the short-transverse direction in parent metal and in weldments.

III. MECHANICAL PROPERTY DATA

In this section, available mechanical property data will be presented and compared. The bulk of the data will be for the 2021 alloy. Although X7007 has been evaluated, virtually no data other than that generated by Alcoa and under this contract are available.

A. TENSILE PROPERTIES

1. Parent Metal

Tensile tests were performed on annealed and solution treated 2021 material (3/4-in. plate) by Lockheed (Ref 2). These data, summarized in Table B-2, show the absence of strain rate sensitivity in the 1.0 to .01%/sec range. The high ductility of both annealed and solution treated material is clearly obvious.

Full heat-treated material (-T81 condition) has been evaluated in thicknesses from 1/16 to 2 1/2 in. The bulk of this work was performed by Coursen of Alcoa as an extension to the original program and is reported in (Ref 1). Available data are summarized in Table B-3. The data show similar properties for the various lots of materials evaluated. There appears to be a tendency toward a reduction in strength with increasing thickness, normal for heat treated aluminum alloys, and low elongation in the long transverse direction in thicknesses of 1 in. or greater. One lot of 1-in. plate exhibited a rather low ultimate strength, 70 ksi, but a normal yield strength level, 65 ksi.

Tensile property data for X7007 alloy are less available than for the 2021 composition because of the lower level of interest in 7000 series alloys. A summary of the available Alcoa and Martin Marietta data is given in Table B-4. This alloy appears to exhibit a wider variation in properties than 2021. Data from the two sources are in general agreement.

Table B-2 Tensile Properties of Annealed and Solution Treated 2021 Alloy

Condition	Strain Rate (sec^{-1})	Ultimate Strength (ksi)	Yield Strength (ksi)	Uniform Strain True (%)	Reduction of Area (%)
ST (1 hr)	1.7×10^{-3}	47	19	21	49
ST (1 hr)	1.7×10^{-2}	44	16	22	54
ST (3 hr)	1.7×10^{-3}	44	22	18	55
ST (3 hr)	1.7×10^{-2}	47	18	20	47
Annealed	1.7×10^{-2}	26	12	13	58
Annealed	1.7×10^{-3}	26	14	14	62

Table B-3 Tensile Properties of Heat Treated 2021 Alloy (-T81 Condition)

Thickness (in.)	Grain Direction	Ultimate Strength (ksi)	Yield Strength (ksi)	Elongation (%)	Reference
1/16	LT	76	66	8	(3)
1/16	L	73	66	7	(1)
	LT	74	64	9	
1/16	L	73	64	9	(4)
	LT	72	63	8	
1/8	L	73	63	10	(1)
	LT	73	62	10	
1/4	L	73	66	12	(1)
	LT	74	66	10	
1/2	L	74	65	10	(1)
	LT	74	64	7	
1	LT	73	64	4	(3)
1	L	73	63	8	This work
	LT	72	61	3	
1	L	70	65	11	This work
1	L	74	67	8	(1)
	LT	74	65	5	
2 1/2	L	72	63	7	(1)
	LT	69	62	4	
	ST	69	60	4	

Table B-4 Tensile Properties of Heat Treated X7007 Alloy (-T6 Condition)

Thickness (in.)	Grain Direction	Ultimate Strength (ksi)	Yield Strength (ksi)	Elongation (%)	Reference
1/16	L	70	68	9	(1)
	LT	74	70	9	
1/8	L	74	68	11	(1)
	LT	71	66	12	
1/4	L	73	67	12	(1)
	LT	71	64	12	
1/2	L	72	65	14	(1)
	LT	71	64	13	
1	L	77	73	13	(1)
	LT	74	69	13	
1	L	77	73	14	This work
1	L	72	69	14	This work
	LT	70	66	14	
2 1/2	L	71	70	14	(1)
	LT	73	68	13	
	ST	74	66	8	

2. Welded Metal

Welded property data for 2021 alloy from Alcoa, Lockheed, and Douglas are summarized in Table B-5. These data show rather typical results for 2000 series alloys. The thin gage (1/16-in.) tests exhibited the highest strength level. Strength level was significantly lower in the plate gage range. With the exception of the Douglas data for 1-in. plate, which exhibited a low strength level, there was generally good agreement of ultimate strength level in the plate range (1/3 to 1 in. thickness). Yield strength levels all appear to be on the high side. In all cases, yield strength was determined over a 2-in. gage length rather than by determining the yield strength of the weld bead only. As a result, yield strength levels are reported to be above the 20-25 ksi normally found for these types of alloys when the local properties of the weld bead are determined.

Data for X7007 alloy are available only from the Alcoa work. These data, from two tests summarized below, show slightly higher strength properties of room temperature aged material than the data obtained in this program. However, this is attributable to the longer room temperature aging period utilized by Alcoa prior to testing.

Postweld Aging Treatment	Lot	Ultimate Strength (ksi)	Yield Strength (ksi)
40 days/70°F	A	55	44
90 days/70°F	A	59	42
133 days/70°F	B	58	49

Table B-5 Weld Tensile Properties of 2021-T81 Alloy

Thick-ness (in.)	Condi-tion*	Weld Technique	Ultimate Strength (ksi)	Yield Strength (ksi)	Reference
1/16	AW	TIG	47	33	(3)
	WA	TIG	54	50	
1/3	AW	TIG	40		(5)
	WA	TIG	44		
1/2	AW	TIG	43	33	(1)
	WA	TIG	48	46	
	AW	MIG	42	38	
	WA	MIG	47	45	
1	AW	TIG	43	38	(1)
	WA	TIG	44	--	
	AW	MIG	43	36	
	WA	MIG	47	46	
1	AW	TIG	36	23	(3)
	WA	TIG	41	36	

*AW = as welded
WA = welded plus aged

B. FRACTURE BEHAVIOR

Alcoa studied the fracture behavior of both alloys (parent metal condition) in thicknesses of 1/4, 1/2, and 1 in. According to current ASTM standards, data were not valid for the 1/4-in. stock of both alloys and much of the 1/2-in. material. Data are summarized in Table B-6.

Table B-6 Room Temperature Fracture Toughness Data

Thickness (in.)	Specimen Type*	Grain Direction	Critical Stress Intensity ksi $\sqrt{in.}$
2021-T81			
1/4	CN	L	25.6†
		T	22.9†
1/2	NB	L	30.6†
		T	21.8
1	NB	L	38.4§
		T	23.9
X7007-T6			
1/4	CN	L	45.4†
		T	37.5†
1/2	NB	L	40.0†
		T	37.3†
1	NB	L	45.5
		T	37.4

*CN = center notched; NB = notched bend.

†Insufficient thickness.

§Out of plane fatigue precrack.

Extensive fracture toughness testing of 2021 weldments has been conducted by Lockheed on 0.30 - 0.33-in. material using the surface flawed specimen (Ref 5). Although the gage was insufficient to permit obtaining valid plane strain data, it nevertheless did provide simulated service type information for the anticipated application. Minimum critical stress intensity values determined in automatic TIG welds, aged after welding, were as follows: weld centerline - 18 ksi $\sqrt{in.}$; near heat affected zone (NHAZ) - 11 ksi $\sqrt{in.}$; NHAZ of repaired weld - 19 ksi $\sqrt{in.}$; and weld centerline of repaired weld - 14 ksi $\sqrt{in.}$ Unaged welds showed the following toughness values: weld centerline - 16 ksi $\sqrt{in.}$ and NHAZ - 15 ksi $\sqrt{in.}$

Sustained load testing of specimens containing weld centerline defects showed no crack growth in a hydrazine environment at 120°F for stress intensities higher than 73% of the critical stress intensity.

C. FATIGUE PROPERTIES

Fatigue properties have been determined at room temperature using various types of fatigue loading methods (Ref 1). No significant directionality effects were found between longitudinal and transverse material.

Flexural and axial stress fatigue strengths of sheet of both alloys were about equal. However, unnotched plate tests of X7007 showed a higher fatigue limit than 2021. This may be attributed to the higher tensile strength level of the X7007 plate stock.

A summary of the average fatigue limits at 5×10^8 cycles is shown below.

Type of Test	Stress Ratio (R)	Fatigue Limit (ksi)			
		2021-T81		X7007-T6	
		Unnotched	Notched ($K_T > 12$)	Unnotched	Notched ($K_T > 12$)
Flexure-Sheet	-1.0	19	--	18	--
Rotating Beam-Plate	-1.0	17	5.5	22	5.5
Axial-Sheet	0.0	27	--	27	--
Axial-Plate	0.0	26	8.0	33	8.0

IV. MANUFACTURING DATA

The properties and behavior of 2021-T81 and X7007-T6 alloys are similar to other aluminum alloys for which a great deal of manufacturing experience exists. Thus, no unique problems or new manufacturing techniques are anticipated.

The X7007-T6 composition has not received sufficient attention by the aerospace industry to account for any manufactured items. The 2021-T81 alloy has received considerably more attention and limited amounts of hardware have been constructed. No unusual manufacturing problems identifiable specifically to alloy 2021, as differentiated from other 2000 series alloys, have been reported. In this section we will briefly summarize the manufacture of two hardware items.

As part of the Air Force Rocket Propulsion Laboratories Hydrazine Storability Test Tank Program, a number of small tanks were designed and fabricated by Martin Marietta Corporation (Ref 6). A total of 35 tanks were constructed from seven materials, thereby providing five tanks of each alloy. Aluminum alloys were 2014-T6, 2219-T6, and 2021-T6.

The tank design incorporated full-scale missile tank features and typical weld stresses. Fabrication and test procedures were based on simulated production tooling and on actual procedures used in the manufacture of production tankage. Tank volume was approximately 15 gallons.

No unusual problems occurred in the fabrication of the 2021 tanks; processing and fabrication were quite similar to those of other 2000 series alloys.

The only known hardware constructed of 2021 alloy for actual service are 62-in.-diameter propellant tanks designed and fabricated by Lockheed (Ref 7). It was reported that selection of 2021 resulted in a weight saving of 20 lb over 2219, and 100 lb over 6061 aluminum. These hydrazine tanks were designed for an operating pressure of 300 psig and a minimum design burst pressure of 600 psig. The tank was spherical in shape and consisted of two 5-ft-diameter shear formed hemispheres welded to an equatorial ring (Y-ring) forging. Membrane thickness for the tank was 0.147 in., weld land thickness was 0.330 in.

To preclude grain coarsening during process annealing or final solution heat treatment, a 2021-H210 temper was developed for the shear forming operation. To prevent differential growth during postweld aging of the hemispheres and ring forging, partial aging before welding was performed.

Welding was performed using the TIG process and 2319 alloy as the filler material. Although 2021 contains only a minor amount of Cd, an overhead venting system was used as a safety precaution. The welding procedure consisted of a three-pass process to attach the Y-ring to the aft hemisphere and a four-pass process to attach the Y-ring to the forward hemisphere. Some weld cracking was found in the process; however, similar cracking was found using 2219 alloy, indicating that the problem was not unique to 2021. Weld process techniques were modified slightly and the cracking was eliminated.

Lockheed concluded that the high strength of 2021 could be used and ease of fabrication maintained. Several characteristics of 2021 that should be considered for the manufacture of space vehicle propellant tanks are noted by Lockheed. These characteristics are:

1) Maximum strength can be attained in the solution treated and aged condition, without the necessity for post-solution treatment cold work;

2) Shear forming in the annealed condition, assures ease of formability and maximum mechanical properties;

3) Freedom from stress corrosion cracking in the as-welded condition;

4) Compatibility in several liquid propellants.

From the experience of both Lockheed and Martin Marietta, it appears that alloy 2021 does not present any unusual manufacturing problems. The present high level of technology available in the construction of aluminum hardware for aerospace applications can be used for 2021 alloy with little modification.

V. REFERENCES

1. R. W. Westerland, W. A. Anderson, H. Y. Hunsicker: *Development of a High Strength Aluminum Alloy, Readily Weldable in Plate Thicknesses, and Suitable for Applications at -423°.* Final Report, Aluminum Co. of America (NASA Contract NAS8-5452), October 13, 1967.

2. P. J. Rowcliffe: *Mechanical and Metallurgical Behavior of 2021 Aluminum Alloy.* Report MRI-510.02. Lockheed Missiles and Space Company, August 29, 1969.

3. R.V. Turley, E. Dash, C. H. Avery: *Stress Corrosion Susceptibility of Welded Aluminum Alloys.* AFML-TR-67-291. Douglas Aircraft Company, August 1967.

4. Martin Marietta Corporation, unpublished data generated under Air Force Contract F04611-70-C-0032.

5. T. M. Morton and J. G. Bjeletich: *Flaw Behavior in 2021 Aluminum Alloy Weldments.* Report F-70-70-1. Lockheed Missiles and Space Company, April 1970.

6. A. W. O'Brien and C. L. Caudill: *Design and Fabrication of Hydrazine Storability Test Tanks.* MCR-69-145. Martin Marietta Corporation, (Air Force Contract F04611-68-C-0080), March 1969.

7. W. Berger and E. Willner: "Development of Space Vehicle Propellant Tankage from the New 2021 Aluminum Alloy." Paper presented at Annual AIAA Meeting, Denver, Colorado, March 1970.

APPENDIX C

DISTRIBUTION

APPENDIX C

DISTRIBUTION

FINAL REPORT NASA CR-72733

Contract NAS3-11203

"Cryogenic Alloy Screening"

Note: Copies of this report have been sent directly to the "Recipient" and "Designee" according to the quantities specified in columns R and D. When no copies are specified in column D, a copy of the letter of transmittal only has been sent to the person named as designee.

Report Copies R	D	Recipient	Designee
		National Aeronautics & Space Administration Lewis Research Center 21000 Brookpark Road Cleveland, Ohio 44135	
1		Attn: Contracting Officer, MS 500-313	
5		Liquid Rocket Technology Branch, MS 500-209	
1		Technical Report Control Office, MS 5-5	
1		Technology Utilization Office, MS 3-16	
2		AFSC Liaison Office, MS 501-3	
2		Library	
1		Office of Reliability & Quality Assurance, MS 500-111	
1		D. L. Nored, Chief, LRTB, MS 500-209	
3		J. R. Faddoul, Project Manager, MS 500-209	
1		W. F. Brown, MS 105-1	
1		R. H. Kemp, MS 49-1	
1		J. E. Sprawley, MS 105-1	
1		J. G. Kennard, MS 3-14	
1		G. T. Smith, MS 500-209	
1		E. W. Conrad, MS 500-204	
1		R. H. Knoll, MS 501-2	
2		Chief, Liquid Propulsion Technology, RPL Office of Advanced Research & Technology NASA Headquarters Washington, D.C. 20546	

Report Copies R	D	Recipient	Designee
1		Director, Launch Vehicles & Propulsion, SV Office of Space Science & Applications NASA Headquarters Washington, D.C. 20546	
1		Chief, Space Vehicles Structures Office of Advanced Research & Technology NASA Headquarters Washington, D.C. 20546	
1		Director, Advanced Manned Missions, MT Office of Manned Space Flight NASA Headquarters Washington, D.C. 20546	
6		NASA Scientific & Technical Information Facility P.O. Box 33 College Park, Maryland 20740	
1		Director, Technology Utilization Division Office of Technology Utilization NASA Headquarters Washington, D.C. 20546	
1		National Aeronautics & Space Administration Ames Research Center Moffett Field, California 94035 Attn: Library	
1		National Aeronautics & Space Administration Flight Research Center P.O. Box 273 Edwards, California 93523 Attn: Library	
1		National Aeronautics & Space Administration Goddard Space Flight Center Greenbelt, Maryland 20771 Attn: Library	
2		Chief, Liquid Propulsion Technology, RPL Office of Advanced Research and Technology, NASA Headquarters, Washington, D.C. 20546	

Report Copies R	D	Recipient	Designee
1		National Aeronautics & Space Administration John F. Kennedy Space Center Cocoa Beach, Florida 32931 Attn: Library	
1		National Aeronautics & Space Administration Langley Research Center Langley Station Hampton, Virginia 23365 Attn: Library	
1		National Aeronautics & Space Administration Manned Spacecraft Center Houston, Texas 77001 Attn: Library	
1	1	National Aeronautics & Space Administration George C. Marshall Space Flight Center Huntsville, Alabama 35812 Attn: Library	M.W. Brennecke SNE-ME-M, Bldg 4712
1	1	Jet Propulsion Laboratory 4800 Oak Grove Drive Pasadena, California 91103 Attn: Library	R. Boundy
1		Defense Documentation Center Cameron Station Building 5 5010 Duke Street Alexandria, Virginia 22314 Attn: TISIA	
1		Office of the Director of Defense Research & Engineering Washington, D.C. 20301 Attn: Office of Asst. Dir. (Chem. Technology)	
1		RTD (RTNP) Bolling Air Force Base Washington, D.C. 20332	
1		Chief, Environmental Factors and Aerodynamics, Code RV-1 Office of Advanced Research and Technology NASA Headquarters Washington, D.C. 20546	

Report Copies R	D	Recipient	Designee
1		Arnold Engineering Development Center Air Force Systems Command Tullahoma, Tennessee 37389 Attn: Library	
1		Advanced Research Projects Agency Washington, D.C. 20525 Attn: Library	
1		Air Force Missile Test Center Patrick Air Force Base, Florida Attn: Library	
1		Air Force FTC (FTAT-2) Edwards Air Force Base, California 93523 Attn: Library	
1		Air Force Office of Scientific Research Washington, D.C. 20333 Attn: Library	SREP, Dr. J. F. Masi
1		Space & Missile Systems Organization Air Force Unit Post Office Los Angeles, California 90045	
1		U.S. Army Missile Command Redstone Scientific Information Center Redstone Arsenal, Alabama 35808 Attn: Document Section	
1		Bureau of Naval Weapons Department of the Navy Washington, D.C. Attn: Library	
1	1	Director (Code 6180) U.S. Naval Research Laboratory Washington, D.C. 20390 Attn: Library	J. M. Krafft

Report Copies R	D	Recipient	Designee
1		Picatinny Arsenal Dover, New Jersey 07801 Attn: Library	
1		Aerojet-General Corporation P.O. Box 296 Azusa, California 91703 Attn: Library	
1		Aerojet-General Corporation 9200 E. Flair Drive El Monte, California 91734 Attn: Library	
1	1	Aerojet-General Corporation P.O. Box 15847 Sacramento, California 95803 Attn: Technical Library 2484-2015A	C. E. Hartbower
1		Aeronutronic Division of Philco Ford Corp. Ford Road Newport Beach, California 92662 Attn: Technical Information Department	
1		Aerospace Corporation 2400 E. El Segundo Blvd. Los Angeles, California 90045 Attn: Library-Documents	
1		Battelle Memorial Institute 505 King Avenue Columbus, Ohio 43201 Attn: Report Library, Room 6A	
1		Beech Aircraft Corporation Boulder Facility Box 631 Boulder, Colorado Attn: Library	

Report Copies R	D	Recipient	Designee
1	1	Bell Aerosystems, Inc. Box 1 Buffalo, New York 14205 Attn: Library	T. Reinhardt
1	1	Boeing Company Space Division P.O. Box 868 Seattle, Washington 98124 Attn: Library	C. F. Tiffany
1		Boeing Company P.O. Box 1680 Huntsville, Alabama 35801	
1		Chemical Propulsion Information Agency Applied Physics Laboratory 8621 Georgia Avenue Silver Spring, Maryland 20910	Tom Reedy
1		Chrysler Corporation Space Division New Orleans, Louisiana Attn: Librarian	
1	1	Syracuse University Research Institute Department of Metallurgy Syracuse, New York	Volker Weiss
1		Curtiss-Wright Corporation Wright Aeronautical Division Wood-Ridge, New Jersey Attn: Library	
1	1 1	General Dynamics/Convair P.O. Box 1128 San Diego, California 92112 Attn: Library	W. Witzel J. Christian
1		Missiles and Space Systems Center General Electric Company Valley Forge Space Technology Center P.O. Box 855 Philadelphia, Pa. 190101 Attn: Library	

Report Copies R	D	Recipient	Designee
1		Grumman Aircraft Engineering Corporation Bethpage, Long Island, New York Attn: Library	
1		Hercules Powder Company Allegheny Ballistics Laboratory P.O. Box 210 Cumberland, Maryland 21501 Attn: Library	
1	1	IIT Research Institute Technology Center Chicago, Illinois 60616 Attn: Library	C. K. Hersh
	1		K. E. Hofer
1		Ling-Temco-Vought Corporation P.O. Box 5907 Dallas, Texas 75222 Attn: Library	
1		Lockheed Missiles and Space Company P.O. Box 504 Sunnyvale, California 94087 Attn: Library	
1		Lockheed-California Company 10445 Glen Oaks Blvd. Pacoima, California Attn: Library	
1		Marquardt Corporation 16555 Saticoy Street Box 2013 - South Annex Van Nuys, California 91409	
1		Martin-Marietta Corporation (Baltimore Division) Baltimore, Maryland 21203 Attn: Library	John Calathes
1	1	Denver Division	R. D. Keys
	1	Martin-Marietta Corporation P.O. Box 179 Denver, Colorado 80201 Attn: Library	F. R. Schwartzberg

Report Copies R	D	Recipient	Designee
1	1	Western Division	R. Rawe
	1	McDonnell Douglas Aircraft Company, Inc. 3000 Ocean Park Blvd. Santa Monica, California 90406 Attn: Library	B. V. Whiteson
1		McDonnell Douglas Aircraft Corporation P.O. Box 516 Lambert Field, Missouri 63166 Attn: Library	
1		Space & Information Systems Division North American Rockwell 12214 Lakewood Blvd. Downey, California Attn: Library	
1		Purdue University Lafayette, Indiana 47907 Attn: Library (Technical)	
1		Stanford Research Institute 333 Ravenswood Avenue Menlo Park, California 94025 Attn: Library	
1		TRW Systems Inc. 1 Space Park Redondo Beach, California 90278 Attn: STL Tech. Lib. Doc. Acquisitions	
1		TRW Incorporated 23555 Euclid Avenue Cleveland, Ohio 44117	E. A. Steigerwald
1		United Aircraft Corporation United Technology Center P.O. Box 358 Sunnyvale, California 94038 Attn: Library	

Report Copies R	D	Recipient	Designee
1		Wright-Patterson Air Force Base, Ohio 45433 Attention: AFML (MAAE)	
1		Wright-Patterson Air Force Base, Ohio 45433 Attention: AFML (MAAM)	
1		Department of the Army U.S. Army Material Command Washington, D.C. 20315 Attention: AMCRD-RC	
1		Commander U.S. Naval Ordnance Laboratory White Oak Silver Spring, Maryland 20910 Attention: Library	
1		Commanding Officer U.S. Naval Weapons Laboratory Dehlgren, Virginia 22448 Attention: Technical Library	
1	1	Colorado State University Fort Collins, Colorado 80521 Attention: Library	F. W. Smith
1	1	Brown University Providence, R. I. 02912 Attention: Library	J. R. Rice
1		California Institute of Technology 1201 E. California Blvd Pasadena, California Attention: Security Officer	
1		General Electric Company Apollo Support Department P.O. Box 2500 Daytona Beach, Florida 32015 Attention: Library	C. Day

Report Copies R	D	Recipient	Designee
1	1	Carnegie Institute of Technology Department of Civil Engineering Pittsburgh, Pennsylvania Attention: Library	R. B. Anderson
1	1	Frankford Arsenal Philadelphia, Pennsylvania 19137 Attention: 1320, Library	Carl Carman
1	1	Cornell University Department of Materials Science & Engineering Ithaca, New York 14850 Attention: Library	H. H. Johnson
1		Sandia Corporation P.O. Box 969 Livermore, California 94550 Attention: Technical Library	H. Lucas
1		Sandia Corporation Sandia Base Albuquerque, New Mexico Attention: Library	H. E. Montgomery B. R. Allen W. Herrmann
1		Brunswick Corporation Defense Products Division P.O. Box 4594 43000 Industrial Avenue Lincoln, Nebraska Attention: Library	J. Carter
1		General Dynamics P.O. Box 748 Fort Worth, Texas 76101 Attention: Library	D. E. Westerheide
1	1	Institution of Aerospace Studies University of Toronto Toronto 5, Ontario Attention: Library	Dr. I. I. Class

Report Copies R	D	Recipient	Designee
1		U. S. Air Force Washington, D.C. Attn: Library	
1		Air Force Systems Command Andrews Air Force Base Washingon, D.C. 20332 Attn: Library	
1		Aeronautical Systems Division Air Force Systems Command Wright-Patterson Air Force Base, Dayton, Ohio Attn: Library	
1		Aerojet-General Corporation 11711 South Woodruff Avenue Downey, California 90241 Attn: Library	
1		ARO, Incorporated Arnold Engineering Development Center Arnold AF Station, Tennessee 37389 Attn: Library	
1		Director Special Projects Office Department of the Navy Washingon, D.C. 20360	
1		Commander U. S. Naval Weapons Center China Lake, California 93557 Attn: Library	
1		Lockheed Propulsion Company P. O. Box 111 Redlands, California 92374 Attn: Library, Thackwell	

Report Copies R	D	Recipient	Designee
1		Arde, Inc 19 Industrial Avenue Mahwah, N. J. 07430	
1		Rocket Research Corporation Willow Road at 116th Street Redmond, Washington 98052 Attn: Library	
1		Rocketdyne Division North American Rockwell, Inc. 6633 Canoga Avenue Canoga Park, California Attn: Library, Department 596-306	
1		Northrop Space Laboratories 3401 West Broadway Hawthrone, California Attn: Library	